Imperial College London
Department of Theoretical Physics

Numerical Calculation of Inflationary Non-Gaussianities

Jonathan Horner

September 14, 2015

Supervised by Prof. Carlo Contaldi

Submitted in part fulfilment of the requirements for the degree of
Doctor of Philosophy in Theoretical Physics of Imperial College London
and the Diploma of Imperial College London

Declaration

All the work presented in this thesis is my own original work unless referenced otherwise. Specifically chapters 5, 6 and 7 are based on papers [1–3] written entirely by me with the collaboration of Carlo Contaldi. Chapter 8 is based on a paper mostly written by Carlo Contaldi in collaboration with myself [4]. The central focus of that paper is a program written completely by myself for the work described in chapters 5, 6 and 7.

Acknowledgements

Throughout my PhD I have received help and advice from countless people. Firstly, and most importantly, I would like to thank my supervisor Carlo Contaldi for taking me on as a student, initiating the project in the first place and his unlimited patience and support over the last few years.

I would like to thank all my fellow students for making my PhD so enjoyable and providing countless hours of physics debates. In particular Ali Mozaffari and Dan Thomas for all the advice they gave me over the last few years. I would like to thank my family for all their support and without them I would never have gotten this far.

And last but not least I would like to thank my wife, Suna, for all her moral support and being there for me during stressful times.

Abstract

In this thesis the numerical calculation of non-Gaussianity from inflation is discussed. Despite a strong interest in non-Gaussianity from inflation models in recent years, not much attention has been devoted to its numerical computation. Calculating the inflationary bispectrum in an efficient and accurate manner will become more important as observational constraints on primordial non-Gaussianity continue to increase.

Despite this, attention given to numerically calculating the primordial bispectrum has been relatively low. The approach presented here differs from previous approaches in that the Hubble Slow-Roll (HSR) parameters are treated as the fundamental parameters. This allows one to calculate the bispectra for a variety of scales and shapes in the out-of-slow-roll regime and makes the calculation ideally suited for Monte-Carlo sampling of the bispectrum.

The work is further extended to include potentials with features and non-canonical kinetic terms, where the standard squeezed limit consistency relation is demonstrated even for models which produce large $f_{\rm NL}$ in the equilateral limit. The method presented here is also independent of the standard field redefinition used in analytic calculations, removing the need for delicate cancellations in the super-horizon limit used in other numerical methods.

Contents

List of Figures

List of Tables

1. A Brief History of Nearly Everything

Compound interest is the most powerful force in the universe.

– Albert Einstein

Cosmology is the study of the history and structure of the universe. From the first moments of the Big Bang, throughout its 13.6 billion year history most of it can be explained by well understood and tested physics. Most of it, except for the first fractions of a second and it is these earliest moments that will be the subject of this thesis.

Looking at the visible universe one of it's most striking features is it's large scale isotropy, that the universe looks roughly the same in all directions. As we have no reason to believe we're in a special place either, we naturally conclude that the universe appears isotropic to observers in other galaxies too. This *isotropy* and *homogeneity* only holds for scales larger than about 100 Mpc [5, 6]. On scales smaller than this, such as the size of individual galaxies and planets, the universe is obviously not homogeneous and isotropic.

Clearly, attempting to explain all the objects in the universe on the smallest scales is outside the bounds of reality. Therefore Cosmology tends to focus on only the largest scales in the universe (those greater 100 Mpc) and many of the non-linearities can be neglected. As it is impossible to model all possible galaxy clusters, observations and predictions tend to focus on statistical properties of the universe. If a theory of the universe can successfully predict properties such as the average density of the universe, its variance etc. then we know we must be on the right track.

These basic observations form the basis of the so-called "Cosmological Principle" where we *assume* to a first approximation, the universe is homogeneous and isotropic. These basic assumptions, a theory of gravity and some initial initial conditions, form the Hot Big Bang model (now more commonly referred to as ΛCDM) and from it the entire history of the universe can be derived.

One such prediction is that everywhere in the universe will be bathed in left-over radiation, a relic from the Big Bang. These photons have been streaming towards us for the past 13.2 billion years and have an average temperature of roughly $T_{\rm CMB} = 2.72548 \pm 0.00057$K [7]. This is referred to as the Cosmic Microwave Background (CMB) and it has a perfect black body spectrum and is probably the most important discovery made in Cosmology. It was first postulated by Gamow [8] in 1946 with the first temperature calculation made by Alpher and Herman in 1950 [9]. It was first discovered in 1964 [10] by Arno Penzias and Robert Wilson who initially found a residual temperature at roughly 3.5K higher than expected when calibrating their antenna and published their work along with an explanation from Dicke, Peebles, Roll and Wilkinson suggesting its Cosmological origin [11].

Using the ΛCDM model and well understood physics we can reconstruct most of the universe's history. At roughly $10^{-10} - 10^{-14}$s the Standard Model of particle physics is a good approximation, the electroweak gauge symmetry is broken and the gauge bosons obtain mass. The density of the universe at this time is dominated by radiation. At 10^{-5}s quarks and gluons become confined forming protons and neutrons. At 0.2s primordial neutrinos decouple and free stream while the neutron-to-proton ratio freezes out. When the universe is 1s old electrons and positrons begin to annihilate resulting in a small amount of leftover electrons. Protons and neutrons begin forming light elements at $200 - 300$s and the ratio of these elements is yet another confirmation of the Hot Big Bang. At 10000 years the density of matter equalises with that of radiation and at 380000 years neutral Hydrogen is formed allowing photons to free stream throughout the universe. Any fluctuations in the density of the universe at this point are preserved by these photons, therefore the CMB is effectively a photograph of the universe when it was 380000 years old. It is not possible to look back to older times in this way as the universe becomes opaque due to electron-photon interactions. This is known as the surface of last scattering. Finally, at $10^9 - 10^{10}$ years initial matter inhomogeneities grow into galaxy clusters from their gravitational attraction [12].

Despite most of the universe's timeline being filled in, there remains a few unanswered but important questions. Why is so much of the universe made of dark matter and dark energy? What are they? Currently our best guess for dark energy is the cosmological constant but this should involve huge corrections from quantum mechanics so what cancels them out? At $t = 1$s, electrons and positrons annihilate resulting a few left over electrons today. What caused this asymmetry and why are there any electrons left at all?

With the recent releases from the Planck satellite [6, 13–19], and especially the recent attention surrounding BICEP2 [20–28], the majority of Theoretical Cosmologists have been concerned with explaining the statistical properties of the CMB. By far their most commonly accepted explanation is called the Inflationary Paradigm and, as it takes place at the very beginning of time before Electroweak symmetry breaking, it is arguably the most fascinating puzzle in Cosmology. On one hand, it takes place at such high temperatures, we can never come close to recreating its conditions in a particle accelerator. Fortunately due to the way inflation imprints on the CMB, its most important predictions are almost completely unaffected by the intermediate particle physics. This is a double edged sword as it means currently we have very little knowledge on how inflation ends. On the other hand as it takes place at such high energies, leaving an imprint on the CMB, this could be one of the only ways to test theories of Quantum Gravity.

Inflation was first proposed by Guth in the 1980's [29] as a solution to certain fine-tuning problems in Cosmology by postulating an early phase of rapid exponential expansion for the universe. Even though this possibility of exponential expansion was first postulated by Starobinsky [30], it wasn't until Guth showed how it could solve outstanding several outstanding Cosmology questions, that Inflation really gained momentum in Theoretical Physics. It wasn't long before cracks started to appear and the paradigm had to be re-thought. This reboot was provided by Linde, Andreas, Albrecht and Steinhardt [31, 32].

Inflation now explains many fine-tuning problems in the universe and the anisotropies in the CMB with an early period of accelerated expansion. One more consequence is that these inflation models predict inflation should continue forever with our observable universe being one out of an infinite set of emergent bubble universes [33, 34]. While this at first sounds like an absurd scenario, from a string theory perspective there are $\sim 10^{1000}$ metastable vacuum-like states [35], each with different laws of physics. Therefore inflation provides a potential mechanism for populating these states and hence explains why the laws of physics are the way they are. While inflation is the most widely accepted explanation of the issues outlined above there is still some disagreement and while alternatives have been proposed, it can remain a heated topic of discussion [36–44].

Inflation's greatest experimental success is also its greatest weakness. The dependence of the variance of the primordial density fluctuations on scale has recently been measured to remarkable precision by the Planck satellite. The current bounds on the relevant parameter, referred to as the spectral index (or tilt) of the primordial scalar perturbation, are $n_s = 0.968 \pm 0.006$ [18]. This value is very close to 1 implying the variance has very little scale dependence, while at the same time decisively rules out $n_s = 1$ exactly. This is in full agreement with standard inflation predictions which state $|n_s - 1| \approx \mathcal{O}(10^{-2})$ and $n_s < 1$. Unfortunately this measurement only fixes one parameter of any given inflationary model meaning we need more information if we are to determine how inflation functions. Attempting to resolve this degeneracy is now a major task in Theoretical Cosmology.

To shed more light on inflation we need more measurements and more predictions. The first candidate is the scale dependence of n_s. Unfortunately this is predicted by inflation to be of order $(n_s - 1)^2$, so very small, and so far all its measurements are consistent with 0 [18], so this doesn't help. The next possibility is gravitational waves. Inflation produces a small amount of gravitational waves which ultimately alter the polarisation of the CMB (so called B-mode polarization). Despite initial excitement from the BICEP2 result there is no evidence of this polarisation effect so far [18, 20]. This is not completely fruitless though. Even if no B-modes are detected, this will continue to place limits on existing inflation models and some progress can be made.

One promising direction is non-Gaussianity. The anisotropies in the CMB are well described by almost-scale-invariant, Gaussian fluctuations, and to a first approximation this is what inflation predicts. However inflation necessarily involves gravity and gravity, in particular General Relativity, is a non-linear theory. This means non-Gaussianities will *always* be generated, albeit very small. Constraints on primordial non-Gaussianity are often given in terms of a parameter $f_{\rm NL}$ [45, 46]. Current observations still show that

f_{NL} is consistent with 0 [19]. However, unlike gravitational waves, the theoretical predictions involve much more intensive calculations and if primordial non-Gaussianity is ever detected our calculations need to be robust and accurate. A flexible and accurate numerical calculation of primordial non-Gaussianity from inflation is the subject of this thesis.

To begin with the basic building blocks of Cosmology are summarised in Chapter 2 along with the various fine-tuning problems of the universe. Chapter 3 introduces inflation as the solution to these problems and discusses how it predicts the primordial power spectrum. Chapter 4 gives a detailed discussion of how we define primordial non-Gaussianity and outlines the methods used to calculate this from the theory side. Chapter 5 describes the numerical calculation of the bispectrum in a Monte-Carlo setting while Chapter 6 discusses non-Gaussian signals from models that would've been required to match the BICEP2 results. Chapter 7 extends this formalism to allow the perturbations to propagate at arbitrary but constant sound speeds and Chapter 8 combines these results with the recent Planck data to put constraints on the inflaton potential.

In this thesis units are used such that $c = \hbar = k_B = 1$ and $M_{pl}^2 = (8\pi G_{\mathrm{N}})^{-1}$.

2. Review of basic cosmology ideas

Today Einstein's General Relativity (GR) is our best theory of gravity. However, it is only a theory, and in particular a classical theory. This means quantum mechanical effects are not taken into account in its description and therefore it is only an approximation. In particular if we study the universe at the beginning of the Big Bang, the temperatures will be so high GR will break down and we need a theory of Quantum Gravity. Currently this is out of our reach. Nevertheless, our understanding of Cosmology is based on the framework of GR so it is of crucial importance.

2.1. FRW metric

GR is a metric theory of gravity, meaning Einstein's equations dictate how the metric of spacetime evolves when we provide a distribution of energy or matter $T_{\mu\nu}$. Given the metric tensor, one can completely describe the motion of particles under gravity as they must follow geodesics on this spacetime. If we observe the universe on large enough angular scales to a good approximation it looks homogeneous (invariant under spacial translations) and isotropic (invariant under rotations). Therefore we can expect to find solutions to the Einstein equations where the spacial parts are homogeneous and isotropic. One possibility is simply flat Euclidean space:

$$\begin{aligned} ds^2 &= g_{ij}dx^i dx^j \\ &= \delta_{ij}dx^i dx^j \\ &= dx^2 + dy^2 + dz^2 \end{aligned} \tag{2.1}$$

However it is not the only possibility. If the space has a constant (i.e. does not vary with position) curvature, K (this still agrees with homogeneity and isotropy), then, in polar coordinates, the spacial metric must take on the form:

$$ds^2 = \frac{dr^2}{1 - Kr^2} + r^2 d\theta^2 + r^2 \sin^2\theta d\phi^2 \tag{2.2}$$

If $K = 0$ this simply becomes equation (2.1). Therefore the full spacetime metric must be the spacial metric above multiplied by an arbitrary function of time $a(t)$.

$$\begin{aligned} ds^2 &= g_{\mu\nu} dx^\mu dx^\nu \\ ds^2 &= dt^2 - a(t)^2 \left[\frac{dr^2}{1 - Kr^2} + r^2 d\theta^2 + r^2 \sin^2\theta d\phi^2 \right] \end{aligned} \tag{2.3}$$

Throughout this thesis $i, j, k, \ldots$ indices are summed only over spacial dimensions whereas $\mu, \nu, \rho, \ldots$ indices are summed over all space-time. This metric is in comoving coordinates, meaning that galaxies will keep their radial and angular coordinates fixed (provided there are no other forces) but the physical distance will increase as $a(t)$ increases i.e. the galaxies will "move with the expansion". The constant K has units $(\text{mass})^2$ and can be 0, positive or negative. The function $a(t)$ is called the "scale factor" and is a rough indication of the size of the universe.

When we can neglect small inhomogeneities and anisotropies (e.g. stars, galaxies etc.), spacetime is then well described by the metric in equation (2.3) called the Friedmann-Robertson-Walker (FRW) metric. Our symmetry principles fixed the form of the FRM metric but so far the function $a(t)$ is arbitrary and undetermined. Many problems in Cosmology, such as calculating the age of the universe, come down to determining the function $a(t)$.

All particles follow geodesics in curved spacetime, representing the path of shortest proper distance, ds, between two events. For photons $ds^2 = 0$ while for non-relativistic particles $ds^2 > 0$. This path can be found by solving the geodesic equation

$$\frac{\mathrm{d}^2 x^\mu}{\mathrm{d}s^2} + \Gamma^\mu_{\alpha\beta} \frac{\mathrm{d}x^\alpha}{\mathrm{d}s} \frac{\mathrm{d}x^\beta}{\mathrm{d}s} = 0, \tag{2.4}$$

where $\Gamma^\mu_{\alpha\beta}$ is the affine connection. Given the FRW metric, the affine connection components can then be easily derived for an arbitrary scale factor. The only none vanishing ones are:

$$
\begin{aligned}
\Gamma^{\rho}_{\mu\nu} &= \frac{1}{2} g^{\rho\sigma} \left(\partial_\mu g_{\sigma\nu} + \partial_\nu g_{\sigma\mu} - \partial_\sigma g_{\mu\nu} \right) \\
\Gamma^{0}_{ij} &= a\dot{a} \left(\delta_{ij} + \frac{K x_i x_j}{1 - K x^2} \right) \\
&= a\dot{a}\tilde{g}_{ij} \\
\Gamma^{i}_{0j} &= \delta_{ij} \frac{\dot{a}}{a} \\
&= \delta_{ij} H \\
\Gamma^{i}_{jk} &= \tilde{\Gamma}^{i}_{jk} \\
&= K x^i \tilde{g}_{jk},
\end{aligned}
\tag{2.5}
$$

where $g^{\mu\nu}$ is the inverse metric satisfying $g^{\mu\alpha} g_{\alpha\nu} = \delta^{\mu}{}_{\nu}$, $\tilde{g}$ is the purely spacial metric and $\tilde{\Gamma}$ are its affine connections [47]. The quantity H is called the Hubble parameter and Hubble's Law says that the recessional velocity of a galaxy, resulting from the expansion of the universe, is proportional to the distance from us. This can be seen from the following simple argument. At any point in time, the physical distance between two objects is $d(t) = \frac{a(t)}{a(t_0)} d(t_0)$, where $d(t_0)$ is the known distance at some earlier time. The velocity of this object is then just $v(t) = \dot{d}(t) = \frac{\dot{a}(t)}{a(t_0)} d(t_0) = \frac{\dot{a}(t)}{a(t)} \frac{a(t)}{a(t_0)} d(t_0) = H(t) d(t)$. This simple relationship was confirmed by Hubble in 1929. Today, the Hubble parameter has a measured value of $H_0 = 67.8 \pm 0.9$ km s^{-1} (Mpc)$^{-1}$ [17].

2.2. The Stress-Energy Tensor

The evolution of the universe is of course dictated by gravity, which in turn depends on the energy content of the universe. In general, matter and radiation (including ultra-relativistic particles whose masses can be neglected) will both contribute to the total energy content of the universe in a different ways. One useful description (like many other astrophysical problems) is to describe the universe as a fluid. The stress-energy tensor for a relativistic perfect fluid is given by

$$T^{\mu\nu} = (\rho + P)u^{\mu}u^{\nu} - Pg^{\mu\nu}, \tag{2.6}$$

where ρ and P are the homogeneous and isotropic density and pressure respectively and u^{μ} is the 4-velocity field of the fluid. This must satisfy the energy-momentum conservation equation:

$$\nabla_{\mu}T^{\mu\nu} = \partial_{\mu}T^{\mu\nu} + \Gamma^{\mu}{}_{\mu\alpha}T^{\alpha\nu} + \Gamma^{\nu}{}_{\mu\alpha}T^{\alpha\mu} = 0 \tag{2.7}$$

These equations give the Navier-Stokes equation after taking the non-relativistic limit, while contracting the the equation with u_{ν} produces the continuity equation.
If we are considering scales where the above assumptions of isotropy and homogeneity hold true the universe is well described a perfect fluid. This means the stress energy tensor of the universe only depends on its rest frame energy density ρ and its isotropic pressure p. Quantities such as shear stresses and viscosities are neglected but arise naturally when considering perturbations.
For example it can be shown that a scalar field $\phi(x)$ with a potential $V(\phi)$ has the following stress-energy tensor

$$T_{\mu\nu} = \partial_{\mu}\phi\partial_{\nu}\phi - g_{\mu\nu}\left(\frac{1}{2}\partial_{\sigma}\phi\partial^{\sigma}\phi - V(\phi)\right). \tag{2.8}$$

Equating equations (2.8) and (2.6) we can see immediately from the term proportional to the metric that

$$p = \left(\frac{1}{2}\partial_{\sigma}\phi\partial^{\sigma}\phi - V(\phi)\right) \tag{2.9}$$

The only 4-vector fields available are u_{μ} and $\partial_{\mu}\phi$ so they must be proportional to each other. But we also know the 4-velocity must always be normalised such that $u^{\mu}u_{\mu} = 1$, this condition then demands that

$$u_{\mu} = \frac{\partial_{\mu}\phi}{\sqrt{\partial_{\sigma}\phi\partial^{\sigma}\phi}} \tag{2.10}$$

It is then straightforward to equate the remaining terms and deduce that a scalar field is a perfect fluid by making the following identifications:

- $u_\mu = \frac{\partial_\mu \phi}{\sqrt{\partial_\sigma \phi \partial^\sigma \phi}}$
- $p = \frac{1}{2}\partial_\sigma \phi \partial^\sigma \phi - V(\phi)$
- $\rho = \frac{1}{2}\partial_\sigma \phi \partial^\sigma \phi + V(\phi)$

Taking the time component of (2.7) determines how the energy density of the fluid evolves in time:

$$\dot{\rho} + 3H(\rho + p) = 0. \tag{2.11}$$

Homogeneity was implicitly assumed here so the ρ and p only depend on time. As ρ and p are both scalars we can always write the fluids equation of state as $p(t) = w(t)\rho(t)$. If w is a constant, equation (2.11) gives an exact solution:

$$\rho \propto a^{-3(1+w)} \tag{2.12}$$

provided $w \neq -1$. For the two special cases mentioned above, $w = 0$ and $w = \frac{1}{3}$. This means for radiation and matter, the energy densities scale as $\rho_{rad} \propto a^{-4}$ and $\rho_{mat} \propto a^{-3}$ respectively, implying the matter dominated era comes later. $w = -1$ is another very important special case in which $T_{\mu\nu} = -\rho g_{\mu\nu}$. Energy conservation then dictates $\partial_\mu \rho = 0$ (as $\nabla_\rho g_{\mu\nu} = 0$) and so the energy density of this fluid must be constant. This case is particularly important when it comes to inflation.
None of this information dictates how $a(t)$ evolves in time. So far our equations only show how the energy density evolves in a background FRW metric. We need to supplement this with the Einstein equation.

2.3. The Einstein Equation

The last ingredient is the Einstein equation [48]:

$$R_{\mu\nu} - \frac{1}{2}g_{\mu\nu}R = \frac{T_{\mu\nu}}{M_{pl}^2} \tag{2.13}$$

or equivalently

$$T_{\mu\nu} - \frac{1}{2}g_{\mu\nu}T = M_{pl}^2 R_{\mu\nu} \tag{2.14}$$

M_{pl} is the Planck mass, defined here as $M_{pl}^2 = \frac{1}{8\pi G_N} = 2.4 \times 10^{18}$ GeV. $G_N = 6.67384(80) \times 10^{-11} \mathrm{m}^3\mathrm{kg}^{-1}\mathrm{s}^{-2}$ is Newton's constant [49]. The Ricci tensor is:

$$R_{\mu\nu} = \partial_\nu \Gamma^\lambda_{\lambda\mu} - \partial_\lambda \Gamma^\lambda_{\mu\nu} + \Gamma^\lambda_{\mu\sigma}\Gamma^\sigma_{\nu\lambda} - \Gamma^\lambda_{\mu\nu}\Gamma^\sigma_{\lambda\sigma} \tag{2.15}$$

and the Ricci scalar is $R = g^{\mu\nu}R_{\mu\nu}$ and $T = g_{\mu\nu}T^{\mu\nu}$. This can be derived from the Einstein-Hilbert action:

$$S = \int \left(\frac{M_{pl}^2}{2} R + \mathcal{L}_{matter} \right) \sqrt{-g}\, \mathrm{d}^4 x \tag{2.16}$$

with

$$T_{\mu\nu} = \frac{2}{\sqrt{-g}} \frac{\delta S_{matter}}{\delta g^{\mu\nu}} \tag{2.17}$$

Using equation (2.5) these quantities can then be calculated:

$$R_{00} = 3\frac{\ddot{a}}{a} \tag{2.18}$$

$$R_{ij} = -(2K + 2\dot{a}^2 + a\ddot{a})\tilde{g}_{ij} \tag{2.19}$$

where $\tilde{g}_{ij}$ is the purely spacial (excluding $a(t)$, so δ_{ij} in Cartesian coordinates when $K = 0$). It is not necessary to calculate R_{0i} as it is a 3-vector and must vanish because of isotropy (no preferred direction) [47].

Using equation (2.6) (in a comoving frame where $u^\mu = (1, \mathbf{0})$) the Einstein equations become:

$$6M_{pl}^2 \frac{\ddot{a}}{a} = -(3p + \rho) \tag{2.20}$$

$$3M_{pl}^2 H^2 = \rho - \frac{3M_{pl}^2 K}{a^2} \tag{2.21}$$

These are known as the Friedmann equations. The second arises after substitution of the (0,0) equation into the (i,j) one (which is proportional to the metric). They can be combined to obtain equation (2.11).

Equation (2.20) tells us that (if ρ is positive) the universe will only stop expanding if $K > 0$. With this in mind, it is useful to define a quantity called the critical density

$$\rho_{0,\text{crit}} = 3M_{pl}^2 H_0^2 = 1.878 \times 10^{-26} h^2 \text{kg m}^{-3} \tag{2.22}$$

0 subscripts indicate the present day quantity and h is H in units of 100 km s^{-1} Mpc $^{-1}$ (i.e. ≈ 0.7). We define the time-dependent critical density

as simply $\rho_{\text{crit}}(t) = 3M_{pl}^2 H^2(t)$.
Using the solutions for $\rho(a)$ described above, we can then use the Friedmann equations to calculate the function $a(t)$ to see how the universe expands with time. With $K = 0$ (the universe is very close to being flat), the scale factor grows:

- $a \propto t^{\frac{2}{3(w+1)}}$
- $a \propto t^{\frac{2}{3}}$ matter dominated
- $a \propto t^{\frac{1}{2}}$ radiation dominated
- $a \propto e^{Ht}$ vacuum dominated (H is a constant in this case)

Therefore the universe is always expanding and there will have been time when $a = 0$, unless the energy density is purely from the vacuum (known as a de Sitter Universe). With this in mind, coupled with how ρ scales with a, if we consider the early time behaviour, its clear that $\rho = \rho_m + \rho_r$ will become very large and will dominate over the curvature term at very early times. Therefore, $\rho(t) \to \rho_{\text{crit}}(t)$ as $a(t) \to 0$. The problem is that today, the total energy density has been measured to be very close to the critical density, even after billions of years. This is known as the "flatness problem" and will be explained in more detail later.
By expressing ρ as a linear combination of all its possible constituents we can re-write the Friedmann equation in a very useful form by dividing out the critical density today. This naturally defines the following quantities:

$$\Omega_K = \frac{-K}{H_0^2} \tag{2.23}$$

$$\Omega_\Lambda = \frac{\rho_{\Lambda,0}}{3M_{pl}^2 H_0^2} \tag{2.24}$$

$$\Omega_m = \frac{\rho_{m,0}}{3M_{pl}^2 H_0^2} \tag{2.25}$$

$$\Omega_r = \frac{\rho_{r,0}}{3M_{pl}^2 H_0^2} \tag{2.26}$$

So the last three Ω's are the corresponding fractions to the critical density measured today. The Friedmann equation then becomes:

$$\left(\frac{H}{H_0}\right)^2 = \Omega_\Lambda + \frac{\Omega_K}{a^2} + \frac{\Omega_m}{a^3} + \frac{\Omega_r}{a^4} \tag{2.27}$$

This is a simple ODE which we can solve for $a(t)$ with the condition $a(0) = 0$. Evaluated at the present day, we obtain the condition $1 = \Omega_\Lambda + \Omega_K + \Omega_m + \Omega_r$ and therefore we only need to measure the fractions of the three energy densities relative to the critical density. With these values measured, we can solve equation (2.27) for $a(t)$ and hence the dynamics of the homogeneous universe are completely specified. In particular, we can invert $a(t)$ or solve for $a(t_0) = 1$ and age of the universe will be a function of the four numbers Ω_Λ,Ω_K, Ω_r and H_0.

2.4. Problems with the cosmological model

From the time of Electro-Weak Unification ($\approx$ 1 TeV) to present day, the universe is described by experimentally verified and well understood physics, particularly with the recent discovery of a Higgs-like particle [50, 51]. For times earlier than this, we can only speculate. We believe that at a high enough energy, Supersymmetry (SUSY) will come in to play, there will be a grand unification of the strong force with the Electro-Weak and at the the Planck scale we know General Relativity must break down and quantum gravity effects must come into play. The exact natures of all of these things are completely unknown and right now the LHC has yet to see any signs of SUSY (the lowest energy phenomenon of those mentioned).
However, everything in Cosmology from the Electro-Weak Unification era onwards is well described by GR supplemented with some initial conditions. In particular we should specify the initial amplitudes of the primordial scalar and tensor perturbations. From these values one can calculate the anisotropies of the CMB, its polarization etc. As we were obviously not around at the very beginning of the radiation era, and this period is not visible to us as the photons were strongly interacting with matter so the universe was opaque, we cannot really know what they were. What we can do though is measure all the relevant quantities today and evolve the universe *backwards* in time to see what initial conditions our universe is compatible with. This is where cracks start to appear our Cosmological model [47, 52].

2.4.1. The Flatness Problem

The first of these problems is the so-called "Flatness Problem". At the end of section 2.3 the quantities Ω_i were defined as the ratio of energy density ρ_i to the critical density today with the condition $1 = \Omega_\Lambda + \Omega_m + \Omega_r + \Omega_K$. The best constraints Ω_K are currently $\Omega_K \approx -0.052^{+0.049}_{-0.055}$ implying it is a small but non-zero value with K being positive. So far all the Ωs are time independent quantities, ratios of energy densities measured today. We now generalise this definition for all time. The critical energy density is $\rho_{crit}(t) = 3M_{pl}^2 H^2(t)$ and $\Omega(t) = \frac{\rho(t)}{\rho_{crit}(t)}$. With these definitions, the Friedman equation becomes:

$$\Omega_K = 1 - \Omega = \frac{-K}{a^2 H^2} \tag{2.28}$$

Now if we take the scale factor to be a power law $a(t) \propto t^n$, such as in the radiation or matter era, periods of the universe which are well understood, trivially:

$$\Omega_K = \frac{-Kt^{2(1-n)}}{n^2} \tag{2.29}$$

In the radiation and matter epochs, n is always less than one and therefore Ω_K will have been growing since the beginning of the radiation era. Therefore to obtain a small value for Ω_K now, an even smaller value must have been specified at some earlier time. To get an idea of how small, it is simpler to work with temperature instead of time: $a \propto T^{-1} \propto t^n$. It is then straightforward to calculate how Ω_K has grown over time [47]

$$\begin{aligned}
\frac{\Omega_K(T_0)}{\Omega_K(T_{pl})} &= \frac{\Omega_K(T_0)}{\Omega_K(T_{eq})}\frac{\Omega_K(T_{eq})}{\Omega_K(T_{pl})} \\
&= \frac{T_{pl}^2}{T_0 T_{eq}} \\
&= \left(\frac{T_{pl}}{T_0}\right)^2 \frac{\Omega_r}{\Omega_m}
\end{aligned}$$

where T_0, T_{eq} and $T_{pl} \sim 10^{32}K$ are today's temperature, the temperature of matter-radiation equality and the Planck temperature respectively and $\Omega_r \approx 10^{-5}\Omega_m$. The important point here is that even though $\Omega_K(T_{Pl})$ clearly must have been tiny, it cannot have been zero. That would mean

$K = 0$ and hence $\Omega_K = 0$ for all time. At this point it becomes convenient to introduce a new time parameter N referred to as the number of e-folding. It is defined as $a_1 = a_0 e^{N_1 - N_0}$ or equivalently $\frac{dN}{dt} = H$. Differentiating $\Omega_K = 1 - \Omega$ with respect to this parameter and using equations (2.11) and (2.20) yields the following differential equation [52]:

$$\frac{d\Omega}{dN} = (1 + 3w)\Omega(\Omega - 1) \tag{2.30}$$

One can easily see that $\Omega = 1$ is an unstable fixed point if $(1 + 3w) > 0$. Ideally one would desire $\Omega = 1$ to be attractor solution. This is the "flatness problem". Why is $\Omega_K(t_0)$ so small but yet non vanishing? The only way $\Omega = 1$ can be an attractor solution is if $(1 + 3w) < 0$.

2.4.2. The Horizon Problem

Two types of horizons exist called "particle" and "event" horizons. They both set an upper limit on how far light can have travelled since within a particular time (mostly $t = 0$) and are given by the integral [47]:

$$d(t_2, t_1) = a(t_2) \int_{t_1}^{t_2} \frac{1}{a(t)} \, \mathrm{d}t \tag{2.31}$$

The differences between the two horizons are the integral limits. Particle horizons measure the maximum distance light may have travelled since the big bang. Event horizons measure how far light may travel from now to a future time. For $a(t) \propto t^n$ with $n < 1$, $d(t_2, t_1)$ can easily be calculated.

$$d(t_2, t_1) = \frac{t_1}{1 - n} \left(\frac{t_2}{t_1} - \left(\frac{t_2}{t_1} \right)^n \right) \tag{2.32}$$

At the time of last scattering, t_L, the universe had evolved through a radiation dominated era, so $n = 1/2$. The particle horizon then at the time of last scattering with $t_L \gg t_1$ is then simply

$$d_H = 2t_L = 2\frac{t_L}{t_0} t_0, \tag{2.33}$$

where t_0 is the time today. At the same time an "angular diameter distance" can be defined. An object at a comoving radial coordinate r emits light at a time t is observed to subtend a small angle θ. The particle (such as a galaxy) at this time will have a length of $L = a(t)r\theta$. The "angular diameter distance" d_A is defined so the usual Euclidean relation is true [47]:

$$\theta = \frac{L}{d_A}. \tag{2.34}$$

Therefore $d_A = a(t)r$ where t is the time light is emitted, i.e. t_L. The angular diameter distance to the surface of last scattering is therefore

$$d_A = \frac{a(t_L)}{a(t_0)}a(t_0)r = \left(\frac{t_L}{t_0}\right)^{2/3} a(t_0)r. \tag{2.35}$$

r the comoving distance to surface of last scattering. It can be easily calculated from the null geodesics of photons travelling towards us from that time, i.e.

$$ds^2 = dt^2 - a^2(t)dr^2 \;\;\rightarrow\;\; a(t_0)r = a(t_0)\int_{t_L}^{t_0} \frac{dt}{a(t)} = 3t_0. \tag{2.36}$$

This gives $d_A = 3t_0(t_L/t_0)^{2/3}$ for the angular diameter distance. With these two results the angle the horizon at the surface of last scattering subtends is $d_H/d_A \sim (t_L/t_0)^{1/3} \sim 10^{-2}$ as $t_L \sim 10^5$ years and $t_0 \sim 10^{10}$ years. This angle is of order 1^{o} so physical interactions during the evolution of the universe (up to last scattering time) can only have smoothed out inhomogeneities for patches in the sky a few degrees across. This is in stark contrast to the fact that the sky is roughly isotropic. This is the "horizon problem". The universe appears to be in a state of thermal equilibrium despite only small patches are in causal contact with each other. More explicitly, equation (2.31) can be written as an integral over the comoving Hubble radius:

$$d = \int_0^a \frac{1}{aH}\, \mathrm{d}(\ln a) \tag{2.37}$$

If the universe is dominated by a fluid with an equation of state given by w, the integrand is [52]:

$$\frac{1}{aH} = H_0^{-1} a^{\frac{1}{2}(1+3w)} \tag{2.38}$$

Calculating the particle horizon for this equation of state yields

$$
\begin{aligned}
d &= \frac{2}{H_0(1+3w)}\left[a^{\frac{1}{2}(1+3w)} - \tilde{a}^{\frac{1}{2}(1+3w)}\right] \\
&= \frac{2}{H_0(-1)(1+3w)}\left(\frac{1}{\tilde{a}}\right)^{-\frac{1}{2}(1+3w)}\left[1-\left(\frac{\tilde{a}}{a}\right)^{-\frac{1}{2}(1+3w)}\right].
\end{aligned} \tag{2.39}
$$

Here a and $\tilde{a}$ are two arbitrary scale factors with $a \gg \tilde{a}$. The factor $(1+3w)$ appears again. From the first line we can see that if $(1+3w) > 0$ the first term will dominate. This is the case for radiation or matter dominated universes. Using this relation results in the horizon problem.
The second line is simply the same quantity but is more helpful when $(1+\ 3w) < 0$. One can now see the particle horizon is dominated by the scale factor at early times, $\tilde{a}$, and we can make the particle horizon as large as we like simply by going to sufficiently early times when $\tilde{a} \to 0$.

2.4.3. The Monopole Problem

As stated above there is a general consensus that at energies around $E \approx 10^{16}$ GeV, a local gauge symmetry is spontaneously broken to Standard Model gauge group $SU(3) \times SU(2) \times U(1)$. In all of these possible models the symmetry breaking mechanism results in an abundance magnetic of monopoles. One can deduce a quick order of magnitude estimate from dimensional grounds. As we have already seen the horizon is roughly t (equation (2.31) when $t_2 \gg t_1$). We also know that at all times $a \propto T^{-1}$ as the Planck distribution is preserved. This holds true even during the matter dominated era as the number of photons vastly outnumbers the number of baryons. Because at these early times the universe is radiation dominated (so $a \propto t^{1/2}$) the horizon is going to be roughly $t \approx M_{pl}/T^2$. Assuming one monopole per causal patch the number density would be t^{-3} evaluated at symmetry breaking energy E, giving $t^{-3} \approx E^6/M_{pl}^3$. The photon energy density is proportional to T^4 so the number density at this time will be around E^3. This ratio of monopole density to photon density will be around $\left(\frac{E}{M_{pl}}\right)^3$ which is of order 10^{-9}. The problem this there are atleast 10^9 photons per nucleon today, meaning we expect one monopole per nucleon. This is clearly wrong. Of course, as everything above the Electro-

Weak scale is mostly just speculation, one may wonder if this is indeed a problem at all. However, it is mentioned as this problem was one of the main reasons people began to take an interest in inflation [47].

From the three main problems outlined above, the horizon and flatness problems are the most serious. It is easy to see that the evolution of the scale factor, determined w, is inherently linked to both of these problems. This suggests that a possible solution would be to postulate some new type of matter with an appropriate equation of state, setting up inflation.

3. Inflation as the solution of the cosmological problems

With the horizon and flatness problems, the main issue arises because the comoving Hubble radius, $1/(aH)$ increases with time. Therefore the solution to these problems is simple: make $1/(aH)$ *decrease* with time [52]. This is the fundamental idea behind inflation and in particular, if "enough" (which we will define shortly) inflation occurs to solve the horizon problem, it automatically solves the other two problems as well [29, 31, 32]. For these reasons we will focus mainly on how inflation solves the horizon and flatness problems.

3.1. Accelerated Expansion

The key to causing $1/(aH)$ decrease with time is evident from equation (2.38). We need the quantity $(1 + 3w) < 0$. This is exactly equivalent to saying the expansion of the universe accelerated via equation (2.20). Alternatively one can simply differentiate $1/(aH) = 1/(\dot{a})$. Another way of parametrizing this is to define a so-called "slow-roll parameter" ϵ. Simply from the definition of H, one can relate $\ddot{a}$ to $\dot{H}$ through the following equation:

$$\frac{\ddot{a}}{a} = H^2\left(1 + \frac{\dot{H}}{H^2}\right) \tag{3.1}$$

$$\frac{\ddot{a}}{a} = H^2\left(1 - \epsilon\right) \tag{3.2}$$

This equation defines ϵ. It also gives a condition for when inflation has to end i.e. when $\epsilon = 1$. So inflation is a period in the universe's history such that the following (completely equivalent) conditions hold [52]:

- $\frac{\mathrm{d}}{\mathrm{d}t}\left(\frac{1}{aH}\right) < 0$

- $\ddot{a} > 0$
- $1 + 3w < 0$
- $\epsilon = -\frac{\dot{H}}{H^2} = -\frac{\mathrm{d}\ln H}{\mathrm{d}N} < 1$

If this is the case, the comoving Hubble radius will decrease, $\Omega_K = 0$ becomes an attractor solution and the horizon integral will be dominated by earlier times. We can be more quantitative though. Let us suppose inflation lasts N e-foldings. That is to say $a_{end} = e^N a_{start}$. Let us also suppose that $\Omega_K = \frac{-K}{a^2H^2}$ is initially of order one. Then, by the end of inflation Ω_K will have decreased by roughly a factor of $e^{-2N} = \frac{|K|}{a_{end}^2 H_{end}^2}$. Using this to solve for K, for today we can say

$$|\Omega_K| = e^{-2N}\left(\frac{a_{end}H_{end}}{a_0 H_0}\right)^2 \tag{3.3}$$

As we desire this quantity to be less than one, the flatness problem ceases to be an issue if

$$e^N > \frac{a_{end}H_{end}}{a_0 H_0} \tag{3.4}$$

To make further progress we have to make an assumption about the end of inflation, in particular that $a_{end}H_{end} \approx a_{rad}H_{rad}$, the quantities don't change much from the end of inflation to the beginning of the radiation era. This is a risky assumption as we have very little idea about what happens during the end of inflation. It is important to note though that this is only a lower bound on how long inflation can last so as long as aH does not reduce too much, the bound should still be valid. During the radiation-matter era the Hubble rate can be written as [47]:

$$H = \frac{H_{\rm eq}}{\sqrt{2}}\sqrt{\left(\frac{a_{eq}}{a}\right)^3 + \left(\frac{a_{\rm eq}}{a}\right)^4} \tag{3.5}$$

where the quantities are evaluated at matter-radiation equality. They can easily be expressed in terms of Ω_m and Ω_r as $a_{\rm eq} = a_0\Omega_r/\Omega_m$ and $H_{\rm eq}^2 = 2H_0^2\Omega_m(a_0/a_{\rm eq})^3$. Using these relations, equation (2.20) and taking the limit $a_{rad} << a_{\rm eq}$ one can show

$$e^N > \Omega_r^{1/4}\sqrt{\frac{H_{\rm rad}}{H_0}} > \left(\frac{\Omega_r \rho_{\rm rad}}{\rho_{0,\rm crit}}\right)^{\frac{1}{4}} = \frac{\rho_{\rm rad}^{\frac{1}{4}}}{0.037h\mathrm{eV}} \tag{3.6}$$

So $\rho_{\rm rad}$ is the energy density at the beginning of the radiation dominated era. We know from the nucleosynthesis that the energy density has to be greater than that at the beginning of neutron-proton conversion which is approximately $(1\mathrm{MeV})^4$. Therefore from this argument we can see that inflation must have lasted atleast 17 e-foldings. Alternatively if $\rho_{end} \approx M_{pl}^4$ then inflation must have lasted around 68 e-foldings [47].
The quantity $1/(aH)$ shrinks during inflation. We need it to shrink enough so that, eventually, the distance $1/(aH)$ covers a smooth patch. After inflation ends $1/(aH)$ will grow, enveloping larger and larger scale perturbations over time. The amount of inflation required is determined by the fact that, observable scales re-entering the horizon today are smooth too. In other words, the effect of inflation will be to "zoom in" on a small smooth patch. The horizon is given by equation (2.31) and as discussed in section 2.4.2 is much too small with just the usual radiation and matter eras. Let us assume that it is dominated by a period of inflation, such that the scale factor increases more or less exponentially, with $N = H_{end}(t_{end} - t_{start})$. It is easy to show that

$$d(t_L) = \frac{a(t_L)}{a_{end}H_{end}}\left(e^N - 1\right) \tag{3.7}$$

To solve the horizon problem we need $d(t_L) > d_A(t_L) > a(t_L)/(H_0 a_0)$. This yields exactly the same condition as before:

$$e^N > \frac{a_{end}H_{end}}{a_0 H_0} \tag{3.8}$$

3.2. A scalar field

It is therefore clear that to solve the three cosmological puzzles we need a period in the universe's history, before the radiation era, where the universe accelerates. This requires the universe to be dominated by a fluid with an equation of state satisfying $1 + 3w < 0$, or $p < -\rho/3$, a fluid with negative pressure. What fluids exhibit a negative pressure? We have already come across a fluid with $w < -\frac{1}{3}$ in the form of vacuum energy. With this case $T_{\mu\nu} = \rho g_{\mu\nu}$ with ρ constant. This clearly satisfies the acceleration condition already discussed with an exponentially growing scale factor $a(t) \propto e^{Ht}$. While it is simple and elegant if it could explain both inflation and dark energy, there needs to be a mechanism which "turns off" inflation and "re activates" it again in the present day.

A much more common way to generate these conditions is to invoke a scalar field ϕ called the inflaton. The simplest possibility is to have a universe where ϕ is the dominant source of $T_{\mu\nu}$. For all practical purposes the action is then

$$S = \int \left(\frac{M_{pl}^2}{2} R + \frac{1}{2} \partial_\mu \phi \partial^\mu \phi - V(\phi) \right) \sqrt{-g}\, \mathrm{d}^4 x \tag{3.9}$$

where $V(\phi)$ is an arbitrary potential in the sense that it essentially defines the inflationary model one is considering. This of course is not the only possibility but it is referred to as a minimally coupled. This ofcourse is not the only possibility. Many inflation models arise from possibly more fundamental theories such as string theory or supergravity [53–55]. From these theories one can postulate many different exotic generalisations of our simple model. Many of these theories naturally predict a large number of scalar fields and so multiple-field inflation has attracted a lot of attention in recent years [56–58]. Multiple field inflation models allow inflation to occur even if their fields individually do not meet the requirements. They also allow natural mechanisms for inflation to end Another possibility is an inflaton field having non-canonical kinetic terms. These type of models generally come with a sound speed $c_s \neq 1$ which can vary over the course of inflation [59–63]. Again, many of these types of models are string theory motivated where the non-canonical kinetic terms arise from brane dynamics. People have of course considered models combining both these concepts [64]. Effective Field Theory has been a valuable tool for theoretical physicists and has had much success in particle and condensed matter physics. It has been successfully applied to Inflation and in a sense unifies all possible single [65, 66] and multi [67] field models into a single framework. Inflation models can also arise from modified gravity [68] the Einstein-Hilbert action R is replaced by something more complicated. Many of these can be related back to scalar field models by a conformal transformation as one can see there a huge number of possibilities of modelling inflation so devising a way to systematically select out the best theories would be incredibly useful.

Continuing with the single, canonical scalar field case, the stress energy tensor takes the form (2.8) and one can easily read off the value for w.

$$w = \frac{p}{\rho} \rightarrow \frac{\frac{1}{2}\dot{\phi}^2 - V(\phi)}{\frac{1}{2}\dot{\phi}^2 + V(\phi)} \tag{3.10}$$

The last statement occurs, as when we take the homogeneous limit, the spacial derivatives disappear. With these identifications, its fairly obvious that a scalar field provides an easy way to get negative pressure. In fact, if the potential energy were to dominate over the kinetic term $w \rightarrow -1$. This system then obeys the following differential equations:

$$\begin{aligned} \ddot{\phi} + 3H\dot{\phi} + \frac{\mathrm{d}V}{\mathrm{d}\phi} &= 0 && (3.11) \\ 3M_{pl}^2 H^2 &= \frac{1}{2}\dot{\phi}^2 + V(\phi) && (3.12) \\ 3M_{pl}^2 \frac{\ddot{a}}{a} &= V(\phi) - \dot{\phi}^2 && (3.13) \end{aligned}$$

As before one of these equations can be derived from the other two. They can be arranged into various forms, for example one particularly useful equation is:

$$\dot{H} = -\frac{\dot{\phi}^2}{2M_{pl}^2} \tag{3.14}$$

Recalling that we can write the acceleration of expansion in terms of a slow roll parameter ϵ, we can see that $\epsilon = 0$ corresponds to the de-Sitter limit. This comes purely from the fact that ϵ is proportional to the derivative of H. This corresponds to the case when the potential energy of the scalar field dominates over its kinetic energy:

$$\dot{\phi}^2 \ll V(\phi) \tag{3.15}$$

In this limit, $w \rightarrow -1$ trivially. On the other hand, accelerated expansion needs to be sustained long enough, therefore the acceleration term cannot contribute too much either:

$$|\ddot{\phi}| \ll |3H\dot{\phi}|, |\frac{\mathrm{d}V}{\mathrm{d}\phi}| \tag{3.16}$$

This can be quantified by introducing another slow roll parameter

$$\eta = -\frac{\ddot{\phi}}{H\dot{\phi}} \tag{3.17}$$

When calculating results from inflationary models one often uses a "slow-roll" approximation, i.e. $\epsilon, |\eta| \ll 1$ as the calculations can become extremely complicated. Under this approximation the equations of motion become

$$\begin{aligned} 3H\dot{\phi} + \frac{\mathrm{d}V}{\mathrm{d}\phi} &= 0 && (3.18) \\ 3M_{pl}^2 H^2 &= V(\phi) && (3.19) \end{aligned}$$

We can also see in this limit

$$\begin{aligned} \epsilon &\approx \frac{M_{pl}^2}{2}\left(\frac{V'(\phi)}{V(\phi)}\right)^2 && (3.20) \\ \eta + \epsilon &\approx M_{pl}^2 \frac{V''(\phi)}{V(\phi)} && (3.21) \end{aligned}$$

And one can calculate how long inflation lasts via

$$N = \ln\frac{a_{end}}{a} = \int_t^{t_{end}} H\,\mathrm{d}t = \int_\phi^{\phi_{end}} \frac{H}{\dot{\phi}}\,\mathrm{d}\phi \approx \int_{\phi_{end}}^{\phi} \frac{V}{M_{pl}^2 V'(\phi)}\,\mathrm{d}\phi \tag{3.22}$$

We need this value to be atleast greater than about 60, the exact value will depend on the exact nature of how the inflationary phase ended, which is still relatively unknown. The slow-roll approximation though tells us that this last integral must be much greater than $|\phi - \phi_{end}|/(\sqrt{2}M_{pl})$. Therefore the slow-roll condition provides the required number of e-foldings if ϕ experiences changes on order of the Planck scale.

It is worth emphasising at this point that, just because ϕ is of order M_{pl}, this does *not* mean General Relativity is no longer an approximation and we need Quantum Gravity. For Quantum Gravity effects to be important $V(\phi) \approx M_{pl}^4$,(the potential energy is dominant in this case). This can easily be satisfied by just having arbitrarily small coupling constants. This does not invalidate the slow-roll approximation as for many cases in this limit, the parameters ϵ and η are independent of these values. This can easily be seen by considering a power law potential $V(\phi) = g\phi^\alpha$.

We can take an exponential potential as an example.

$$V(\phi) = ge^{-\lambda\phi} \tag{3.23}$$

One exact solution to the equations of motion can be deduced by the ansatz $\phi = a\ln(bt)$. This gives the following solution:

$$\begin{aligned} \phi(t) &= \frac{1}{\lambda}\ln\left(\frac{g\epsilon^2 t^2}{M_{pl}^2(3-\epsilon)}\right) \\ \epsilon &= \eta = \frac{M_{pl}^2}{2}\lambda^2 \\ a &\propto t^{1/\epsilon}. \end{aligned} \tag{3.24}$$

Therefore in this case, both slow roll conditions are satisfied if $\epsilon \ll 1$. This does not depend on the value of g or ϕ. It is also clear from this solution that if $\epsilon < 1$ the expansion accelerates and if $\epsilon > 1$ it decelerates.

3.3. The Power Spectrum

Inflation has two main successes. The first is solving the three cosmological puzzles already explained in section 2.4. This is solved essentially by construction in section 3.1. Inflation's second major success is linking the initial cosmological perturbations to microscopic quantum fluctuations of the the field ϕ.

3.3.1. ADM formalism and the Scalar Power Spectrum

Working in the ADM formalism [48, 69] the metric takes the form:

$$ds^2 = -N^2dt^2 + h_{ij}(dx^i + N^i dt)(dx^j + N^j dt) \tag{3.25}$$

and the action

$$\begin{aligned} S &= \frac{1}{2}\int\Bigg(NM_{pl}^2 R^{(3)} + \frac{M_{pl}^2}{N}(E_{ij}E^{ij} - E^2) \\ &\quad + N^{-1}(\dot{\phi} - N^i\partial_i\phi)^2 - Nh^{ij}\partial_i\phi\partial_j\phi - 2NV(\phi)\Bigg)\sqrt{h}\,\mathrm{d}^4x \end{aligned} \tag{3.26}$$

where

$$
\begin{aligned}
E_{ij} &= \frac{1}{2}(\dot{h}_{ij} - \nabla_i N_j - \nabla_j N_i) \\
E &= h^{ij} E_{ij} \\
h &= \det(h_{ij}) \\
R^{(3)} &= h^{ij} R^{(3)}_{ij}
\end{aligned}
\tag{3.27}
$$

Repeated $i, j, k...$ imply summation over 1,2,3. The system is then perturbed to second order around a homogeneous (in space) solution. So $\phi(t, \mathbf{x}) = \bar{\phi}(t) + \delta\phi(t, \mathbf{x})$ etc. So far a gauge has not been specified. Following [70] and focusing on scalar perturbations the gauge used here will be

$$
\delta\phi = 0, \qquad h_{ij} = a^2 e^{2\zeta} \delta_{ij}. \tag{3.28}
$$

The quantities E_{ij}, Γ^i_{jk} etc. can be calculated exactly in terms of the curvature perturbation ζ. Varying the action with respect to N and N^i, remembering ϕ is homogeneous, yields two equations:

$$
R^{(3)} - 2V - \frac{1}{N^2}(E_{ij}E^{ij} - E^2) - \frac{1}{N^2}\dot{\phi}^2 = 0, \tag{3.29}
$$

$$
\nabla_i \left(\frac{1}{N}(E^{ij} - E h^{ij}) \right) = 0. \tag{3.30}
$$

We are perturbing around an FRW metric. One can see by inspection that $N = 1, N^i = 0$ and $h_{ij} = a^2(t)\delta_{ij}$ correspond to the FRW metric. Indeed, plugging in these values trivially satisfies the second equation (as nothing depends on $\mathbf{x}$) and the first yields the Friedmann equation. In this case $R^{(3)}$ obviously vanishes and H enters through the $\dot{h}_{ij}$ dependence in E_{ij}.

The strategy then is to perturb these equations to 1st order, plug the solutions back into the action and expand the action up to 2nd order. One may be concerned that, in that case, we should really be expanding these equations up to second order for the perturbation expansion to be valid. This is unnecessary as the second order terms will necessarily be multiplied by 0th order terms which must vanish by the equations of motion [70].

So expanding both to 1st order, then taking the divergence of the second equation yields:

$$\begin{aligned}
N &= 1 + N_1 \\
N_i &= \partial_i \psi \\
N_1 &= \frac{\dot{\zeta}}{H} \\
\partial^2 \psi &= a^2 \epsilon \dot{\zeta} - \frac{\partial^2 \zeta}{H}
\end{aligned} \tag{3.31}$$

Many of the affine connections can be ignored at this order as they are order ζ so will only contribute to second order. We then insert these expression into the action and expand up to 2nd order. After some work, which is left to the appendix, one arrives at

$$S = M_{pl}^2 \int \mathrm{d}^4 x \, a\epsilon \left(a^2 \dot{\zeta}^2 - (\partial \zeta)^2 \right) \tag{3.32}$$

and we can see that the second order action is of order ϵ.

As discussed previously, ideally one would like top predict $\zeta(t, \mathbf{x})$ at every point in the universe. This is obviously completely intractable so we choose to make statistical predictions. To this end we model $\zeta(t, \mathbf{x})$ as a random field and aim to calculate $\langle \zeta(t, \mathbf{x}) \zeta(t, \mathbf{y}) \rangle$. $\langle \zeta(t, \mathbf{x}) \rangle$ is obviously zero as we are perturbing around a homogeneous background. These averages are technically ensemble averages over many different realisations of the universe. As we only have one universe to observe this could potentially be a problem however, under reasonable assumptions, the Ergodic Theorem [47] states that these are ensemble averages become the same as averages over position.

At this point it is useful to recall some basic facts about Gaussian random fields [12]. Any real random function $f(\mathbf{x})$ can be written as a Fourier transform.

$$f(\mathbf{x}) = \frac{1}{(2\pi)^3} \int f_{\mathbf{k}} e^{i\mathbf{k}.\mathbf{x}} \, \mathrm{d}^3 \mathbf{k} \tag{3.33}$$

The coefficients are complex $f_{\mathbf{k}} = a_{\mathbf{k}} + i b_{\mathbf{k}}$ but a reality condition imposes $a_{\mathbf{k}} = a_{-\mathbf{k}}$ and $b_{\mathbf{k}} = -b_{-\mathbf{k}}$. A Gaussian random field is then defined to be a random field where the coefficients $a_{\mathbf{k}}, b_{\mathbf{k}}$ are drawn from uncorrelated normal distribution. Because we need to randomly draw each Fourier mode this will necessarily involves functional integrals over $a_{\mathbf{k}}$ and $b_{\mathbf{k}}$. We can define the following quantity

$$Z[M] = C \int \mathcal{D}a_{\mathbf{k}} \mathcal{D}b_{\mathbf{k}} e^{-\frac{1}{2}\int d^3\mathbf{k} \int d^3\mathbf{k}' M(\mathbf{k},\mathbf{k}')(a_{\mathbf{k}}a_{\mathbf{k}'}+b_{\mathbf{k}}b_{\mathbf{k}'})} = \frac{1}{\det M} \tag{3.34}$$

where C is an arbitrary normalisation constant and $\det M$ is the functional determinant of the symmetric matrix $M(\mathbf{k}, \mathbf{k}')$, which is so far arbitrary. $\mathcal{D}a_{\mathbf{k}}$ represents an infinite product of integrals over $a_{\mathbf{k}}$, one for each Fourier mode $\mathbf{k}$. This represents a Gaussian distribution for the coefficients $a_{\mathbf{k}}$,$b_{\mathbf{k}}$ and at the moment they are not necessarily uncorrelated between the various Fourier modes. Gaussianity is not a statement about correlation. Functionally differentiating $Z[M]$ with respect to $M(\mathbf{k}, \mathbf{k}')$ produces the following expectation value.

$$\frac{-2}{Z[M]} \frac{\delta Z[M]}{\delta M(\mathbf{k}, \mathbf{k}')} = \langle a_{\mathbf{k}} a_{\mathbf{k}'} + b_{\mathbf{k}} b_{\mathbf{k}'} \rangle = 2M^{-1}(\mathbf{k}, \mathbf{k}') \tag{3.35}$$

$M^{-1}(\mathbf{k}, \mathbf{k}')$ is the inverse of the matrix $M(\mathbf{k}, \mathbf{k}')$. We are interested in the quantity $\langle f_{\mathbf{k}} f_{\mathbf{k}'} \rangle$

$$\begin{aligned} \langle f_{\mathbf{k}} f_{\mathbf{k}'} \rangle &= \langle a_{\mathbf{k}} a_{\mathbf{k}'} - b_{\mathbf{k}} b_{\mathbf{k}'} + i\left(a_{\mathbf{k}} b_{\mathbf{k}'} + b_{\mathbf{k}} a_{\mathbf{k}'}\right) \rangle \\ &= \langle a_{\mathbf{k}} a_{-\mathbf{k}'} + b_{\mathbf{k}} b_{-\mathbf{k}'} \rangle \\ &= 2M^{-1}\left(\mathbf{k}, -\mathbf{k}'\right) \end{aligned} \tag{3.36}$$

Choosing $M(\mathbf{k}, \mathbf{k}') \propto \delta^{(3)}(\mathbf{k} - \mathbf{k}')$ so the Fourier modes are uncorrelated produces our key result with a scale dependant variance σ_k^2

$$\langle f_{\mathbf{k}} f_{\mathbf{k}'} \rangle = (2\pi)^3 \delta^{(3)}\left(\mathbf{k} + \mathbf{k}'\right) \sigma_k^2 \tag{3.37}$$

Statistical isotropy is encoded by demanding σ_k^2 as opposed to $\sigma_{\mathbf{k}}^2$. Higher order statistical moments can be calculated by further functional differentiating with respect to $M(\mathbf{k}, \mathbf{k}')$. This produces Wick's theorem while odd statistical moments trivially vanish. The two-point correlation, defined as $\xi_f(|\mathbf{x} - \mathbf{y}|) = \langle f(\mathbf{x}) f(\mathbf{y}) \rangle$ is then

$$\xi_f(|\mathbf{x} - \mathbf{y}|) = \xi_f(r) = \int \frac{\sigma_k^2 k^3}{2\pi^2} \frac{\sin(kr)}{kr} \frac{\mathrm{d}k}{k} \tag{3.38}$$

The quantity σ_k^2 is the power spectrum while $\sigma_k^2 k^3/(2\pi^2)$ is the dimensionless power spectrum. On scales $1/k$ the dimensionless power spectrum represents the squared amplitude of the fluctuations. A scale invariant power spectrum means the two-point function must be invariant under $\mathbf{x} \to \lambda\mathbf{x}$ for $\lambda > 0$. This implies $\sigma_k^2 \propto k^{-3}$. Any even-point correlation function will expressed as sums of products of the two-point correlation function while any odd-point function will vanish. Therefore the power spectrum encodes all the statistics of the random function $f(\mathbf{x})$.

Returning to our second order action, equation (3.32), we wish quantize the curvature perturbation ζ and use the methods of quantum field theory to calculate the two-point correlation function. The most illuminating way to do this is to make the substitution $v = z\zeta$ with $z = M_{pl}a\sqrt{2\epsilon}$. Swapping to conformal time, defined as $a(t)\mathrm{d}\tau = \mathrm{d}t$, the action then takes the form of a scalar field with a time-dependant mass

$$S = \frac{1}{2}\int \left((v')^2 - (\partial v)^2 + \frac{z''}{z}v^2 \right) \mathrm{d}\tau \mathrm{d}^3\mathbf{x} \tag{3.39}$$

Varying this action with respect to v and performing a Fourier transform gives the Mukhanov-Sasaki equation [71, 72]

$$v_k'' + (k^2 - \frac{z''}{z})v_k = 0 \tag{3.40}$$

The function z''/z will be proportional to a^2H^2 multiplied by some long expression in slow roll parameters.

$$\frac{z''}{z} = a^2H^2(2 + 2\epsilon - 3\eta + 2\epsilon^2 + \eta^2 - 4\epsilon\eta + \xi) \tag{3.41}$$

η and ξ are related to the first and second derivative of ϵ. They will be defined more precisely but for now it sufficient to say they are of order ϵ and ϵ^2 respectively. As we know inflation ends when $\epsilon = 1$, unless the slow roll parameters behave extremely erratically, $z''/z \approx 2a^2H^2$. If we look at early enough times, $H \approx$ const and the scale factor will shrink exponentially. For each mode k, there will be some early enough time where the scale of the perturbation is deep within the horizon i.e $1/\lambda^2 \approx k^2 \gg z''/z$. In this limit v_k will behave like a simple harmonic oscillator. At the other extreme if $k \ll z''/z$ we can see v will grow rapidly. To be more precise, it is the ζ variable which becomes constant very quickly. For this case it is more convenient to work with the ζ variable. Then the Mukhanov-Sasaki equation is

$$\zeta_k'' + 2\frac{z'}{z}\zeta_k' + k^2\zeta_k = 0 \tag{3.42}$$

In the de Sitter limit, if k is very small, ζ_k' will decay like z^{-2} and so ζ_k will rapidly become a constant. With the v variable the sub horizon behaviour is more apparent while for super-horizon behaviour the ζ variable is better. It is more straightforward to quantize in the v variable as it is just a free scalar field with a time-dependant mass and its early time behaviour is simpler. We quantise in the usual way by promoting v to an operator and writing it as a Fourier transform.

$$v(\tau, \mathbf{x}) = \int \frac{\mathrm{d}^3\mathbf{k}}{(2\pi)^3}\left[v_{k,cl}(\tau)\hat{a}_{\mathbf{k}}e^{i\mathbf{k.x}} + v^*_{k,cl}(\tau)\hat{a}^\dagger_{\mathbf{k}}e^{-i\mathbf{k.x}}\right] \tag{3.43}$$

If we were just dealing with a free scalar field, the functions $v_{k,cl}(\tau)$ would simply be the solutions of $v_k'' + \omega_k v_k = 0$ i.e $v_k(\tau) = e^{-i\omega_k\tau}$ with $\omega_k = \sqrt{k^2+m^2}$. So our quantum field is a sum of the classical solutions of the equations of motion. The only difference is that now our field is a collection of simple harmonic oscillators with time-dependant masses so in the expansion above, the functions $v_k(\tau)$ are the classical solutions of the equation of motion, equation (3.40).
The annihilation and creation operators a, $a^\dagger$ will again satisfy the usual commutation relations

$$\left[\hat{a}_{\mathbf{k}}, \hat{a}^\dagger_{\mathbf{k}'}\right] = (2\pi)^3\delta^{(3)}(\mathbf{k}-\mathbf{k}') \tag{3.44}$$

If we use this to calculate $[\hat{x}, \hat{p}] = i$ we obtain:

$$\left[v(\tau,\mathbf{x}), v'(\tau,\mathbf{y})\right] = \int \frac{\mathrm{d}^3\mathbf{k}}{(2\pi)^3}\left(v_k v_k'^\star - v_k' v_k^\star\right)e^{i\mathbf{k}\cdot(\mathbf{x}-\mathbf{y})} = i\delta^{(3)}(\mathbf{x}-\mathbf{y}) \tag{3.45}$$

The only difference here is the factor $i(v_k^\star v_k' - v_k'^\star v_k)$ which we can set to 1 [52]. The *cl* subscripts and τ dependence have been dropped to simplify the notation. This fixes one of the boundary conditions of the Mukhanov-Sasaki equation.

We have already seen that in the limit $k \gg aH$, the classical solutions behave like simple harmonic oscillators. We can therefore choose the standard

Minkowski vacuum for comoving observers in the far past because all the modes deep within the horizon at a given time are effectively in flat space. To this end we define the vacuum state $\hat{a}_{\mathbf{k}}|0\rangle = 0$ in the usual way and then calculate the Hamiltonian density acting on the ground state [52]:

$$\begin{aligned} H|0\rangle = \int \frac{\mathrm{d}^3\mathbf{k}}{(2\pi)^3} \Big[& \left(v_k'^2 + k^2 v_k^2\right)^\star \hat{a}^\dagger_{\mathbf{k}} \hat{a}^\dagger_{-\mathbf{k}} \\ & + (2\pi)^3 \delta^{(3)}(0) \left(|v_k|^2 + k^2 |v_k|^2\right) \Big] |0\rangle \end{aligned} \tag{3.46}$$

If we require the ground state to be an eigenstate of the Hamiltonian the first term must vanish. For modes deep inside the horizon this gives

$$v_k' = \pm i k v_k \tag{3.47}$$

Therefore we specify the initial conditions by demanding that $v(\tau, \mathbf{x})$ is a free quantum scalar field, satisfying the usual commutation relations and require the ground state to be an eigenstate of the Hamiltonian at very early times. Combining these equations picks out the minus sign and gives the following Bunch-Davies initial conditions [73]

$$\lim_{\tau \to -\infty} v_{k,cl} = \frac{e^{-ik\tau}}{\sqrt{2k}}. \tag{3.48}$$

This completely fixes all the classical solutions v_k. We can then compute the power spectrum using the basic methods of quantum field theory.

$$\langle 0 | v(\tau, \mathbf{x}) v(\tau, \mathbf{y}) | 0 \rangle = \int \frac{|v_k(\tau)|^2 k^3}{2\pi^2} \frac{\sin(kr)}{kr} \frac{\mathrm{d}k}{k} \tag{3.49}$$

We can therefore identify $\sigma_k^2 = |v_{k,cl}(\tau)|^2$. If we know the exact analytic solution for equation (3.40) the power spectrum is then

$$\langle \zeta_k(\tau) \zeta_{k'}(\tau) \rangle = (2\pi)^3 \delta^{(3)}(\mathbf{k} + \mathbf{k}') \frac{|v_k(\tau)|^2}{2a^2 \epsilon} = (2\pi)^3 \delta^{(3)}(\mathbf{k} + \mathbf{k}') |\zeta_{k,cl}(\tau)|^2 \tag{3.50}$$

The time that the classical solution is evaluated at is such that the mode is well outside the horizon, $k \ll aH$. But because the mode perturbations freeze out so quickly, one can effectively evaluate this at horizon crossing. This freeze out is important as it means the spectrum of perturbations will be conserved until each mode re-enters the horizon in the radiation era, regardless of the physics of reheating [47, 70, 74, 75].

Only one analytic solution for $\zeta_k(\tau)$ exists and that is when the slow-roll parameters are constant. However one can use this as an approximation for more general potentials. In reality the slow-roll parameters are only ever constant when $\eta = \epsilon$, $\xi = \epsilon^2$ but we can neglect this small change under most circumstances. $\zeta_k(\tau)$ then becomes a Hankel function:

$$\zeta_k(\tau) = \frac{H}{2M_{pl}}\sqrt{\frac{\pi}{2}}\frac{(1-\epsilon)}{\sqrt{\epsilon k^3}}(-k\tau)^{\frac{3}{2}}H_\nu^{(1)}(-k\tau)e^{i\frac{\pi}{2}(\nu+\frac{1}{2})} \tag{3.51}$$

$H_\nu^{(1)}(x)$ has the following limits:

$$\lim_{x\to\infty} H_\nu^{(1)}(x) \;\;\rightarrow\;\; \sqrt{\frac{2}{\pi x}}\exp\left(i\left(x - \frac{\nu\pi}{2} - \frac{\pi}{4}\right)\right) \tag{3.52}$$

$$\lim_{x\to 0} H_\nu^{(1)}(x) \;\;\rightarrow\;\; -\frac{i}{\pi}\Gamma(\nu)\left(\frac{x}{2}\right)^{-\nu}. \tag{3.53}$$

The first limit picks out the solution and normalisation of ζ when we impose Bunch-Davies initial conditions. Using the second limit and the slow-roll approximation one can calculate the power-spectrum as series in slow roll parameters [76].

$$P_\zeta(k) = (1 + (2 - \ln 2 - \gamma)(2\epsilon + \eta) - \epsilon)^2\,\frac{H^2}{4M_{pl}^2 k^3\epsilon} \tag{3.54}$$

Here γ is the Euler-Mascheroni constant. This is the dimension*ful* power-spectrum. The dimension*less* power spectrum is defined as

$$\Delta_\zeta(k) = \frac{P_\zeta(k)k^3}{2\pi^2} \tag{3.55}$$

In the slow roll approximation the power spectrum is approximately given by a power law and can be parametrized by

$$\Delta_\zeta(k) \propto k^{n_s-1} \tag{3.56}$$

Alternatively we can define a parameter called the "tilt" of the power spectrum as

$$n_s(k_\star) = 1 + \left.\frac{\mathrm{d}\ln P_\zeta(k)}{\mathrm{d}\ln k}\right|_{k=k_\star}, \tag{3.57}$$

where $k_\star$ is a pivot scale usually taken to be $k = 0.05$ Mpc^{-1}. This quantity

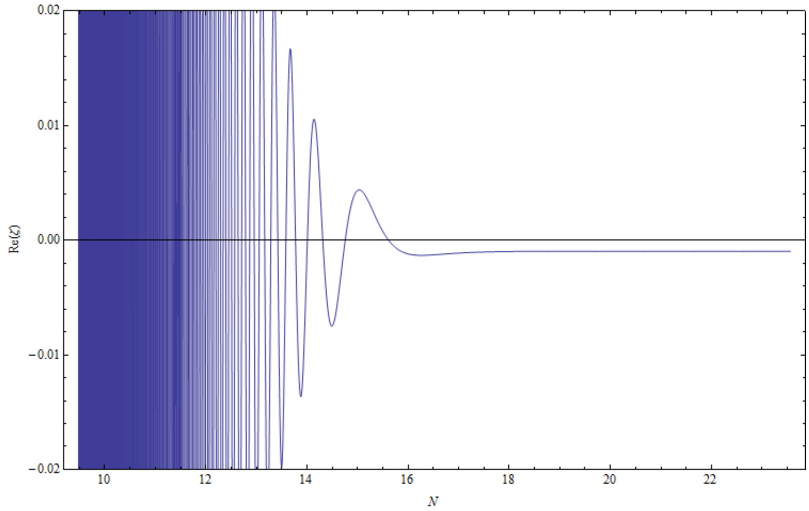

Figure 3.1.: A typical solution to equation (3.40) with some arbitrary normalisation. The imaginary part of ζ behaves in a similar fashion. The freeze-out time N is roughly proportional to $\ln(k)$ assuming H is roughly constant. For typical inflationary backgrounds the functional form of ζ doesn't change much.

can be calculated as a series in slow-roll parameters, for example [76]

$$n_s \approx 1 - 4\,\epsilon + 2\,\eta - 2\,(1+C)\,\epsilon^2 - \frac{1}{2}(3-5C)\,\epsilon\,\eta + \frac{1}{2}(3-C)\,\xi \qquad (3.58)$$

$C = 4(\ln 2 + \gamma) - 5 \approx 0.08$. What is important is that in the slow-roll limit the power spectrum becomes nearly scale-invariant. The observational bounds on n_s are currently $n_s = 0.968 \pm 0.012$. This is another justification for assuming the slow-roll parameters to be small.

3.3.2. Tensor Power Spectrum

Inflation also produces a small amount of gravitational waves proportional to the slow-roll parameter ϵ. As tensor perturbations are not the main focus of this thesis we summarize the calculation below, emphasizing where the normalisation differences come from [70, 76]. The calculation is proceeds in much the same way but we can ignore scalar perturbations and choose the following gauge:

$$h_{ij} \quad = \quad a^2\left(\delta_{ij} + 2\gamma_{ij}\right). \tag{3.59}$$

The second order action becomes

$$S_2 = \frac{M_{pl}^2}{8}\int \mathrm{d}\tau \mathrm{d}^3\mathbf{x}\; a^2\left(\gamma'_{ij}\gamma'_{ij} - \partial_k\gamma_{ij}\partial_k\gamma_{ij}\right) \tag{3.60}$$

We decompose the gravitational waves as

$$\gamma_{ij} = \sum_{\lambda=1}^{2}\int \frac{\mathrm{d}^3\mathbf{k}}{(2\pi)^{\frac{3}{2}}} h_{\mathbf{k},\lambda}(\tau)e_{ij}(\mathbf{k},\lambda)e^{i\mathbf{k}\cdot\mathbf{x}} \tag{3.61}$$

and the polarisation tensor satisfies

$$e_{ij} = e_{ji}, \qquad e_{ii} = 0, \qquad k_i e_{ij} = 0, \tag{3.62}$$

$$e_{ij}(\mathbf{k},\lambda)e^{\star}_{ij}(\mathbf{k},\rho) = \delta_{\lambda\rho}, \tag{3.63}$$

$$e_{ij}(-\mathbf{k},\lambda) = e^{\star}_{ij}(\mathbf{k},\lambda). \tag{3.64}$$

We also make the change of variables $2v_{\mathbf{k},\lambda} = M_{pl}ah_{\mathbf{k},\lambda}$ so it looks like a familiar scalar field. With this substitution the second order action becomes

$$S_2 = \frac{1}{2}\int \mathrm{d}\tau \mathrm{d}^3\mathbf{k}\;\left(|u'_{\mathbf{k},\lambda}|^2 - \left(k^2 - \frac{a''}{a}\right)|u_{\mathbf{k},\lambda}|^2\right) \tag{3.65}$$

Now $u_{\mathbf{k},\lambda} = u^{\star}_{-\mathbf{k},\lambda}$ from our polarisation conditions and requiring γ_{ij} to be real. We quantise in the same way as before

$$\hat{u}_{\mathbf{k},\lambda}(\tau) = u_k(\tau)\hat{a}_{\mathbf{k},\lambda} + u^{\star}_k(\tau)\hat{a}^{\dagger}_{-\mathbf{k},\lambda} \tag{3.66}$$

$u_k(\tau)$ satisfies a similar Mukhanov equation with identical Bunch-Davies conditions

$$u''_k + \left(k^2 - \frac{a''}{a}\right)u_k = 0 \tag{3.67}$$

producing a similar solution. u_k is now normalised with an extra factor of $1/2$ relative to v_k for the scalar case as the action was originally proportional to $M_{pl}^2/8$. When calculating the contribution to the power spectrum this becomes a factor of 4. In addition each polarisation λ contributes to the total tensor power in an identical way giving an extra factor of 2 for a total of 8. The tensor-to-scalar ratio is thus [76]

$$r = \frac{P_h}{P_\zeta} = 8\frac{|h_{\mathbf{k},\lambda}|^2}{|\zeta_k|^2} \approx 16\,\epsilon\,\left[1 + \frac{1}{2}(C-3)(\epsilon - \eta)\right] \tag{3.68}$$

We now have good analytical approximations for some key inflation results. The current Planck constraints on these observations are $n_s = 0.968 \pm 0.006$ and $r < 0.11$ [18]. To first order this gives two linear equations $r = 16\epsilon$ and $n_s = 1 - 4\epsilon + 2\eta$ which we can solve for ϵ, η which in turn will give us information about the inflation potential. Unfortunately no gravitational waves have been detected yet so we can only use the equation for r to put limits ϵ.

3.4. Formalising slow-roll

The first part of the calculation involves integrating essentially the Friedmann equations numerically to obtain the background solutions. However, the formalism behind the equations needs some explanation, in particular the definitions and relations between the slow roll parameters need to be more precise. What will now be discussed is called the "Hamilton-Jacobi" formulation [77–79].

We start be re-writing the Friedmann equations into an equivalent form

$$\begin{aligned} \dot{\phi} &= -2M_{pl}^2 H'(\phi) \\ 3M_{pl}^2 H(\phi)^2 &= 2M_{pl}^4 \left[H'(\phi)\right]^2 + V(\phi). \end{aligned} \tag{3.69}$$

All the variables are now functions of ϕ and primes denote derivatives with respect to ϕ. Obviously when solving the Friedmann equations each potential $V(\phi)$ along with a set of initial conditions $(\phi(t_0), \dot{\phi}(t_0))$ will specify a unique evolution of the background $H(t), \phi(t)$. Writing the Friedmann equations this way means that its easy to do the reverse. That is, specifying a background function $H(\phi)$ trivially produces the corresponding potential $V(\phi)$ which is what we wish to constrain when comparing to observations. For example if $H(\phi)$ is linear, this will correspond to a quadratic potential. The usual conditions for $\ddot{a} > 0$ can be derived as usual like before this means that a slow-roll parameter $\epsilon_H < 1$ which is defined as

$$\epsilon_H = 2M_{pl}^2 \left(\frac{H'(\phi)}{H(\phi)}\right)^2 \tag{3.70}$$

The subscript H indicates that this is a *Hubble Slow Roll* (HSR) parameter as opposed to the *Potential Slow Roll* (PSR) [78] parameter defined as

$$\epsilon_V = \frac{M_{pl}^2}{2} \left(\frac{V'(\phi)}{V(\phi)}\right)^2 \tag{3.71}$$

The two are only equivalent in the slow roll limit and importantly, inflation ends when $\epsilon_H = 1$ or $\epsilon_V \approx 1$. One can find a simple relation between the two.

$$\epsilon_V = \epsilon \left(\frac{3-\eta}{3-\epsilon}\right)^2 \tag{3.72}$$

η is defined as

$$\eta = 2M^2 \frac{H''(\phi)}{H(\phi)}. \tag{3.73}$$

We have dropped the subscript H as these will be the parameters we will be from now on. It is easy to see that $\epsilon = -\dot{H}/H^2$ by the chain rule. Therefore we can already see that the HSR parameter will be a more convenient quantity to work with numerically. We can then define an infinite hierarchy of slow roll parameters [78]:

$$\begin{aligned} \epsilon &= 2M_{pl}^2 \left(\frac{H'(\phi)}{H(\phi)}\right)^2 && (3.74) \\ {}^l\lambda &= \left(2M_{pl}^2\right)^l \frac{(H')^{l-1}}{H^l} \frac{d^{(l+1)}H}{d\phi^{(l+1)}} && (3.75) \end{aligned}$$

We will also define $\eta = {}^1\lambda$ and $\xi = {}^2\lambda$ and for consistency one can take $1 = {}^0\lambda$ and $\epsilon^{-1} = {}^{-1}\lambda$. One can easily check that $\eta = -\ddot{\phi}/(H\dot{\phi})$.

Now our slow-roll hierarchy is defined it becomes convenient to use $e-$foldings N as our time variable. We know inflation lasts atleast roughly 60 $e-$folds at it is dimensionless so is more natural numerically. Recall it is effectively defined as $a(N) = a_0 e^N$. So

$$\frac{\mathrm{d}N}{\mathrm{d}t} = H \tag{3.76}$$

In the literature it is sometimes defined with a minus sign calculating backwards from the end of inflation. We define it this way as it is conceptually simpler to have it increasing with time. However as all our variables are now functions of ϕ we use the chain rule and the equations of motion to get

$$\frac{\mathrm{d}\phi}{\mathrm{d}N} = -M_{pl}\sqrt{2\epsilon} \tag{3.77}$$

With this relation there is a sign choice when substituting for $\sqrt{\epsilon}$ relating to which direction ϕ rolls down its potential. With this last ingredient the slow-roll parameters then satisfy an infinite set of differential equations:

$$\begin{aligned}
\frac{\mathrm{d}H}{\mathrm{d}N} &= -\epsilon H && (3.78)\\
\frac{\mathrm{d}\epsilon}{\mathrm{d}N} &= 2\epsilon(\epsilon - \eta) && (3.79)\\
\frac{\mathrm{d}\,{}^{l}\lambda}{\mathrm{d}N} &= [l\epsilon - (l-1)\eta]\,{}^{l}\lambda - {}^{l+1}\lambda && (3.80)
\end{aligned}$$

These differential equations, with a set of initial conditions, will define a trajectory in slow-roll parameter space. No slow roll approximation has been made so far so this system is an infinite set of differential equations. These equations could alternatively be taken to be the definition of ${}^{l}\lambda$.

3.4.1. Correspondence with a potential and some analytical solutions

The slow-roll hierarchy defined above, the set of differential equations and some initial conditions will completely define an inflationary model.

From this perspective the parameters that define an inflationary model will be the initial conditions of the slow-roll parameters and H. Therefore there will be a mapping between $H(N=0), \epsilon(N=0), \eta(N=0)$... and the potential function $V(\phi)$. This is best illustrated with some examples.

Exponential Potential

We can first solve equation (3.69) analytically. Unfortunately the non-linear nature of equation (3.69) makes it difficult to solve for general $V(\phi)$. The easiest case is the exponential potential $V(\phi) = \Lambda e^{g\phi}$ with the solution

$$\begin{aligned}
H(\phi) &= \sqrt{\frac{2\Lambda}{M_{pl}^2(6 - M_{pl}^2 g^2)}} e^{-g\phi/2} \\
\epsilon &= \frac{M_{pl}^2}{2} g^2 \\
{}^l\lambda &= \epsilon^l \\
\phi(t) &= -\frac{1}{g} \ln\left(\frac{\Lambda\epsilon^2 (t - t_0)^2}{(3-\epsilon)M_{pl}^2}\right) \\
\phi(N) &= -M_{pl}\sqrt{2\epsilon}(N - N_0)
\end{aligned} \tag{3.81}$$

for some arbitrary constants t_0, N_0. This is the only solution where ϵ is a constant and our Hankel function solutions for the power spectrum apply exactly. For the case $\epsilon = 3$, $V(\phi) = 0$ for all t which is the kinetic dominating limit, the opposite limit of interest for inflation. Assuming $g > 0$ we choose $\dot{\phi}$ to be negative so in the inflaton rolls down the potential.

Quadratic Potentials

We know the exponential potential solution cannot be real (atleast exactly) because ϵ is constant so inflation would never end. We are therefore interested in finding solutions where the slow-roll parameters are dynamical variables. The simplest case is then to set ${}^l\lambda = 0$ for $l > 0$ leaving the simple equation

$$\frac{\mathrm{d}\epsilon}{\mathrm{d}N} = 2\epsilon^2 \tag{3.82}$$

with the solution

$$\epsilon(N) = \frac{\epsilon_0}{1 - 2\epsilon_0 N}. \tag{3.83}$$

$\epsilon_0 = \epsilon(N = 0)$. Setting $\epsilon(N_f) = 1$ where $N_f > 60$ is the $e-$folds gives a rough limit of $\epsilon < 1/121 \approx 0.008$. From the definition of ϵ we can immediately write down $H(\phi) = \alpha\phi + \beta$ and map α, β to some initial conditions which will produce a quadratic potential

$$V(\phi) = M_{pl}^2 H_0^2 \left[3 - \epsilon_0 + 3\sqrt{2\epsilon_0}\left(\frac{\phi - \phi_0}{M_{pl}}\right) + \frac{\epsilon_0}{2}\left(\frac{\phi - \phi_0}{M_{pl}}\right)^2\right] \tag{3.84}$$

$\phi_0 = \phi(N = 0)$. This simple model shows how choosing initial conditions on the slow-roll parameters maps to some potential $V(\phi)$ when solving equations (3.69). Note while we can choose ϕ_0 so that either the constant or the linear term disappears (and the background evolution remains unchanged), we can't choose to model a pure $m^2\phi^2$ in this manner. We can use the first order relations for n_s and r to conclude that it will be very difficult for this simple model to be valid as the tensor power spectrum it produces is too strong.

Quartic Potentials

We can also obtain some analytic results for quartic potentials. In a similar manner we truncate the slow-roll parameter hierarchy so that the only non-vanishing parameters are $\epsilon(N), \eta(N)$. Our equations become

$$\frac{\mathrm{d}\epsilon}{\mathrm{d}N} = 2\epsilon(\epsilon - \eta) \tag{3.85}$$

$$\frac{\mathrm{d}\eta}{\mathrm{d}N} = \epsilon\eta \tag{3.86}$$

These two equations become the linear differential equation

$$\frac{\mathrm{d}\epsilon}{\mathrm{d}\eta} = 2\frac{\epsilon}{\eta} - 2 \tag{3.87}$$

which has the family of solutions

$$\epsilon(\eta) = 2\eta + \alpha\eta^2 \tag{3.88}$$

where α is an integration constant. We can use our initial condition on ϕ to choose $H(\phi) = a\phi^2 + c$. Using the definitions of our slow-roll parameters as derivatives with respect to ϕ the potential is then

$$\begin{aligned} V(\phi) &= \Lambda + \frac{m^2}{2}\phi^2 + \frac{\lambda}{4!}\phi^4 \\ \Lambda &= 3M_{pl}^2 H_0^2 (1 + \alpha\eta_0)^2 \\ m^2 &= -H_0^2\eta_0 \left(3 + (3\alpha + 1)\eta_0\right) \\ \lambda &= \frac{9H_0^2\eta_0^2}{2M_{pl}^2}. \end{aligned} \tag{3.89}$$

In this case the simple relation $H(N)\eta(N) = H_0\eta_0$ is quite helpful. The 0 subscript indicates the initial conditions evaluated at any desired time. The time dependence of η, and hence all other quantities can be solved exactly, although solving for $\eta(N)$ produces an non-invertible function.

$$\eta = \frac{2\eta_0}{(2+\alpha\eta_0)e^{-\eta_0 H_0(t-t_0)} - \alpha\eta_0} \tag{3.90}$$

Looking at the early/late time limits when $t \to \infty$, $\eta \to -2/\alpha$ and when $t \to -\infty$ $\eta \to 0$. In both cases $\epsilon \to 0$. Therefore for inflation to end in this model we need ϵ to have some maximum value $\epsilon_{\max} > 1$. One easily arrives at $\epsilon_{\max} = -1/\alpha$ telling us that if this model can support enough $e-$folds by itself, $-1 > \alpha$. Demanding $\epsilon > 0$ therefore fixes $\eta > 0$.

At this point one could easily do a more complex analysis looking at the precise dependence of the solutions on α and η_0. However our slow-roll formulae are only valid when ϵ,η are very small. Deviating from this assumption would require us to solve the power spectrum numerically anyway so there is little value in pursuing this avenue here.

With this in mind we assume the scales observable today exit the horizon at a time where we can neglect the non-linear term and assume $\epsilon \approx 2\eta$. Using the first order results for n_s to fix η gives $r \approx 0.17$. Therefore assuming the result doesn't drastically change when varying α and η_0 it is safe to say that this model is ruled out too.

Other Potentials

Finally we consider a potential which has an infinite number of slow-roll parameters, but unlike the exponential potential, they are all dynamic. We look for solutions of the form ${}^l\lambda = a_l\epsilon^l$. Plugging this expression into equations (3.69) gives the following recursion relation

$$a_{l+1} = a_l\left(\alpha(l+1) - l\right) \tag{3.91}$$

with $\alpha = a_1$ and ϵ has the time dependence.

$$\epsilon = \frac{\epsilon_0}{1 - 2(1-\alpha)\epsilon_0 N}. \tag{3.92}$$

$\alpha = 0$ gives our earlier simple quadratic potential. $\alpha = 1$ gives the exponential potential.

Using $\epsilon = \alpha\eta$ and their definitions as derivatives with respect to ϕ gives a simple differential equation for $H(\phi)$. Solving this gives the following potential for real $\alpha \neq 1$

$$V(\phi) = 3M_{pl}^2 H_0^2 \epsilon_0 \left(\frac{3}{\epsilon_0}x^2 - 1\right) x^{\frac{2\alpha}{(1-\alpha)}} \tag{3.93}$$

$$x = (1-\alpha)\sqrt{\frac{\epsilon_0}{2}}\frac{\phi}{M_{pl}} \tag{3.94}$$

Again using the first order results for n_s and r as well as $\eta = \alpha\epsilon$ gives the constraint $\alpha < -0.33$.

It is clear then that specifying the initial conditions for the slow roll parameters and H is enough to completely determine the inflation model we are working with, sometimes referred to as a *trajectory.* The advantage of this method is then very apparent when modelling large numbers of potentials. To model a specific potential it is simpler to work with equations (3.11). However, if one is considering many potentials, one will have to modify equations (3.11) for every potential. With the Hamilton-Jacobi formalism, one merely needs to specify many initial conditions. It also easy to deduce which trajectories are physically viable as inflation ends when $\epsilon = 1$ and it must last for atleast 60 $e-$foldings. Many quantities of interest are also easily expressed as functions of the slow roll parameters such as z in the Mukhanov equation.

The first aim of the project then is to generate large numbers of trajectories (or potentials) by randomly selecting the initial conditions. The slow-roll parameters as a function of N are then solved exactly. Any trajectory for which inflation lasts atleast 60 e-foldings but still ends ($\epsilon \to 1$) are stored for further calculation. Any others are discarded. For example trajectories where the slow-roll parameters shrink to zero are eliminated as inflation will never end.

Technically we must include the whole infinite hierarchy of slow-roll parameters. This obviously cannot be done numerically but if we truncate the hierarchy at a finite order L, the generated solutions will still be exact but will only cover a subset of the total number of solutions. One might wonder how one might take into account exponential-like potentials, which require an infinite series. We know for inflation to occur though that $\epsilon < 1$ and since ${}^l\lambda = \epsilon^l$ we know this will be a good enough approximation for high enough L. Of course a pure exponential potential is ruled out anyway as inflation will never end as the slow-roll parameters remain constant.

3.4.2. Anisotropies from the Primordial Power Spectrum

Ultimately we are concerned with predicting statistical properties of the universe and in particular, the CMB. Experiments such as WMAP [80–85] and more recently PLANCK [6,13,14] have mapped the CMB temperature variations with astonishing detail.

We can expand the temperature variations $\Theta(\theta, \phi) = \delta T(\theta, \phi)/T_{\mathrm{CMB}}$ in terms of spherical harmonics $Y_{lm}(\theta, \phi)$, defining the complex coefficients a_{lm} [12,52,86]

$$\Theta(\theta, \phi) = \sum_{l=0}^{l=\infty} \sum_{m=-l}^{m=l} a_{lm} Y_{lm}(\theta, \phi). \tag{3.95}$$

Averaged over position, in an isotropic and homogeneous universe the variance of a_{lm} takes on the simple form

$$\langle a_{lm} a^{\star}_{l'm'} \rangle = C_l \delta_{ll'} \delta_{mm'}. \tag{3.96}$$

The quantity C_l is called the angular power spectrum and is a clear analogue to the primordial power spectrum $P_\zeta(k)$ calculated earlier. We would expect in the realm of linear perturbation theory that $\Theta \sim \zeta$ so any variations in temperature are ultimately sourced from the curvature perturbation. It follows that C_l should be a linear functional of $P_\zeta(k)$

$$C_l = \frac{2}{\pi} \int_0^\infty k^2 P_\zeta(k) \Delta^2_{Tl}(k) \, \mathrm{d}k. \tag{3.97}$$

This defines the transfer function $\Delta^2_{Tl}(k)$ [86]. It is a complicated function which takes into account projecting the perturbations as a function of 3 dimensional space onto the two dimensional surface of a sphere. This necessarily involves integrating out the radial component and requires evolving the initial perturbations over the history of the universe by solving the linearised Einstein-Boltzmann equations. Needless to say, calculating $\Delta^2_{Tl}(k)$ in detail would take half a textbook [12, 47, 86] and most of the time it is calculated numerically using programs like CMBFAST [87, 88] and CAMB [89, 90].

When comparing the CMB to theoretical predictions $P_\zeta(k)$ is often parametrised in the form $A_s k^{n_s-4}$ and the recent PLANCK results [17, 18] confirm that this form is in excellent agreement the observations. In summary inflation predicts the function $P_\zeta(k)$ from the initial quantum fluctuations ζ, the rest of the ΛCDM model produces the function $\Delta^2_{Tl}(k)$ which depends on cosmological parameters such as H_0, Ω_i etc. and the theoretical prediction for the angular power spectrum is given by equation (3.97).

Of course to arrive at this prediction we initial expanded the Einstein-Hilbert action, equation (3.26), to second order. Because there is no reason why all the higher order contributions should vanish this generates small deviations from Gaussianity in the primordial curvature perturbation. This leads us into non-Gaussianity, a major prediction of inflation and a subject of great theoretical interest in recent years.

4. What is non-Gaussianity?

In the previous chapter it was shown how to computer the power spectrum, or scale dependant variance, for the fluctuations of the scalar perturbations in inflation. These perturbations become the seeds for the initial perturbations in the radiation era, for which, the rest of Cosmology is well explained by the Λ-CDM model. The fluctuations are, to a high degree of accuracy, Gaussian fluctuations. Over the next few years though, *non-Gaussianity* will become a crucial tool to help us understand two important areas of cosmology and astrophysics [91]:

- The physics of inflation and how it created the primordial perturbations of the universe at early times, leading to large-scale structure formation
- How gravitational instability and gas physics leads to the growth of these structures at late times

We will be focusing on how non-Gaussianity can help to probe the physics of inflation. Non-Gaussianity, is simply the deviations from a pure Gaussian distribution. A pure Gaussian distribution implies that all of the statistical information is encoded in its variance, the two-point correlation function, and all odd correlation functions must vanish. Therefore, for a non-Gaussian distribution, there will be some contribution to higher order correlation functions other than the variance, or the odd - correlation functions will be non-vanishing.

For inflation this is best understood in terms of quantum fields, as this is how we derived the power spectrum. If we have a non-interacting quantum field, its action is quadratic and we can calculate its two-point function exactly which is obviously just the propagator. Because its action is quadratic this is equivalent to a Gaussian probability distribution. If we wish to calculate higher order correlation functions we know, because there are no interactions, all odd-functions vanish while all even functions are various

combinations of the propagator, in line with summing up Feynman diagrams. We know though from section 8.9, that to second order in scalar perturbations, ζ is equivalent to a free quantum field with a time dependant mass. So to lowest order we expect the scalar fluctuations to be Gaussian as there are no interaction terms.
It is clear then that if there are interaction terms in the action for the scalar perturbations, these will induce non-Gaussianity. For example, if there is a ζ^3 term, this will provide a 3-point vertex and hence a non-vanishing 3-point function. Furthermore, if we expand the action up to third order, as we should if we desire a more accurate calculation, this will necessarily induce interaction terms. Therefore we *expect* deviations from a Gaussian distribution simply because we have no reason to suspect all higher order terms in the perturbation expansion to magically vanish after second order.

4.1. A probe of inflationary models

We expect inflation to leave residual non-Gaussian corrections to the temperature and density distributions. How is this is a useful probe on inflationary physics? The answer is in two parts.

The first reason is, as outlined in Section 3.3, the power spectrum is largely independent of the inflationary model. There exists a huge degeneracy between the observed power spectrum and the inflationary models which predict it. We arrived at the second order action assuming very little about the inflaton field. When expanding the action to third order we start including more terms from the same model using the same parameters, for example the slow-roll parameters which are ultimately related to the inflaton potential. So far the scalar and tensor power spectrum constrains two of these parameters so observations of higher order moments will provide more measurements to constrain more parameters.

The second reason is simply because the 3-point function, or bispectrum, as a third-order moment provides a much more information than the power spectrum. The power spectrum is a function of two momenta $\mathbf{k}$ and $\mathbf{k}'$. Because of homogeneity or momentum conservation, a Dirac delta function enforces the condition $\mathbf{k} + \mathbf{k}' = 0$. So the power spectrum is immediately reduced to a function of a single vector $\mathbf{k}$. Isotropy removes any preference in direction and so the power spectrum is a function of just a single number

k.

Equivalently consider the 3-point function as a function of three momenta $\mathbf{k}_1, \mathbf{k}_2$ and $\mathbf{k}_3$. Statistical isotropy means we expect the bispectrum to be a scalar under rotations. There are only 6 rotational invariants we can form: k_1^2, k_2^2, k_3^2, $\mathbf{k}_1 \cdot \mathbf{k}_2$, $\mathbf{k}_1 \cdot \mathbf{k}_3$ and $\mathbf{k}_2 \cdot \mathbf{k}_3$ so the bispectrum must be a function of these 6 numbers. Homogeneity implies that the three vectors must form a closed triangle due to momentum conservation, fixing the vector $\mathbf{k}_3$ and reducing the bispectrum dependence down to: k_1^2, k_2^2 and $\mathbf{k}_1 \cdot \mathbf{k}_2$. Using the cosine rule to eliminate the dot product we can reduce the bispectrum down to a function of the three scales k_1, k_2, k_3. We therefore parametrise the bispectrum as [52]

$$\langle \zeta_{\mathbf{k}_1} \zeta_{\mathbf{k}_2} \zeta_{\mathbf{k}_3} \rangle = (2\pi)^3 \delta^{(3)}(\mathbf{k}_1 + \mathbf{k}_2 + \mathbf{k}_3) B(k_1, k_2, k_3). \tag{4.1}$$

If we also assume scale invariance, as the power spectrum is close to being scale invariant, the bispectrum will no longer depend on the size of the triangle. This means the 3-point function is now a function of the *shape* of the triangle i.e $S(x_1, x_2)$ where $x_{1,2} = k_{1,2}/k_3$. A function of two numbers gives a lot more information than a function of a single variable.

For single-field slow-roll inflation we expect the level of non-Gaussianity to be small and effectively non-observable. A "large amount" (which we will define shortly) of non-Gaussianity can be produced however if any of the following are violated [91]:

- **Initial Vacuum State** When calculating the power spectrum, we needed to supply some initial conditions to the Mukhanov-Sasaki equation, demanding that at early times all modes were effectively Minkowski space. This vacuum state is called the Bunch-Davies vacuum.

- **Slow Roll** We have frequently referred to slow roll parameters and provided some results based on these parameters being small. While there is some justification for these parameters being small we only need inflation to last a certain number of $e-$foldings to solve certain problems. The simplest way to achieve this is by assuming the slow-roll approximation is valid, although there is no strict reason this has to be true.

- **Canonincal Kinetic term** The Lagrangian for the inflaton may contain more derivatives than the standard $(\partial\phi)$ appearing in most Lagrangians. Allowing flexibility in the kinetic term will necessarily relax constraints on the inflaton potential as we are necessarily adding more parameters.

- **Multiple Fields** In addition to all the above there is no reason to expect the inflation period to be dominated by a single scalar field.

4.1.1. Defining f_{NL}

The amount of non-Gaussianity inflation generates is related to its 3-point correlation function which will take on the form

$$\langle\zeta(t,\mathbf{k}_1)\zeta(t,\mathbf{k}_2)\zeta(t,\mathbf{k}_3)\rangle = (2\pi)^3\delta^{(3)}(\mathbf{k}_1+\mathbf{k}_2+\mathbf{k}_3)B(k_1,k_2,k_3) \tag{4.2}$$

An early way of parametrizing non-Gaussianity was through a parameter f_{NL} [45, 52, 92–94]

$$\zeta(\mathbf{x}) = \zeta_g(\mathbf{x}) + \frac{3}{5}f_{NL}^{\text{local}}\left(\zeta_g(\mathbf{x})^2 - \langle\zeta_g(\mathbf{x})^2\rangle\right). \tag{4.3}$$

This parametrisation is referred to as *local* non-Gaussianity. Here ζ_g is a pure Gaussian field and satisfies

$$\langle\zeta(t,\mathbf{k}_1)\zeta(t,\mathbf{k}_2))\rangle = (2\pi)^3\delta^{(3)}(\mathbf{k}_1+\mathbf{k}_2)P(k). \tag{4.4}$$

After a straightforward calculation one can show

$$B(k_1,k_2,k_3) = \frac{6}{5}f_{NL}^{\text{local}}\left[P(k_1)P(k_2)+P(k_2)P(k_3)+P(k_1)P(k_3)\right]. \tag{4.5}$$

Assuming $P(k)\propto k^{n_s-4}$ f_{NL}^{local} peaks in the "squeezed limit" where $k_3 \ll\ k_1 \approx\ k_2$ and

$$B(k_1,k_2,k_3\to 0) = \frac{12}{5}f_{NL}^{\text{local}}P(k_1)P(k_3) \tag{4.6}$$

In this limit it is possible to prove for single field inflation models f_{NL}^{local} is merely given by the tilt of the power spectrum [70, 95, 96]

$$f_{NL}^{\text{local}} = -\frac{5}{12}(n_s-1). \tag{4.7}$$

The proof relies on the fact that when $k_3 \ll k_1, k_2$, the mode ζ_{k_3} freezes out long before the other two modes and hence acts as a an effective background for them, so

$$\langle\zeta(k_1)\zeta(k_2)\zeta(k_3)\rangle \approx \langle\langle\zeta(k_1)\zeta(k_2)\rangle_{\bar{\zeta}}\ \bar{\zeta}(k_3)\rangle. \tag{4.8}$$

We therefore need $P(k_1)$ evaluated with a perturbed background $\bar{\zeta}$ which takes into account all the relevant frozen modes. Following [96] we can absorb this background into a rescaling of the coordinates

$$\tilde{x}^i = e^{\bar{\zeta}} x^i. \tag{4.9}$$

In position space the correlation function takes the form

$$\langle\zeta(\mathbf{x}_2)\zeta(\mathbf{x}_3)\rangle = \int \frac{\mathrm{d}^3\mathbf{k}}{(2\pi)^3} P(k) e^{i\mathbf{k}\cdot(\mathbf{x}_2-\mathbf{x}_3)} = \xi\left(|\mathbf{x}_2-\mathbf{x}_3|\right) \tag{4.10}$$

We need to evaluate this function in the rescaled coordinates $\tilde{x}$. If the $\bar{\zeta}$ is small we can express these as

$$\tilde{\mathbf{x}}_2 - \tilde{\mathbf{x}}_3 = \left(1+\bar{\zeta}(\mathbf{x}_m)\right)(\mathbf{x}_2-\mathbf{x}_3). \tag{4.11}$$

Assuming $\bar{\zeta}$ is roughly constant it is convenient to evaluate it at the midpoint $\mathbf{x}_m = (\mathbf{x}_2+\mathbf{x}_3)/2$. The the two point function becomes

$$\xi\left(|\tilde{\mathbf{x}}_2-\tilde{\mathbf{x}}_3|\right) = \xi\left(|\mathbf{x}_2-\mathbf{x}_3|\right) + \bar{\zeta}(\mathbf{x}_m)\nabla\xi\left(|\mathbf{x}_2-\mathbf{x}_3|\right)\cdot(\mathbf{x}_2-\mathbf{x}_3). \tag{4.12}$$

We can then evaluate the three-point function in position space

$$
\begin{aligned}
\langle\zeta(k_1)\zeta(k_2)\zeta(k_3)\rangle &\approx \int\mathrm{d}^3\mathbf{x}_1\int\mathrm{d}^3\mathbf{x}_2\langle\langle\zeta(\mathbf{x}_1)\zeta(\mathbf{x}_2)\rangle_{\bar{\zeta}}\ \zeta(\mathbf{k}_3)\rangle e^{i(\mathbf{k}_1\cdot\mathbf{x}_1+\mathbf{k}_2\cdot\mathbf{x}_2)} \\
&= \frac{1}{(2\pi)^3}\iiint\mathrm{d}^3\mathbf{x}_1\mathrm{d}^3\mathbf{x}_2\mathrm{d}^3\mathbf{k}\langle\zeta(\mathbf{k}_3)\zeta(\mathbf{x}_m)\rangle P(k)\times \\
&\qquad (\mathbf{x}_2-\mathbf{x}_1)\cdot\nabla e^{i\mathbf{k}\cdot(\mathbf{x}_2-\mathbf{x}_1)}e^{i(\mathbf{k}_1\cdot\mathbf{x}_1+\mathbf{k}_2\cdot\mathbf{x}_2)} \\
&= \frac{1}{(2\pi)^3}\iiint\mathrm{d}^3\mathbf{x}_1\mathrm{d}^3\mathbf{x}_2\mathrm{d}^3\mathbf{k}\langle\zeta(\mathbf{k}_3)\zeta(\mathbf{x}_m)\rangle P(k)\times \\
&\qquad k_i\frac{\partial}{\partial k_i}e^{i\mathbf{k}\cdot(\mathbf{x}_2-\mathbf{x}_1)}e^{i(\mathbf{k}_1\cdot\mathbf{x}_1+\mathbf{k}_1\cdot\mathbf{x}_1)} \\
&= -\frac{1}{(2\pi)^3}\iiint\mathrm{d}^3\mathbf{x}_1\mathrm{d}^3\mathbf{x}_2\mathrm{d}^3\mathbf{k}\langle\zeta(\mathbf{k}_3)\zeta(\mathbf{x}_m)\rangle P(k)\times \\
&\qquad \frac{\mathrm{d}\ln k^3P(k)}{\mathrm{d}\ln k}e^{i\mathbf{k}\cdot(\mathbf{x}_2-\mathbf{x}_1)}e^{i(\mathbf{k}_1\cdot\mathbf{x}_1+\mathbf{k}_1\cdot\mathbf{x}_1)} \\
&= -(2\pi)^3\delta^{(3)}(\mathbf{k}_1+\mathbf{k}_2+\mathbf{k}_3)P(k_3)P(k)\left.\frac{\mathrm{d}\ln k^3P(k)}{\mathrm{d}\ln k}\right|_{k=\bar{k}},
\end{aligned}
$$

with $\bar{k}=|\mathbf{k}_1-\mathbf{k}_2|/2$.In integrating by parts with respect to $\mathbf{k}$ we have neglected a boundary term proportional to $P(k)$ which decays as $k\to\infty$. In the limit $k_3\to 0$, $\mathbf{k}_1$ and $\mathbf{k}_2$ become equal in magnitude and opposite in direction.

Equation (4.5) suggests a much more convenient way to parametrise the bispectrum. We define a $k-$dependent f_{NL} as

$$
f_{\mathrm{NL}}(k_1,k_2,k_3)=-\frac{5}{6}B(k_1,k_2,k_3)/\left[P(k_1)P(k_2)+P(k_2)P(k_3)+P(k_3)P(k_1)\right]. \tag{4.13}
$$

Our definition of f_{NL} is different to that which is observationally constrained[1]. Estimating CMB non-Gaussianity is numerically very challenging and assuming the bispectrum can be written as a product of factorisable functions provides a significant simplification [94, 97, 98]. In [16, 19] various "shape templates" are considered, each with their corresponding f_{NL}:

[1] In particular our definition of f_{NL}differs by a minus sign from that which is commonly found in the literature.

$$
\begin{aligned}
B^{\mathrm{local}}(k_1,k_2,k_3) =&\ 2A_s^2 f_{\mathrm{NL}}^{\mathrm{local}}\left[\left(\frac{1}{k_1k_2}\right)^{4-n_s} + \ 2 \text{ perm.}\right]\\
B^{\mathrm{equil}}(k_1,k_2,k_3) =&\ 6A_s^2 f_{\mathrm{NL}}^{\mathrm{equil}}\left[-2\left(\frac{1}{k_1k_2k_3}\right)^{2(4-n_s)/3}\right.\\
&\left. -\left(\left(\frac{1}{k_1k_2}\right)^{4-n_s} + \ 2 \text{ perm.}\right) + \left(\left(\frac{1}{k_1k_2^2k_3^3}\right)^{(4-n_s)/3} + \ 5 \text{ perm.}\right)\right]\\
B^{\mathrm{ortho}}(k_1,k_2,k_3) =&\ 6A_s^2 f_{\mathrm{NL}}^{\mathrm{ortho}}\left[-8\left(\frac{1}{k_1k_2k_3}\right)^{2(4-n_s)/3}\right.\\
&\left. -3\left(\left(\frac{1}{k_1k_2}\right)^{4-n_s} + \ 2 \text{ perm.}\right) + 3\left(\left(\frac{1}{k_1k_2^2k_3^3}\right)^{(4-n_s)/3} + \ 5 \text{ perm.}\right)\right].
\end{aligned}
\tag{4.14}
$$

The current bounds on the various bispectra are [19]

$$
\begin{aligned}
f_{\mathrm{NL}}^{\mathrm{local}} &= 0.8 \pm 5.0,\\
f_{\mathrm{NL}}^{\mathrm{equil}} &= -4 \pm 43,\\
f_{\mathrm{NL}}^{\mathrm{ortho}} &= -26 \pm 21.
\end{aligned}
\tag{4.15}
$$

This is analogous to assuming for the power spectrum, $k^3P(k) = A_s k^{n_s-1}$, as opposed to the more general definition of the spectral index

$$
n_s(k) = 1 + \frac{\mathrm{d}\ln k^3 P(k)}{\mathrm{d}\ln k} \tag{4.16}
$$

where $P(k)$ is in principle an arbitrary function of k.

The shape functions given in equations (4.14) are chosen to be sums of factorisable functions to aid data analysis and are a good approximation to the bispectra expected from various theoretical models.

For example multi-field models of inflation generally give bispectra which can be well approximated by the local type and peak in the squeezed limit ($k_3 \ll k_1 \approx k_2$) [94, 99–106]. Single field models generally give bispectra that can be well approximated by either the equilateral or orthogonal type and peak in the equilateral limit($k_1 \approx k_2 \approx k_3$) [61, 65, 107–110].

4.2. The Bispectrum from Inflation

In Section 3.3.1 we showed how general models on Inflation predict primordial power spectrum by relating it to the quantum fluctuations of the primordial curvature perturbation ζ. This was done by simply evaluating the quantum expectation value of ζ at late times.

$$\langle \zeta_{\mathbf{k}_1} \zeta_{\mathbf{k}_2} \rangle = \langle 0 | \zeta_{\mathbf{k}_1} \zeta_{\mathbf{k}_2} | 0 \rangle \tag{4.17}$$

Naively performing the same procedure for the bispectrum gives 0 because we now have unequal $\hat{a}$ and $\hat{a}^\dagger$ operators in each term, annihilating the vacuum in each case. This is because when calculating the power spectrum we are implicitly assuming the field is Gaussian by truncating the action to second order so all non-Gaussian contributions trivially vanish. We therefore have two problems to address before we can calculate the bispectrum.

First of all we need to know what interaction terms arise when expanding the inflationary action to higher orders. This is a non-trivial calculation highly prone to error so will be dealt with in the next section. This calculation was first done by Maldacena [70] for the basic single canonical scalar field and has since been generalised to many different models [111, 112]. It is important to note that we only need to expand up to third order as higher order terms only contribute via loops. Such terms are typically negligible as they are higher order in both the slow-roll parameters and H/M_{pl} [113–119]. We expect higher order moments to be smaller still and indeed for even moments they will be dominated by the Gaussian contribution from Wick's Theorem.

Secondly, given the interaction terms, we need to know how to perform the calculation correctly. The method in question is most commonly referred to as the "In-In Formalism" [120–123]. It was first used by Jordan, Calzetta and Hu [124, 125] for Cosmological calculations but it wasn't until Maldacena first used it in the same paper [70] that it became the standard method for calculating quantum corrections to cosmological perturbations [108, 111–113, 115–117, 126–129].

4.2.1. The In-In Formalism

The naive approach to the bispectrum is

$$\langle \zeta_{\mathbf{k}_1}(t)\zeta_{\mathbf{k}_2}(t)\zeta_{\mathbf{k}_3}(t)\rangle = \langle 0\,|\zeta_{\mathbf{k}_1}(t)\zeta_{\mathbf{k}_2}(t)\zeta_{\mathbf{k}_3}(t)|\,0\rangle. \tag{4.18}$$

This is only correct at zero-th order because we need to take into account how the vacuum changes in time. We impose our Bunch-Davies initial conditions on ζ at very early times which makes use of the free vacuum state $|0\rangle$. What we would like to do is evaluate the bispectrum at a time t when all relevant scales have exited the horizon which means evaluating the vacuum expectation value of ζ^3 with the true vacuum state $|\Omega(t)\rangle \neq |0\rangle$. Unlike flat-space QFT the vacuum is time-dependent because we are perturbing around a time-dependant background. We therefore need to look at the effect of the Hamiltonian in more detail.

In addition we would like to use our solutions to equation (3.40) to determine the time evolution of ζ. Similarly to standard QFT we want to define an "interaction picture" and the interaction Hamiltonian. We follow [113] dealing with a general field $\phi(t,\mathbf{x})$ and look at its quantum perturbation $\delta\phi(t,\mathbf{x})$ around a classical background $\bar{\phi}(t,\mathbf{x})$.

$$\phi(t,\mathbf{x}) = \bar{\phi}(t,\mathbf{x}) + \delta\phi(t,\mathbf{x}) \tag{4.19}$$

In our case $\bar{\phi}(t,\mathbf{x})$ will represent quantities like $a(t), H(t)$ etc. while $\delta\phi(t,\mathbf{x})$ will become $\zeta(t,\mathbf{x})$. There is a corresponding conjugate momenta.

$$\pi(t,\mathbf{x}) = \bar{\pi}(t,\mathbf{x}) + \delta\pi(t,\mathbf{x}) \tag{4.20}$$

$\bar{\phi}$ and $\bar{\pi}$ satisfy Hamilton's equations while $\delta\phi$ and $\delta\pi$ satisfy the usual commutation relations. Expanding the Hamiltonian in powers of $\delta\phi$ and $\delta\pi$, it can be shown they satisfy Heisenberg's equations of motion. For example

$$\dot{\delta\phi}(t,\mathbf{x}) = i\left[\tilde{H}[\delta\phi(t),\delta\pi(t);t],\delta\phi(t,\mathbf{x})\right]. \tag{4.21}$$

$\tilde{H}$ contains only terms in $\delta\phi$ and $\delta\pi$ which are quadratic and higher. The explicit time dependence arises from the classical background fields. We now separate the quadratic part of $\tilde{H}$, H_0 from the interaction terms H_I:

$$\tilde{H}[\delta\phi(t), \delta\pi(t); t] = H_0[\delta\phi(t), \delta\pi(t); t] + H_I[\delta\phi(t), \delta\pi(t); t]. \tag{4.22}$$

The "interaction picture" is then defined so that the evolution of the operators $\delta\phi_I$ is given by the free Hamiltonian H_0:

$$\dot{\delta\phi}_I(t, \mathbf{x}) = i\left[H_0[\delta\phi(t_0), \delta\pi(t_0); t], \delta\phi_I(t, \mathbf{x})\right], \tag{4.23}$$

with initial conditions $\delta\phi_I(t_0) = \delta\phi(t_0)$ and $\delta\pi_I(t_0) = \delta\pi(t_0)$. This allows to use solutions of equation (3.40) to calculate the bispectrum as opposed to solving a non-linear partial differential equation.

The solutions of equations (4.21) and (4.23) can be written in terms of some unitary operators $U(t, t_0)$ and $U_0(t, t_0)$. They are

$$\begin{aligned} \delta\phi(t) &= U^{-1}(t, t_0)\, \delta\phi(t_0)\, U(t, t_0) & (4.24) \\ \delta\phi_I(t) &= U_0^{-1}(t, t_0)\, \delta\phi(t_0)\, U_0(t, t_0) & (4.25) \end{aligned}$$

Eliminating $\delta\phi(t_0)$ gives

$$\begin{aligned} \delta\phi(t) &= F^{-1}(t, t_0)\, \delta\phi(t)\, F(t, t_0) & (4.26) \\ F(t, t_0) &= U_0^{-1}(t, t_0)\, U(t, t_0) & (4.27) \end{aligned}$$

where $F(t, t_0)$ satisfies

$$\frac{\mathrm{d}}{\mathrm{d}t} F(t, t_0) = -iH_I(t) F(t, t_0), \qquad F(t_0, t_0) = 1. \tag{4.28}$$

$H_I(t)$ is the interaction Hamiltonian where the fields are evaluated in the interaction picture. The solution for $F(t, t_0)$ can be written as a time-ordered exponential

$$F(t, t_0) = T \exp\left(-i \int_{t_0}^{t} H_I(t)\, dt\right). \tag{4.29}$$

Putting it all together gives

$$\langle Q(t) \rangle = \left\langle \left[T \exp\left(-i \int_{t_0}^{t} H_I(t)\, dt\right)\right]^{\dagger} Q_I(t) \left[T \exp\left(-i \int_{t_0}^{t} H_I(t)\, dt\right)\right] \right\rangle \tag{4.30}$$

where $Q_I(t)$ refers to the operator $Q(t)$ evaluated in the interaction picture.

We impose our initial conditions when the relevant modes are deep inside the horizon so we typically take $t_0 \to -\infty$. For our purposes we are only interested in the first order result due to higher orders being negligible as mentioned earlier. Also as mentioned earlier we will only expand the action up to third order. Our first order expression for bispectrum is then

$$\langle \zeta_{\mathbf{k}_1}(t)\zeta_{\mathbf{k}_2}(t)\zeta_{\mathbf{k}_3}(t)\rangle = -i\int_{-\infty}^{t} \mathrm{d}t' \left\langle \left[\zeta_{\mathbf{k}_1}(t)\zeta_{\mathbf{k}_2}(t)\zeta_{\mathbf{k}_3}(t), H_I(t')\right]\right\rangle \,, \tag{4.31}$$

The curvature perturbations inside the commutator are evaluated at t and not t' and $H_I(t')$ will be cubic in $\zeta(t')$. All mode functions $\zeta_{\mathbf{k}}(t)$ will satisfy equation (3.40) with Bunch-Davies initial conditions. The whole expression is to be evaluated at a time t when all three modes have exited the horizon.

4.2.2. The Third Order Action

Equation (4.31) is our main formula for the bispectrum expressed in terms of the solution of equation (3.40). Calculating the last ingredient $H_I[\zeta(t,\mathbf{x})]$ will be the focus of this section. We will follow the original calculation in [70].

To begin with the procedure is identical to that outlined in Section 3.3.1. This time however we will completely ignore tensor perturbations. As we have yet to measure the primordial tensor power spectrum we expect 3-point functions involving tensor perturbations to be unobservable. We therefore decompose the action using the ADM formalism and focus only the scalar perturbations. There are two gauges we can consider. We define gauge 1 as

$$\phi(t,\mathbf{x}) = \phi(t), \quad h_{ij} = a^2(t)e^{2\zeta(t,\mathbf{x})}\delta_{ij}, \tag{4.32}$$

and gauge 2 as

$$\phi(t,\mathbf{x}) = \phi(t) + \varphi(t,\mathbf{x}), \quad h_{ij} = a^2(t)\delta_{ij}. \tag{4.33}$$

These two gauges are related by a complicated gauge transformation. Starting from gauge 2, one can perform a time re-parametrization $t \to t' = t + T(t,\mathbf{x})$ to set $\varphi = 0$ from an arbitrary initial $\varphi(t,\mathbf{x})$. This change of coordinates produces a new metric. Writing the metric in the form of gauge

1 requires a further spacial re-parametrization. This leaves the inflaton field unaffected as it is now homogeneous. Performing these steps allows us to write a lengthy expression for ζ in terms of φ.

$$
\begin{aligned}
T &= -\frac{\varphi}{\dot{\phi}} - \frac{\ddot{\phi}\varphi^2}{\dot{\phi}^3} + \frac{\dot{\varphi}\varphi}{\dot{\phi}^2} && (4.34)\\
\partial^2\chi &= -M_{pl}\epsilon\frac{\mathrm{d}}{\mathrm{d}t}\left(\frac{H}{\dot{\phi}}\varphi\right) && (4.35)\\
\zeta &= HT + \frac{1}{2}\dot{H}T^2 - \frac{1}{4a^2}(\partial T)^2 + \frac{1}{2}\partial_i\chi\partial_i T && (4.36)\\
&\quad + \frac{1}{4a^2}\partial^{-2}\partial_i\partial_j(\partial_i T\partial_j T) - \frac{1}{2}\partial^{-2}\partial_i\partial_j(\partial_i\chi\partial_j T)
\end{aligned}
$$

This expression is important for checking the third-order action we calculate is correct. In calculating our expressions for the third order action we only need to find N and N_i up to first order. Any third order terms would necessarily multiply the zero-th order constraints, in this case the Friedmann equations, meaning the term would subsequently vanish. Similarly any second order terms would appear in combination with the first order constraints which again vanish for the same reasons. Expanding the action up to third order in gauge 1 then yields

$$
\begin{aligned}
\frac{S_3}{M_{pl}^2} &= \int \mathrm{d}^4x \left[\frac{a}{H}\left(H+\dot{\zeta}\right)\left(-2\partial^2\zeta - (\partial\zeta)^2\right)e^{\zeta} + Ha^3\epsilon\dot{\zeta}^2\left(H-\dot{\zeta}\right)e^{3\zeta}\right.\\
&\quad \left. + \frac{1}{a^2}\left(\frac{1}{2H}(\partial_i\partial_j\psi\partial_i\partial_j\psi - (\partial^2\psi)^2)(H-\dot{\zeta}) - 2\partial_i\psi\partial\zeta\partial^2\psi\right)e^{3\zeta}\right]\\
\psi &= a^2\epsilon\dot{\zeta} - \frac{\partial^2\zeta}{H} && (4.37)
\end{aligned}
$$

Doing the equivalent calculation in gauge 2 gives:

$$
\begin{aligned}
S_3 &= \int \mathrm{d}^4x\, a^3 \left[-\frac{\dot{\phi}}{4M_{pl}^2 H}\varphi\dot{\varphi}^2 - \frac{1}{a^2}\frac{\dot{\phi}}{4M_{pl}^2 H}\varphi(\partial\varphi)^2 - \dot{\varphi}\partial_i\chi\partial_i\varphi\right.\\
&\quad + \left(\frac{3}{4}H\epsilon - \frac{H\dot{\phi}\epsilon}{4M_{pl}^2} - \frac{\dot{\phi}V''}{4M_{pl}^2 H} - \frac{V'''}{6}\right)\varphi^3 + \frac{\dot{\phi}\epsilon}{2M_{pl}^2}\varphi^2\dot{\varphi} + \frac{H\epsilon}{2}\varphi^2\partial^2\chi\\
&\quad \left.\frac{\dot{\phi}}{4H}\left((\partial^2\chi)^2 - \partial_i\chi\partial_j\chi\partial_i\chi\partial_j\chi\right)\varphi\right] && (4.38)\\
\partial^2\chi &= \epsilon\frac{\mathrm{d}}{\mathrm{d}t}\left(-\frac{H\varphi}{\dot{\phi}}\right)
\end{aligned}
$$

Comparing these two results one can see that the action is zero-th order in ϵ for gauge 1 whereas in gauge 2 it is of order ϵ^2 after using the first order relation between ζ and φ. In gauge 1 we know ζ is conserved outside the horizon whereas in gauge 2 it is not obvious any quantity is conserved because the φ^3 terms will typically lead to evolution outside the horizon. Therefore the action in the two different gauges appear inconsistent.

To resolve this apparent inconsistency one has take the third order action for ζ and integrate by parts many many times dropping all total space and time derivatives. This can potentially be a cyclic calculation but our target form is to keep only terms proportional to ϵ^2 and higher. We also introduce the second order equation of motion

$$a^3\epsilon\ddot{\zeta} = a\epsilon\partial^2\zeta - Ha^3\epsilon\,(3+2\epsilon-2\eta)\,\dot{\zeta} - \frac{1}{2}\frac{\delta L_2}{\delta\zeta} \tag{4.39}$$

which is used to eliminate any terms proportional to $\ddot{\zeta}$ when we integrate by parts. After performing all these steps we find

$$\begin{aligned}
S_3 &= M_{pl}^2\int \mathrm{d}^4x\,\Big[a^3\epsilon^2\dot{\zeta}^2\zeta + a\epsilon^2(\partial\zeta)^2\zeta - 2a^3\epsilon\dot{\zeta}\partial_i\chi\partial_i\zeta \\
&\quad -\frac{1}{2}a^3\epsilon^3\dot{\zeta}^2\zeta + a^3\epsilon\frac{\mathrm{d}}{\mathrm{d}t}\left[\epsilon-\eta\right]\zeta^2\dot{\zeta} + \frac{1}{2}a^3\epsilon\partial_i\partial_j\chi\partial_i\partial_j\chi\zeta \\
&\quad +f(\zeta)\frac{\delta L_2}{\delta\zeta}\Big], \qquad\qquad (4.40)\\
f(\zeta) &= -\frac{1}{2}\left[\epsilon-\eta\right]\zeta^2 - \frac{1}{H}\dot{\zeta}\zeta + \frac{1}{4H^2a^2}(\partial\zeta)^2 - \frac{1}{2H}\partial_i\chi\partial_i\zeta \\
&\quad -\frac{1}{4H^2a^2}\partial^{-2}\partial_i\partial_j(\partial_i\zeta\partial_j\zeta) + \frac{1}{2H}\partial^{-2}\partial_i\partial_j(\partial_i\chi\partial_j\chi),\\
\partial^2\chi &= \epsilon\dot{\zeta}.
\end{aligned}$$

The action is now of order ϵ^2 with some excess terms proportional to the equations of motion. Any interaction term can be removed by performing a suitable field redefinition but at the cost of producing higher order interaction terms. As we are limiting the calculation to third order, this is not a problem for us so we can remove all the terms proportional to the equations of motion by performing a field redefinition. In this case the field redefinition is especially simple and takes the form

$$\zeta = \zeta_n - f(\zeta_n). \tag{4.41}$$

The terms involving ∂^{-2} are reminiscent of the gauge transformation, equation (4.34) and this leads us to make the identification

$$\zeta_n = -\frac{H}{\dot{\phi}}\varphi. \tag{4.42}$$

With this identification, performing the field redefinition then converts equation (4.40) to equation (4.38) and is equivalent to the gauge transformation given in equation (4.34) [70]. In both cases the action is second order in the slow-roll parameters. It is also apparent that while ζ stays constant outside the horizon, ζ_n does not.

The outline of this field redefinition was important for several reasons. First of all it establishes a consistency check for a calculation which is highly prone to error and at first glance appears inconsistent. In [70], the author makes numerous field redefinitions. The first, outlined here, serves as a consistency relation and is not used in subsequent calculations. When calculating the bispectrum the author introduces another field redefinition defined via

$$\zeta = \zeta_c + \frac{1}{2}\frac{\ddot{\phi}}{\dot{\phi}H}\zeta_c^2 + \frac{1}{4}\epsilon\zeta_c^2 + \frac{1}{2}\epsilon\partial^{-2}(\zeta_c\partial^2\zeta_c) + \dots \tag{4.43}$$

where the dots indicate terms higher in slow-roll or vanish outside the horizon. This allows the author to simplify the action so that at leading order in slow-roll it becomes a single term.

We are interested in calculating the bispectrum for ζ, not ζ_n or ζ_c, therefore if we do a field redefinition we need to include an extra term in our calculations. If $\zeta = \zeta_c + \lambda\zeta_c^2$ then the bispectrum becomes

$$\langle\zeta(x_1)\zeta(x_2)\zeta(x_3)\rangle = \langle\zeta_c(x_1)\zeta_c(x_2)\zeta_c(x_3)\rangle + \lambda\left[\langle\zeta_c(x_1)\zeta_c(x_2)\rangle\langle\zeta_c(x_1)\zeta_c(x_3)\rangle + \dots\right] \tag{4.44}$$

where the dots refer to all the permutations expected from applying Wick's Theorem. These extra terms are important because only the field redefinition terms involving derivatives of ζ vanish at late times when all scales have exited the horizon. Many authors use field redefinitions of this manner to remove the terms proportional to the equation of motion in order to simplify calculations, for example [111, 112, 127, 130]. At this point we depart from the usual literature and not do a field redefinition at all.

First of all performing a non-linear field redefinition in quantum field theory has several non-trivial effects, see [131] and its corresponding references for details. These effects arise from operator-ordering issues or the Jacobian when one changes variables in the path-integral which generally give rise to extra terms in the action. The situation is non-trivial at best even for simple toy models with explicitly local field redefinitions. For our case where there are complex derivative interactions and necessarily non-local field redefinitions it is no doubt much worse. This then casts doubt on weather performing the field redefinition and quantising ζ_n really produces the same results for ζ as quantising ζ itself. It could be that these issues can be argued away on grounds of renormalisation but this is not obvious and is certainly not emphasised in the literature.

Secondly the terms removed by the field redefinition are those proportional to the equation of motion(by construction). To calculate the bispectrum we use the "In-In" formalism and to this end we work in the interaction picture so the interaction Hamiltonian is expressed in terms of the interaction picture fields. By definition the interaction picture fields will satisfy the equation of motion. Therefore in perturbation theory whenever a term arises proportional to the equation of motion it must vanish by construction. This leads us to conclude that any interaction term proportional to the equation of motion provides no contribution to all orders in perturbation theory and so removing them achieves nothing.

In summary performing the usual field redefinition does nothing to make the bispectrum calculation easier, possibly introduces non-trivial quantum field theory effects and requires us to calculate more terms in the spirit of equation (4.44). It seems then we can just simply ignore the $f(\zeta)$ term in equation (4.40) and proceed with our calculation. Unfortunately this is not the case.

In equation (4.40) there is a single term,

$$a^3\epsilon\frac{\mathrm{d}}{\mathrm{d}t}\left[\epsilon-\eta\right]\zeta^2\dot{\zeta}, \tag{4.45}$$

which causes problems. It can be easily shown that outside the horizon ζ tends to a constant and $\dot{\zeta}$ decays as a^{-2}. Therefore this whole term grows like a implying the bispectrum doesn't converge outside the horizon. We could argue away such a contribution if we restrict ourselves to background models where the time derivative vanishes but this is counter-productive to calculating the bispectrum for general potentials.

This terms appears when integrating by parts equation (4.37) to obtain (4.40) so we can easily compare the action in two different gauges. This diverging term is therefore cancelled by an appropriate boundary term.

At this point we generalise our action to the case $k-$inflation [59, 132] to prove a simple general result. $k-$inflation, see Chapter 7 for more details, involves generalising the kinetic term in single field inflation models. Instead of simply $L = X - V(\phi)$ where $X = \frac{1}{2}\partial_\mu\phi\partial^\mu\phi$, the Lagrangian is now a general function $P(X, \phi)$. The key new feature is that the perturbations now propagate with a general time dependent sound speed $c_s \neq 1$.

The third order action for this class of models was derived in [111] and takes the form [111, 112]

$$\begin{aligned}
S_3 &= M_{pl}^2 \int \mathrm{d}^4x \left[\frac{2a^3\epsilon}{3Hc_s^2}\left(\left(\frac{1}{c_s^2}-1\right)-g\right)\dot{\zeta}^3 \right. \\
&\quad + \frac{a^3\epsilon}{c_s^2}\left(\frac{\epsilon}{c_s^2}+3\left(1-\frac{1}{c_s^2}\right)\right)\zeta\dot{\zeta}^2 + \frac{a\epsilon}{c_s^2}(\epsilon - 2\epsilon_s + 1 - c_s^2)\zeta(\partial\zeta)^2 \\
&\quad - \frac{2a^3\epsilon^2}{c_s^4}\left(1-\frac{\epsilon}{4}\right)\dot{\zeta}\partial_i\zeta\partial_i\partial^{-2}\dot{\zeta} + \frac{a^3\epsilon^3}{4c_s^4}\partial^2\zeta\partial_i\partial^{-2}\dot{\zeta}\partial_i\partial^{-2}\dot{\zeta} \\
&\quad \left. + \frac{a^3\epsilon}{2c_s^2}\frac{\mathrm{d}}{\mathrm{d}t}\left(\frac{\dot{\epsilon}}{H\epsilon c_s^2}\right)\zeta^2\dot{\zeta} + f(\zeta)\frac{\delta L}{\delta\zeta}\right], \qquad (4.46) \\
\frac{\delta L}{\delta \zeta} &= \frac{\mathrm{d}}{\mathrm{d}t}\left(\frac{a^3\epsilon}{c_s^2}\dot{\zeta}\right) - a\epsilon\partial^2\zeta\,, \\
f(\zeta) &= \frac{\dot{\epsilon}\zeta^2}{2H\epsilon c_s^2} + \ldots\,.
\end{aligned}$$

g and ϵ_s are terms which vanish for constant $c_s \neq 1$, so in this thesis they are unimportant, and the dots indicate terms which vanish outside the horizon. We are concerned with the final line in the above action. According to [133] there is a single total time derivative equal of the form

$$\int \mathrm{d}^4x \, \frac{\mathrm{d}}{\mathrm{d}t}\left(-\frac{a^3\dot{\epsilon}}{2Hc_s^4}\zeta^2\dot{\zeta}\right), \qquad (4.47)$$

which also contributes to the bispectrum. Noting the similarity between this term and the last line in the third order action we consider all the terms as a single contribution and integrate by parts.

$$\frac{a^3\epsilon}{2c_s^2}\frac{\mathrm{d}}{\mathrm{d}t}\left(\frac{\dot{\epsilon}}{H\epsilon c_s^2}\right)\zeta^2\dot{\zeta}-\frac{\mathrm{d}}{\mathrm{d}t}\left(\frac{a^3\dot{\epsilon}}{2Hc_s^4}\zeta^2\dot{\zeta}\right)+f(\zeta)\frac{\delta L}{\delta\zeta} \tag{4.48}$$

$$=-\frac{a^3\dot{\epsilon}}{Hc_s^4}\dot{\zeta}^2\zeta-\frac{a\dot{\epsilon}}{2Hc_s^2}\zeta^2\partial^2\zeta+f'(\zeta)\frac{\delta L}{\delta\zeta}. \tag{4.49}$$

The new function $f'(\zeta)$ now only contains terms which vanish outside the horizon. They can be removed by a field redefinition as before but as we are evaluating the bispectrum after horizon exit, there will be no new contributions. Alternatively we can include the terms in the action but they will also give no contribution when we use the In-In formalism to evaluate the Hamiltonian on the solutions of the Mukhanov equation. We can therefore simply ignore the terms proportional to the equation of motion and, specialising to the case of constant c_s, write the action as

$$\begin{aligned}
S_3 &= M_{pl}^2\int \mathrm{d}^4x\,\Bigg[\frac{2a^3\epsilon}{3Hc_s^2}\left(\frac{1}{c_s^2}-1\right)\dot{\zeta}^3+\frac{a^3\epsilon}{c_s^2}\left(\frac{2\eta-\epsilon}{c_s^2}+3\left(1-\frac{1}{c_s^2}\right)\right)\zeta\dot{\zeta}^2\\
&\quad+\frac{a\epsilon}{c_s^2}(\epsilon+1-c_s^2)\zeta(\partial\zeta)^2+\frac{a\epsilon}{c_s^2}(\eta-\epsilon)\zeta^2\partial^2\zeta\\
&\quad-\frac{2a^3\epsilon^2}{c_s^4}\left(1-\frac{\epsilon}{4}\right)\dot{\zeta}\xi_i\partial_i\zeta+\frac{a^3\epsilon^3}{4c_s^4}\partial^2\zeta\xi^2\Bigg]\,, \qquad (4.50)\\
&= \int \mathrm{d}t\,L_3\,,\\
\xi_i &= \partial_i\partial^{-2}\dot{\zeta}\,.
\end{aligned}$$

From this action it is straightforward to work out the interaction Hamiltonian $H_3=-L_3$.

4.2.3. The tree-level calculation

Taking the equations (4.50), (4.31) and (3.43) we can evaluate the 3-point correlation function.

$$\langle\zeta(t,\mathbf{k}_1)\zeta(t,\mathbf{k}_2)\zeta(t,\mathbf{k}_3)\rangle=(2\pi)^3\delta^{(3)}\left(\mathbf{k}_1+\mathbf{k}_2+\mathbf{k}_3\right)\left[i\zeta_1^\star\zeta_2^\star\zeta_3^\star\,\mathcal{I}+\mathrm{c.c.}\right] \tag{4.51}$$

with

$$
\begin{aligned}
\mathcal{I} &= \mathcal{I}_{\dot{\zeta}^3} + \mathcal{I}_{\dot{\zeta}^2\zeta} + \mathcal{I}_{\zeta(\partial\zeta)^2} + \mathcal{I}_{\zeta^2\partial^2\zeta} + \mathcal{I}_{\dot{\zeta}\xi_i\partial_i\zeta} + \mathcal{I}_{\partial^2\zeta\xi^2} \\
\mathcal{I}_{\dot{\zeta}^3} &= -\int_{-\infty}^{t} \mathrm{d}t\, \frac{2a^3\epsilon}{3Hc_s^2}\left(\frac{1}{c_s^2}-1\right) \times 6\,\dot{\zeta}_1\dot{\zeta}_2\dot{\zeta}_3 \\
\mathcal{I}_{\dot{\zeta}^2\zeta} &= -\int_{-\infty}^{t} \mathrm{d}t\, \frac{a^3\epsilon}{c_s^2}\left(3\left(1-\frac{1}{c_s^2}\right)+\frac{2\eta-\epsilon}{c_s^2}\right) \times 2\left(\zeta_1\dot{\zeta}_2\dot{\zeta}_3 + 2 \text{ perm.}\right) \\
\mathcal{I}_{\zeta(\partial\zeta)^2} &= -\int_{-\infty}^{t} \mathrm{d}t\, a\epsilon\left(1-\frac{1}{c_s^2}-\frac{\epsilon}{c_s^2}\right) \times 2\,\left(\mathbf{k}_1\cdot\mathbf{k}_2 + 2 \text{ perm.}\right)\zeta_1\zeta_2\zeta_3 \\
\mathcal{I}_{\zeta^2\partial^2\zeta} &= -\int_{-\infty}^{t} \mathrm{d}t\, \frac{a\epsilon}{c_s^2}(\epsilon-\eta) \times 2\,\left(k_1^2+k_2^2+k_3^2\right)\zeta_1\zeta_2\zeta_3 \\
\mathcal{I}_{\dot{\zeta}\xi_i\partial_i\zeta} &= -\int_{-\infty}^{t} \mathrm{d}t\,(-2)\frac{a^3\epsilon^2}{c_s^4}\left(1-\frac{\epsilon}{4}\right)\left(\frac{\mathbf{k}_2\cdot\mathbf{k}_3}{k_2^2}\dot{\zeta}_1\dot{\zeta}_2\zeta_3 + 5 \text{ perm.}\right) \\
\mathcal{I}_{\partial^2\zeta\xi^2} &= -\int_{-\infty}^{t} \mathrm{d}t\, \frac{a^3\epsilon^3}{4c_s^4}\left(\frac{k_1^2}{k_2^2k_3^2}\left(\mathbf{k}_2\cdot\mathbf{k}_3\right)\zeta_1\dot{\zeta}_2\dot{\zeta}_3 + 5 \text{ perm.}\right),
\end{aligned}
\tag{4.52}
$$

where $\zeta_i = \zeta(t, k_i)$ and t is to be taken as any time after all 3 modes have exited the horizon [112, 128, 129].

We can then make the identification $B(k_1, k_2, k_3) = i\zeta_1^\star\zeta_2^\star\zeta_3^\star\,\mathcal{I} + \text{c.c.}$ Writing the bispectrum as the imaginary part, $\Im$, of a complex number Z, rescaling by 5/3 and converting to $e-$foldings N allows us to write $f_{\rm NL}$ as

$$
\begin{aligned}
f_{\rm NL} &= -\frac{\Im[Z]}{(P_1P_2 + 2 \text{ perm.})} \qquad (4.53)\\
Z &= \zeta_1^\star\zeta_2^\star\zeta_3^\star \int_{-\infty}^{N} \mathrm{d}N\,\left[g_1\zeta_1'\zeta_2'\zeta_3' + g_2\zeta_1\zeta_2\zeta_3 + \left(g_3(k_1,k_2,k_3)\zeta_1\zeta_2'\zeta_3' + 2 \text{ perm.}\right)\right].
\end{aligned}
$$

The functions g_i are defined as

$$
\begin{aligned}
g_1 &= \frac{20Ha^3\epsilon}{3c_2^2}\left(1-\frac{1}{c_s^2}\right) \\
g_2 &= \frac{10a\epsilon}{3H}\left[\left(\frac{1}{c_s^2}-1+\frac{\epsilon}{c_2^2}\right)(\mathbf{k}_1\cdot\mathbf{k}_2+\mathbf{k}_2\cdot\mathbf{k}_3+\mathbf{k}_1\cdot\mathbf{k}_3)\right. \\
&\qquad \left.+\frac{(\eta-\epsilon)}{c_s^2}(k_1^2+k_2^2+k_3^2)\right] \\
g_3(k_1,k_2,k_3) &= \frac{5Ha^3\epsilon}{3c_s^2}\left[6\left(\frac{1}{c_s^2}-1\right)+\frac{(\epsilon-2\eta)}{c_s^2}-\frac{\epsilon^2}{2c_s^2}\frac{k_1^2}{k_2^2k_3^2}\mathbf{k}_2\cdot\mathbf{k}_3\right. \\
&\qquad \left.+\frac{2\epsilon}{c_s^2}\left(1-\frac{\epsilon}{4}\right)\mathbf{k}_1\cdot\left(\frac{\mathbf{k}_2}{k_2^2}+\frac{\mathbf{k}_3}{k_3^2}\right)\right],
\end{aligned}
$$

with $\zeta' = \mathrm{d}\zeta/\mathrm{d}N$. This provides us with a formula to calculate $f_{\rm NL}$ for arbitrary triangle shapes. At this point we specialise to isosceles triangles with $k_1 = k_2 = k$ and $k_3 = \beta k$. In this notation $\beta = 0, 1, 2$ corresponds to the squeezed, equilateral and folded limits respectively. This covers most shapes of interest for single field inflation models [52]. In the squeezed limit all single field models the consistency relation [70, 95, 96]. $|f_{\rm NL}|$ generally peaks in the equilateral limit for single field models and theories with excited initial states generally peak in the folded limit [61, 108, 134]. Restricting ourselves to this set of shapes gives the final equation for the variable Z

$$
\begin{aligned}
Z(N) &= \zeta_1^\star\zeta_2^\star\zeta_3^\star\int_{-\infty}^{N}\frac{5Ha^3\epsilon}{3c_s^2}\left(f_1\zeta'^2\zeta'_\beta+f_2\zeta^2\zeta_\beta+f_3\zeta\zeta'\zeta'_\beta+f_4\zeta'^2\zeta_\beta\right), \\
f_1 &= 4u\,, \\
f_2 &= \left(2+\beta^2\right)\left(\frac{c_sk}{aH}\right)^2\left(u+\frac{1}{c_s^2}(2\eta-3\epsilon)\right), \\
f_3 &= 12u-\frac{2}{c_s^2}\left(4\eta+(1-\beta^2)\epsilon+\left(\frac{\beta^2}{4}-1\right)\epsilon^2\right), \\
f_4 &= 6u-\frac{1}{c_s^2}\left(4\eta+2(\beta^2-1)\epsilon+\left(\frac{\beta^2}{4}-1\right)\beta^2\epsilon^2\right),
\end{aligned}
\tag{4.54}
$$

from which we can calculate $f_{\rm NL}$. In equation (7.26) $\zeta = \zeta_k$ and $\zeta_\beta = \zeta_{\beta k}$.

The remainder of this thesis focuses on solving this equation numerically in the context of a Monte-Carlo approach. In particular all the numerical integration was carried out using a 5th order Rung-Kutta Cash-Karp algorithm [135, 136]. Unfortunately evaluating this integral numerically is quite challenging and is the focus for the rest of the thesis with the remaining chapters based on papers released during the PhD [1–4, 137].

Chapter 5 provides a detailed overview on how to evaluate the bispectrum in the context of Monte Carlo sampling inflationary trajectories. Chapter 6 focuses on models motivated by the recent BICEP2 results [20]. Chapter 7 extends the Monte Carlo framework to non-canonical models and chapter 8 reconstructs the inflaton potential from the Planck 2013 results [15, 16].

While it is only mentioned in passing in Chapter 5, the nature of the Monte-Carlo approach means that each bispectrum calculation is independent and therefore can be easily parallelised. This, in combination with the large number of samples makes it an environment for utilising Graphics Processing Units (GPUs) for the computation. To achieve this the code was written using C++AMP [138], a set of libraries included in the free Microsoft Visual Studio compiler. The advantage of this over more popular choices is that it is hardware independent while maintaining a fairly simple code interface. Excluding this, the code written to perform the calculations of the bispectrum was completely self contained.

5. Non-Gaussian signatures of general inflationary trajectories

5.1. Introduction

The recent results from Planck satellite have confirmed that the universe is well described by the ΛCDM model [13, 15]. A cornerstone of this model is the behaviour of the primordial perturbations to the background homogeneous model which seed the formation of structure in the observed universe. The model assumes the perturbations are almost Gaussian and very close to but *not exactly* independent of scale. The latter statement following from the observational bounds on the scalar-spectral index $n_s = 0.9603 \pm 0.0073$ [15].

A period of accelerated expansion in the very early universe driven by the potential energy of a slowly evolving scalar field, the inflaton, [29–32, 71, 139–145] is the most commonly accepted explanation for the near scale invariance of the primordial perturbations on scales larger than the Hubble length. The inflation scenario also explains why the universe is very homogeneous, isotropic and devoid of monopoles. Inflation has been criticised on the grounds of requiring fine tuning [41–44] and alternatives have been proposed (see e.g. [36–40]), however none are as simple as the basic inflation scenario involving a single scalar field.

This statement is simultaneously Inflation's greatest strength and weakness since the observational bounds on n_s can be satisfied easily by a large selection of potentials defining even the simplest single field model. To pin down the exact model of inflation more precise observations that can constrain higher order statistics of the perturbations will be required. This is particularly important if even more complicated models requiring multiple fields are to be constrained.

A wealth of information could be gained by measuring the non-Gaussianity

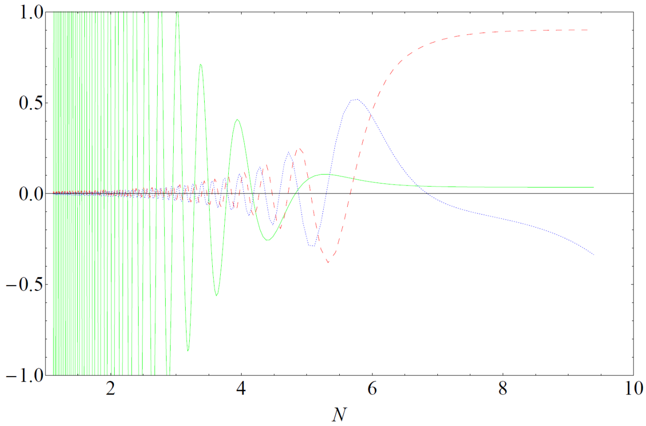

Figure 5.1.: The evolution of ζ and $f_{\rm NL}$ as a function of e-fold N for a typical random trajectory. The curves are normalised arbitrarily for the purpose of visualisation. The green (solid) line shows the real part of ζ for a mode that crosses the horizon at $N \sim 6$. ζ converges to a constant shortly after horizon crossing as expected. The blue (dotted) and red (dashed) curves show the evolution of the real and imaginary parts of the integral in (5.47). Only the imaginary part that converges after horizon exit contributes to the value of $f_{\rm NL}$ whilst the real, diverging component is discarded.

of the perturbations. If Inflation did occur then the deviations from scale-independence and a pure Gaussian distribution are inherently linked. In the simplest cases both are small and of order the slow-roll parameter ϵ, representing deviations from pure de-Sitter space [70, 76]. Non-Gaussianity is encoded in the bispectrum, or 3–point function of the perturbations. The bispectrum has a much richer structure than the power spectrum as it is, in principle, a function of three different scales and therefore contains a lot more information. It may therefore be a very effective tool for breaking the degeneracy of inflationary models. The bispectrum is often parametrised by the dimensionless quantity $f_{\rm NL}$ [45]. Most often $f_{\rm NL}$ is quoted in some limit for the configuration of the mode triangle involved in the 3–point function and in addition it is usually assumed to be very nearly scale invariant. Thus $f_{\rm NL}$ is usually regarded as a single amplitude for a particular configuration of the 3–point function.

The calculation of $f_{\rm NL}$ from inflationary models has received a lot of

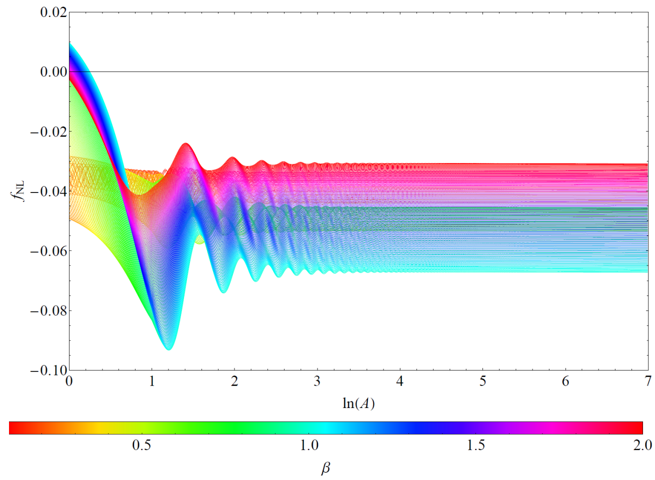

Figure 5.2.: This figure shows how $f_{\rm NL}$ for different shape parameter β depends on the integration start scale parameter A. Each of the curves is generated from the same HSR trajectory for comparison. The parameter A represents how deep inside the horizon the mode *smallest* k in the triangle was at the start of the integration. $f_{\rm NL}$ converges for all shapes as A becomes large, signifying earlier start times with respect to horizon exit. Note that, as expected, $f_{\rm NL}$ peaks at roughly $\beta \sim 1$. Typically when $A \sim 400$ $f_{\rm NL}$ has converged with only residual numerical noise at the a level of $\lesssim 1\%$. The source of the residual noise is the early-time oscillatory integral approximation (see below).

attention in recent years [46]. In particular much focus has been placed on models which generate a large value of $f_{\rm NL}$ yet retain the near scale invariance of the observed power spectrum [60, 61, 103, 105, 112]. It was hoped that a large $f_{\rm NL}$ could be observed, potentially confirming any theory matching the amplitude and shape dependence of $f_{\rm NL}$, or at the very least, ruling out all the models which do not. Unfortunately, this did not happen with the Planck satellite results which showed that $f_{\rm NL}$ as measured from Cosmic Microwave Background (CMB) anisotropies, is consistent with zero with standard deviation of $\mathcal{O}(10)$ in all "types" of $f_{\rm NL}$ [16]. This means the simplest models of inflation are still perfectly consistent with observations.

Despite this, an accurate calculation of $f_{\rm NL}$ will still be valuable in future as bounds get stronger and stronger. This is particularly important for comparisons with future Large Scale Structure (LSS) surveys that may constrain $f_{\rm NL}\sim \mathcal{O}(1)$ (see e.g. [146, 147]). Obtaining *accurate* estimates of the bispectrum and its scale dependence for generic inflationary solutions will be important for these comparisons. This work will require a numerical evaluation of the primordial bispectrum arising from higher-order correlations of the curvature perturbations. The full numerical treatment of the bispectrum has received little attention over the years, most calculations being analytical and relying on various approximations. Most numerical work carried out so far has been concerned only with specific potentials with features that are known to result in large non-Gaussianity and still rely on slow-roll approximations to simplify the calculations [128–130, 148].

This *paper* describes the full numerical calculation of non-Gaussianity for inflationary, single-field trajectories generated in the Hamilton-Jacobi (HJ) formulation [77]. Initial results from this treatment were reported in [137]. The numerical treatment allows the calculation of non-Gaussianity in cases where the field is not in the slow-roll regime, but still in the perturbative regime where the higher-order interaction couplings are still $\ll 1$. It also allows us to calculate the contribution to all possible "shapes" and "types" of non-Gaussianity.

In this framework large ensembles of inflating solutions, or *trajectories*, can be generated. These are related to a large class of single field potentials and can, in principle, be compared to observations without restrictions on the the model of inflation [4]. Here we examine the resulting distribution in various shapes of *local* type non-Gaussianity and verify the well-known consistency relation for squeezed, single-field inflation [70, 95]. We also confirm that the equilateral configuration of the bispectrum follows a similar distribution.

The *paper* is organised as follows. In Section 5.2 we outline the HJ approach and the analytical framework we are using for our computations. In Section 5.3 we describe our computational method, recapping the calculation of the power spectrum, followed by the subtleties involved in the calculation of the bispectrum. In Section 5.4 we outline the main results of the paper and verify them through some simple consistency checks. We discuss our results in Section 5.5.

5.2. Hamilton Jacobi approach to inflationary trajectories

We start by briefly reviewing the HJ approach to inflationary trajectories where we consider the Hubble-Slow-Roll (HSR) parameters to be the fundamental quantities of interest, as opposed to the frequently used Potential-Slow-Roll (PSR) parameters [77, 78, 149, 150].

If ϕ is a monotonic function of time, we can change the independent variable in the Friedmann equations from t to ϕ and consider all quantities as functions of ϕ. The Friedmann equation and the inflaton's equation of motion then take on the following form

$$\begin{aligned} \dot{\phi} &= -2M_{\rm pl}^2 H'(\phi)\,, & (5.1)\\ \left[H'(\phi)\right]^2 - \frac{3}{2M_{\rm pl}^2}H(\phi)^2 &= -\frac{1}{2M_{\rm pl}^4}V(\phi)\,, & (5.2)\end{aligned}$$

where overdots and primes denote a derivative with respect to t and ϕ respectively, H is the Hubble rate, and $M_{\rm pl}^2 = (8\pi G)^{-1}$. One of the advantages of performing this change of variable is that one can merely pick a function $H(\phi)$ and this will correspond to an exact solution of a corresponding potential $V(\phi)$. It is straightforward to verify that inflation will occur if the following condition holds

$$\epsilon = 2M_{\rm pl}^2\left[\frac{H'(\phi)}{H(\phi)}\right]^2 \equiv -\frac{\dot{H}}{H^2} \equiv \frac{\dot{\phi}^2}{2M_{\rm pl}^2 H^2} < 1\,. \quad (5.3)$$

This relation is exact, unlike the equivalent expression for the PSR parameter $\epsilon_V \propto (V'/V)^2 < 1$ which is only approximate.

We can define an infinite hierarchy of HSR parameters labelled by index l

$${}^l\lambda = \left(2M_{\rm pl}^2\right)^l \frac{(H')^{l-1}}{H^l}\frac{d^{(l+1)}H}{d\phi^{(l+1)}}\,. \quad (5.4)$$

From these we can define $\eta \equiv {}^1\lambda = -(\ddot{\phi}/H\dot{\phi})$ and $\xi \equiv {}^3\lambda$. The last ingredient required is the number of e-foldings N specifying the change in scale factor a during the inflationary phase $\ln(a) = N$. It is useful to relate this to the Hubble rate as

$$\frac{\mathrm{d}N}{\mathrm{d}t} = H\,. \quad (5.5)$$

Combining all of these equations produces the following set of differential equations dictating the evolution of the background

$$
\begin{aligned}
\frac{\mathrm{d}H}{\mathrm{d}N} &= -\epsilon H\,, \\
\frac{\mathrm{d}\epsilon}{\mathrm{d}N} &= 2\epsilon(\epsilon-\eta)\,, \\
\frac{\mathrm{d}^l\lambda}{\mathrm{d}N} &= (l\epsilon-(l-1)\eta)\ {}^l\lambda - {}^{l+1}\lambda\,.
\end{aligned} \tag{5.6}
$$

This is the most natural set of variables to use when describing a general inflationary trajectory. These equations will be the starting point of our f_{NL} calculation. The HSR parameters will evolve in time and each particular inflation model with a particular set of initial conditions will correspond to a distinct trajectory in HSR-space. In other words, specifying the HSR parameters at some particular time and solving the system (8.5) is precisely equivalent to specifying $\phi(t_0)$, $\dot{\phi}(t_0)$, and $V(\phi)$ and solving the Friedmann equations.

The HJ system (5.6) is an infinite hierarchy of equations that describe *all* possible background solutions. For the purpose of computing observables the system is usually truncated by fixing ${}^l\lambda = 0$ for $l \geq l_{\mathrm{max}}$. The truncated system still describes *exact* solutions for the background quantities but restricts the space of solutions to a subset of the infinite system.

Relating the HSR picture to a specific model is straightforward for the simplest cases. For example if we set ${}^l\lambda = 0$ for all $l > 1$ the only remaining non-zero HSR parameters are ϵ and η. This implies $H(\phi) = a\phi^2 + b\phi + c$ is a quadratic function and hence $V(\phi)$ is quartic. If one specifies an initial condition H_0 this fixes the potential $V(\phi)$ up to a constant shift $\phi \to \phi + C$. This shift will have no impact on observations because the energy scale is specified by H_0. We can use this symmetry to remove the linear term in $H(\phi)$ and write the potential as

$$
V(\phi) = \frac{\lambda}{4!}\phi^4 + \frac{m^2}{2}\phi^2 + \Lambda\,. \tag{5.7}
$$

If one specifies ϵ_0 and η_0 at the same time as H_0 this is then equivalent to solving for the model parameters and initial conditions

$$\begin{aligned}
\phi_0 &= \pm\frac{\sqrt{2\epsilon_0}}{\eta_0}M_{\rm pl}\,,\\
\dot{\phi}_0 &= \mp\sqrt{2\epsilon_0}H_0M_{\rm pl}\,,\\
\frac{\lambda}{4!} &= \frac{3H_0^2\eta_0^2}{16M_{\rm pl}^2}\,,\\
\frac{m^2}{2} &= \frac{H_0^2}{2}(3\eta_0-\frac{3}{2}\epsilon_0-\eta_0^2)\,,\\
\Lambda &= \frac{2}{27}\lambda M_{\rm pl}^4\left(1+\frac{27}{2}\frac{m^2}{\lambda M_{\rm pl}^2}\right)^2\,.
\end{aligned} \tag{5.8}$$

Note that although we have three degrees of freedom we cannot specify λ, m^2, and Λ independently. This is simply because we have used our freedom in initial condition ϕ_0 to write H as $H(\phi)=a\phi^2+c$. This leaves two degrees of freedom to specify λ, m^2 and Λ. In practice, if one only requires the shape of the potential $V(\phi)$ it is much simpler to solve for $\phi(N)$, $H(N)$, and $\epsilon(N)$ and use the relation

$$V(\phi)=3M_{\rm pl}^2H^2\left(1-\frac{\epsilon}{3}\right)\,. \tag{5.9}$$

The only remaining information that needs to be specified in the model above is the total number of e-foldings ΔN. When integrating the Friedmann equations for a given potential $V(\phi)$ there is no clear way of ensuring inflation ends, or if it provides enough inflation. Inflation ends exactly when $\epsilon=1$. The only constraint on the length of inflation is that it must last at least roughly 60 e-foldings [15] in order for all scales up to the present Hubble scale to have been inflated to super horizon scales before the deceleration phase of the standard Big Bang picture. Converting this into some length in time necessarily requires some knowledge of H (which may vary significantly over the whole of inflation) so N is clearly the most natural time variable to use. These constraints on inflation are then easy to implement using the HSR parameter system - to ensure inflation ends we choose the initial condition $\epsilon(N_{\rm tot})=1$. To ensure inflation provides enough e-foldings we integrate *back* in time from $N_{\rm tot}\to N=0$ where $N_{\rm tot}\sim 60$. In practice the exact value of $N_{\rm tot}$ is not known due to uncertainties in the physics of reheating. When generating random trajectories ΔN can be drawn from a proposal density distribution to account for this uncertainty.

To generate large ensembles of random inflationary trajectories we can then draw the remaining HSR parameters ${}^{l}\lambda$ at the end of inflation from proposal densities. In the following the proposal densities are uniform over a specified range in each HSR but could also take different forms e.g. normal distribution. The choice of proposal shape and *where* the boundary conditions are drawn can lead to significant differences in the distributions of the final observable quantities. A number of different choices have been made in the literature [150–153].

It is important to emphasise that the evolution of these trajectories need not have anything to do with inflationary dynamics as $H(\phi)$ can be completely decoupled from the system. One is perfectly able to solve for $\epsilon(N)$, $\eta(N)\ldots$ without mentioning inflation. The key ingredients to connect with inflation are $H(N)$ and $V(\phi)$ or (8.8), both of which only require an input function $\epsilon(N)$. The HSR parameters themselves, along with their differential equations, only provide an efficient tool for generating valid functions $\epsilon(N)$ which may *then* be correctly interpreted as inflationary models [153].

5.2.1. Monte Carlo generation of HJ trajectories

The generation of large ensembles of consistent inflationary trajectories in the HJ formalism lends itself to Monte Carlo Markov Chain (MCMC) comparisons of the inflationary model space with observations such as the Planck CMB measurements. The HSR definition is particularly useful since in the slow roll limit the proposal parameters are closely related to the observables such as n_s, the tensor-to-scalar ratio r, running $dn_s/d\ln k$ etc. For example, at second order in HSR parameters

$$n_s = 1 - 4\,\epsilon + 2\,\eta - 2\,(1+C)\,\epsilon^2 - \frac{1}{2}(3-5C)\,\epsilon\,\eta + \frac{1}{2}(3-C)\,\xi\,, \tag{5.10}$$

$$r = 16\,\epsilon\left[1 + \frac{1}{2}(C-3)(\epsilon-\eta)\right]\,, \tag{5.11}$$

$$n_t = -2\,\epsilon + (3+C)\,\epsilon^2 + (1+C)\,\epsilon\,\eta\,, \tag{5.12}$$

where $C = \ln 2 + \gamma - 2$ and γ is the Euler-Mascheroni constant [76]. As described below we calculate all observables numerically and use (5.10)-

(5.12) for comparison.

Here, we explore the proposal densities for observables resulting from the HJ formalism and including non-Gaussianity. The use of the proposal densities for comparison with the data will be explored in [4]. As a simple assumption for the proposal densities from which to draw HSR boundary conditions we use uniform distributions in the range

$$ {}^{l}\lambda = [-1, 1]e^{-s\,l}\,, \tag{5.13} $$

for $l > 0$ and where s is a suitable suppression factor. Our boundary conditions will be imposed at the end of inflation so $\epsilon = 1$ and $N_{\rm tot}$ is also drawn from a uniform distribution $N_{\rm tot} = [60, 80]$. In our formulation N increases with time so $N \sim 0$ represents the time at which the largest scales observable today were exiting the horizon and $N = N_{\rm tot}$ is the end of inflation. The observable window spanned by e.g. CMB observations corresponds approximately to the interval $N \sim 0 \to N \sim 10$. Note that the normalisation of H does not affect the evolution of the parameters so we may specify the initial condition for H at any time in order to correctly normalise the amplitude of perturbations. In practice we have to truncate the HSR series for some finite value of $l = l_{\rm max} - 1$ (so $l_{\rm max} = 3$ implies ϵ, η, ξ are non-zero) [1].

5.3. Computational method

5.3.1. Computation of the power spectrum

We introduce a comoving curvature perturbation $\zeta(t, \mathbf{x})$ and work in a gauge where the spatial part of the perturbed metric is given by $g_{ij} = a^2\,(t)e^{2\zeta(t,\mathbf{x})}\delta_{ij}$ and the inflaton perturbation vanishes everywhere $\delta\phi(t, \mathbf{x}) = 0$. The primordial power spectrum of the curvature perturbations is related to the variance of the Fourier expanded mode ζ_k

$$ \langle \zeta_{k_1} \zeta^{\star}_{k_2} \rangle = (2\pi)^3 \delta^{(3)}(\mathbf{k}_1 + \mathbf{k}_2) P_\zeta(k_1)\,, \tag{5.14} $$

[1] An alternative "model-independent" method is to parametrise the potential via a Taylor expansion of a certain order as done in [15]. The two method are complementary.

where $\mathbf{k}$ is the Fourier wavevector and $k \equiv |\mathbf{k}|$. The mode $\zeta_k(t)$ satisfies the Mukhanov-Sasaki equation [71, 72]. Expressed in terms of N instead of t this equation becomes

$$\frac{\mathrm{d}^2\zeta_k}{\mathrm{d}N^2} + (3 + \epsilon - 2\eta)\frac{\mathrm{d}\zeta_k}{\mathrm{d}N} + \frac{k^2}{a^2H^2}\zeta_k = 0 \,. \tag{5.15}$$

In this form it is trivial to see that outside the horizon the derivative of ζ_k decays exponentially with respect to N or as a^{-2} so ζ_k quickly goes to a constant. The power spectrum of interest is then related to the freeze-out value of ζ_k on scales $k \ll aH$

$$P_\zeta(k) = |\zeta_{k \ll aH}|^2 \,. \tag{5.16}$$

The initial conditions for the solutions to (5.15) can be set when the mode is much smaller than the horizon $k \gg aH$ and takes on the Bunch-Davies form [73]

$$\zeta_k \to \frac{1}{M_{\mathrm{pl}}} \frac{e^{-ik\tau}}{2a\sqrt{k\epsilon}} \,, \tag{5.17}$$

where τ is conformal time defined by $\mathrm{d}N/\mathrm{d}\tau = aH$.

For our f_{NL} calculation we are interested in solving this equation for an observable range of $10^{-5} < k < 10^{-1}$ in units of $(\mathrm{Mpc})^{-1}$ for each inflationary trajectory obtained via the HJ system. Each background model is completely defined from the solutions of (5.6) up to an overall normalisation of H. To choose this normalisation we need to look at our calculation of ζ_k more closely.

We integrate (5.15) from a time satisfying $k = A\,aH$ to $k = B\,aH$ where $A \gg 1$ and $B \ll 1$ representing sub and super-horizon times respectively. Whatever units we wish to work in, we can fix the normalisation of a so that at $N = 0$ the following condition is satisfied

$$k_{\mathrm{min}} = A\,aH \,. \tag{5.18}$$

Here k_{min} represents the smallest k of interest, in practice the mode corresponding to the largest scales observable today. For this particular mode one can then approximate the time of horizon crossing as $N_c \approx \ln A$ (this is exact if H is exactly constant and is the only time we use this approximation). The initial condition on H will have a direct effect on the amplitude of the power spectrum. Therefore during the background integration of the flow parameters we fix the initial condition on H to be

$$H(N_c) = 4\pi\sqrt{2\pi\epsilon(N_c)}M_{\rm pl}A_s\,, \tag{5.19}$$

where A_s is the normalisation of the canonical form of the dimensionless primordial curvature perturbation

$$k^3\, P_\zeta(k) = A_s\, k^{n_s-1}\,, \tag{5.20}$$

and is typically of the order of 10^{-5} to reproduce typical density fluctuations amplitudes.

We also need to increase the total number of $e-$folds $N_{\rm tot} \to N_{\rm tot} + \ln A$. If this was ignored, as A increases the mode would start deeper inside the horizon but the initial conditions on the HSR parameters would remain constant. This would effectively change the trajectory so the HSR values at horizon crossing would be different. Shifting the total $e-$folds by $\ln A$ and enforcing (5.19) ensures that H and the HSR parameters, evaluated at horizon crossing, are independent of A (how deep the modes start inside the horizon). Neglecting these effects would affect the convergence of the power spectrum as $A \to \infty$.

A simpler way of normalising H would be to specify the initial condition at the end of inflation (with all the other HSR parameters) but that choice is not as physically transparent. In addition, H may vary by orders of magnitudes during the approximately 60 e-foldings of evolution. This can lead to a large variation in the overall normalisation of the primordial power which can lead to numerical problems if one wishes to use the results as the input to standard boltzmann codes such as `CAMB` [154].

To be consistent we require (5.17) to be satisfied for each k. Therefore in order for each mode to start "equally deep" inside the horizon we integrate the background forward in time (from $N = 0$) until $k = A\,aH$ for every mode of interest. Applying (5.17) we integrate the background and (5.15) until each mode crosses the horizon and satisfies $k = B\,aH$. This ensures the modes have sufficiently converged to their super-horizon values. In practice it was found that, for the calculation of the bispectrum, the solutions converged for $A \approx e^6$ and $B \approx 0.1$. Larger values of A significantly added to computational time due to the erratic early time behaviour of ζ_k with no real benefit.

This completely determines the mode evolution and hence their value on super-horizon scales. We can then calculate physical observables such as n_s and r from their definitions directly without resorting to any approximations

$$\begin{aligned} n_s(k_\star) &= 1 + \left.\frac{\mathrm{d}\ln\left[k^3 P_\zeta(k)\right]}{\mathrm{d}\ln k}\right|_{k=k_\star} \\ r(k_\star) &= 2\,\frac{P_h(k_\star)}{P_\zeta(k_\star)} \end{aligned} \tag{5.21}$$

where we evaluate the quantities at a scale $k_\star$ normally chosen to be the largest mode in the system. P_h is the power spectrum of either the tensor mode polarisations h_+ and $h_\times$. The factor of 2 accounts for the fact that in parity invariant models both polarisations contribute the same exact power. Solutions for both gravitational wave polarisations can be obtained by integrating an equation similar to (5.15)

$$\frac{\mathrm{d}^2 h_k}{\mathrm{d}N^2} + (3-\epsilon)\frac{\mathrm{d}h_k}{\mathrm{d}N} + \frac{k^2}{a^2H^2}h_k = 0\,, \tag{5.22}$$

with initial condition

$$h_k \to \frac{1}{M_{\rm pl}}\,\frac{e^{-ik\tau}}{a\sqrt{2k}}\,, \tag{5.23}$$

in the limit where $k \gg aH$.

It is worth noting that choosing $B = 1$ (terminating *exactly* at horizon crossing) produces the the best agreement between equations (6.9) and (5.10)-(5.12) and for very small values of B the results can disagree by $\mathcal{O}(\epsilon)$. This is purely because the slow-roll parameters *evolve* while the power spectrum remains constant and so the slow-roll formula (which is specified at horizon-crossing) ceases to be valid for sufficiently small B. This gives us confidence in our numerical results.

It is important to stress that our choice of priors (in particular our choice of *location* for the priors) typically generates trajectories where the HSR parameters become small during the time we calculate P_k. But the method outlined above works for *arbitrary* values of these parameters. We could specify the initial conditions at the beginning of inflation to begin with, easily breaking slow roll, but we cannot guarantee the trajectory will provide enough inflation.

5.3.2. Computation of the bispectrum

The non-Gaussianity of the primordial curvature perturbations is encoded in the third order moment of ζ_k which, in the isotropic limit, is a function of the wavenumbers of three wavevectors forming closed triangles in momentum space

$$\langle \zeta_{k_1} \zeta_{k_2} \zeta_{k_3} \rangle = (2\pi)^3 \delta^{(3)}(\mathbf{k}_1 + \mathbf{k}_2 + \mathbf{k}_3) B(k_1, k_2, k_3)\,. \tag{5.24}$$

For convenience the bispectrum B is re-written in a dimensionless form $f_{\rm NL}(k_1, k_2, k_3)$ by dividing it by different combinations of the squares of the power spectra of the three modes. $f_{\rm NL}$ is defined in terms of the bispectrum [45]

$$\begin{aligned} f_{\rm NL}(k_1, k_2, k_3) &= \frac{5}{6} B(k_1, k_2, k_3) / \left(|\zeta_{k_1}|^2 |\zeta_{k_2}|^2 + \right. \\ & \left. |\zeta_{k_1}|^2 |\zeta_{k_3}|^2 + |\zeta_{k_2}|^2 |\zeta_{k_3}|^2 \right)\,, \end{aligned} \tag{5.25}$$

and the 5/6 factor has been introduced by convention.

The weighting introduced in (5.25) is often called the "local" type and others have also been used when motivated by the expected signal-to-noise of different shaped triangles in the observations. In particular [16] analysed the data with respect to two additional weightings - equilateral and orthogonal. The limits reported in [16] are $f_{\rm NL}^{\rm local} = 2.7 \pm 5.8$, $f_{\rm NL}^{\rm equil} = -42 \pm 75$, $f_{\rm NL}^{\rm ortho} = -25 \pm 39$.

The $f_{\rm NL}$ function is normally reduced to a single, scale invariant amplitude for a particular shaped triangle, as above. This motivates the different choice of weightings in analysing observations and reporting results. In our case we will consider the k_1, k_2, k_3 dependence of $f_{\rm NL}$ explicitly and the choice of weighting in relating the bispectrum to the dimensionless $f_{\rm NL}$ is irrelevant. Throughout this work we use (5.25) as the definition of $f_{\rm NL}$ even when we take the limit of different shaped triangles.

In order to calculate $f_{\rm NL}$ the third order correlator of (5.24) needs to be calculated at late times in the super-horizon limit. To do this we consider the expansion of the action for ζ at third order which in terms of the HSR parameters can be written as [70, 103, 112]

$$
\begin{aligned}
S_3 \;=\; & M_{\rm pl}^2\int d^4x \, \Big[a^3\epsilon^2\zeta\dot{\zeta}^2 + a\epsilon^2\zeta(\partial\zeta)^2 \\
& -2a^3\epsilon^2\left(1-\frac{\epsilon}{4}\right)\dot{\zeta}\partial_i\zeta\partial_i\partial^{-2}\dot{\zeta} + \frac{a^3\epsilon^3}{4}\partial^2\zeta\partial_i\partial^{-2}\dot{\zeta}\partial_i\partial^{-2}\dot{\zeta} \\
& +a^3\epsilon\frac{\mathrm{d}}{\mathrm{d}t}\left(\epsilon-\eta\right)\dot{\zeta}\zeta^2 + 2f(\zeta)\frac{\delta L}{\delta\zeta}\Big] \, ,
\end{aligned}
$$

where $\partial_i \equiv \partial/\partial x_i$, ∂^2 and ∂^{-2} are the Laplacian and inverse Laplacian operators respectively, and $\delta L/\delta\zeta$ is the equation of motion (5.15)

$$
\frac{\delta L}{\delta\zeta} = a\left(\frac{\mathrm{d}}{\mathrm{d}t}\left(a^2\epsilon\dot{\zeta}\right) + Ha^2\epsilon\dot{\zeta} - \epsilon\partial^2\zeta\right) . \tag{5.26}
$$

The function $f(\zeta)$ is

$$
\begin{aligned}
f(\zeta) \;=\; & \frac{\epsilon-\eta}{2}\zeta^2 + \frac{1}{H}\zeta\dot{\zeta} + \\
& \frac{1}{4a^2H^2}\left(-(\partial\zeta)^2 - \partial^{-2}\left(\partial_i\partial_j(\partial_i\zeta\partial_j\zeta)\right)\right) + \\
& \frac{\epsilon}{2H}\left(\partial\zeta\partial\partial^2\dot{\zeta} - \partial^{-2}\left(\partial_i\partial_j(\partial_i\zeta\partial_j\partial^{-2}\dot{\zeta})\right)\right) ,
\end{aligned} \tag{5.27}
$$

which gathers terms proportional to the equation of motion $\delta L/\delta\zeta$ that do not contribute to the third order action.

In analytical estimates of $f_{\rm NL}$ it is helpful to introduce a number of field redefinitions that simplify the calculations by suppressing the terms proportional to $\delta L/\delta\zeta$ explicitly and isolate the dominant contributions to (5.26) [70, 103]. The redefinitions are not strictly required when calculating the contributions numerically and introduce slow-roll approximations which are against the approach being taken here. The approach described below is equivalent but avoids making some assumptions inherent in the slow-roll limit.

We are interested in calculating the bispectrum using the "in-in" formalism. At tree-level this requires the calculation of [70, 103, 115]

$$
\langle\zeta^3(t)\rangle = -i\int_{-\infty}^{t}\mathrm{d}t'\langle\left[\zeta^3(t), H_{\rm int}(t')\right]\rangle \, , \tag{5.28}
$$

where $H_{\rm int}$, the interaction Hamiltonian, is essentially S_3 without the integral over time. Each of the terms in S_3 contribute separately to the correlation (5.28) and can be considered individually. We are treating ζ as a quantised curvature perturbation that is expanded in term of a time dependent amplitude and standard momentum space creation and annihilation operators

$$\zeta(t,\mathbf{x}) = \int \frac{\mathrm{d}^3\mathbf{p}}{(2\pi)^3} \left(\zeta_{\mathbf{p}}(t)\, a_{\mathbf{p}} + \zeta^*_{-\mathbf{p}}(t)\, a^\dagger_{-\mathbf{p}} \right) e^{i\mathbf{p}\cdot\mathbf{x}} \,. \tag{5.29}$$

Here $\zeta_{\mathbf{p}}(t)$ is by definition the solution of equation (5.15) or (5.26) in Fourier space. Therefore any interaction term proportional to (5.26) will necessarily vanish and give no contribution because we are expanding in terms of the solutions to that equation.

Since ζ on super-horizon scales converges at late times we should expect both power spectra and bispectra to converge too. This is not obvious from the form of the action (5.26) as it requires all terms in S_3 to converge fast enough at late times. After horizon crossing $\dot{\zeta} \propto a^{-2}$ therefore the $a^3\zeta\dot{\zeta}^2$ terms in S_3 decay like a^{-3} and a^{-1} at late times respectively. The same is true for the terms involving $\partial^{-2}\dot{\zeta}$. The $a\zeta(\partial\zeta)^2 \to ak^2\zeta_k^3$ term grows like a at late times however. This appears problematic but it will turn out that this divergence gives no contribution to f_{NL} and will ultimately be discarded.

The final term $\propto a^3\dot{\zeta}\zeta^2$ is problematic. It grows like a at late times and unlike the $a\zeta(\partial\zeta)^2$ term we are not be able to disregard it. One may neglect this term if one assumes certain certain conditions[2] on $\epsilon - \eta$ but this goes against the spirit of the HSR approach.

The HSR approach also requires a more thorough treatment of boundary terms that have previously been assumed to vanish. Several total derivatives arise from integration by parts during the derivation of the action in the form of (5.26) and while all the total spatial derivatives can be safely ignored, one total time derivative may give a non-vanishing contribution [133]. The contribution, in terms of HSR parameters, is

$$-\int \mathrm{d}^4x \, \frac{\mathrm{d}}{\mathrm{d}t} \left[(\epsilon - \eta)\epsilon a^3 \zeta^2 \dot{\zeta} \right] , \tag{5.30}$$

Noting the similarity between the boundary term, the apparently diver-

[2] For example if $\epsilon - \eta$ is sufficiently constant as assumed in analytical approximations or if it decays rapidly enough at late times as done in [128, 129].

gent $a^3\zeta^2\dot{\zeta}$ term, and the first term in $f(\zeta)$, we write the final line in (5.26) as

$$\int \mathrm{d}^4x \left[a^3\epsilon\frac{\mathrm{d}t}{\mathrm{d}t}\left(\epsilon-\eta\right)\zeta^2\dot{\zeta} + a(\epsilon-\eta)\frac{\delta L}{\delta\zeta} - \frac{\mathrm{d}}{\mathrm{d}t}\left(a^3\epsilon(\epsilon-\eta)\right) + f'(\zeta)\frac{\delta L}{\delta\zeta}\right] . \tag{5.31}$$

Here the function $f'(\zeta)$ contains only derivatives of ζ. It is then straightforward to verify that several cancellations occur in the first three terms resulting in

$$-2a^3\epsilon(\epsilon-\eta)\zeta\dot{\zeta}^2 - a\epsilon(\epsilon-\eta)\zeta^2\partial^2\zeta\,. \tag{5.32}$$

The divergent $\zeta^2\dot{\zeta}$ disappears in exchange of $\zeta^2\partial^2\zeta$ which can be dealt with in the same manner as the $\zeta(\partial\zeta)^2$ term as described below[3] We can then finally write the action as

$$\begin{aligned} S_3 \;=\; & \int d^4x\, a^3\epsilon \left[\left(2\eta-\epsilon\right)\zeta\dot{\zeta}^2 + \frac{1}{a^2}\epsilon\zeta(\partial\zeta)^2 \right. \\ & -(\epsilon-\eta)\zeta^2\partial^2\zeta - 2\epsilon\left(1-\frac{\epsilon}{4}\right)\dot{\zeta}\partial_i\zeta\partial_i\partial^{-2}\dot{\zeta} \\ & \left. +\frac{\epsilon^2}{4}\partial^2\zeta\partial_i\partial^{-2}\dot{\zeta}\partial_i\partial^{-2}\dot{\zeta}\right] , \end{aligned} \tag{5.33}$$

where we have dropped terms proportional to the first order equation of motion.

Numerical Calculation of $f_{\rm NL}$

Using (5.33) to define the interaction Hamiltonian one can use equations (5.28) and (5.29) to calculate the bispectrum. It can be written in the general form

$$B(k_1,k_2,k_3) = \mathcal{I}\left[\zeta_1^*\zeta_2^*\zeta_3^*\int_{N_0}^{N_2} dN\, Z(N)\right] , \tag{5.34}$$

where $\mathcal{I}[z]$ distinguishes the imaginary part of z, N_2 and N_0 are defined e-folds (times) defined such that all modes are deep inside and far outside

[3]Note also that the remaining terms proportional to the equation of motion contain only derivatives of ζ and can be disregarded exactly at the boundary (late times) in the approach taken by [70].

the horizon respectively (using the previously defined A and B parameters), $\zeta_i = \zeta_{k_i}$. There is a contribution to $Z(N)$ for each term in the action. For example, the $\zeta(\partial\zeta)^2$ and $\zeta^2\partial^2\zeta$ terms give the following contribution

$$\frac{10}{3H}\left[a\epsilon^2(\mathbf{k}_1\cdot\mathbf{k}_2+\mathbf{k}_1\cdot\mathbf{k}_3+\mathbf{k}_2\cdot\mathbf{k}_3)+\right.\\ \left.a\epsilon(\eta-\epsilon)(k_1^2+k_2^2+k_3^2)\right]\zeta_1\zeta_2\zeta_3\,. \tag{5.35}$$

From (8.20), these are the only terms which do not obviously converge. However, we know at late times $\zeta_k \to A_k + \frac{B_k}{a^2}$ for some k-dependant constants. Considering the case $k = k_1 = k_2 = k_3$ for simplicity

$$\zeta_k^{*3}\int dN\, a\zeta_k^3 \approx |A|^6\int dN\, a + \dots\,, \tag{5.36}$$

where $\dots$ denote terms that converge at late times like a^{-1}. Only the real part of this expression diverges and we are only interested in the imaginary part for the bispectrum. Therefore these terms cause no issues at late times, unlike the $a^3\zeta^2\dot{\zeta}$ term.

We now specialise to the case where $k_1 = k_2 = k$ and $k_3 = \beta k$. This allows us to parametrise most shapes of interest via the parameter β separately from the overall scale dependence given by wavenumber k. Squeezed, equilateral and folded limits correspond to $\beta = 0$, 1 and 2 respectively. In terms of this classification we can write down our full expression for $f_{\rm NL}$ as

$$\begin{aligned} f_{\rm NL} &= \frac{1}{|\zeta|^2\left(|\zeta|^2+2|\zeta_\beta|^2\right)}\times \\ &\mathcal{I}\left[\zeta^{*2}\zeta_\beta^*\int_{N_0}^{N_2} dN\, f_1\zeta^2\zeta_\beta + f_2\zeta\zeta'\zeta_\beta' + f_3\zeta_\beta\zeta'^2\right]\,, \end{aligned} \tag{5.37}$$

where $\zeta = \zeta_k, \zeta_\beta = \zeta_{\beta k}$ and $\zeta' = \mathrm{d}\zeta/\mathrm{d}N$. The functions f_i are given by

$$\begin{aligned} f_1 &= \frac{5k^2a\epsilon}{3H}(2+\beta^2)(2\eta-3\epsilon)\,, \\ f_2 &= -\frac{10Ha^3\epsilon}{3}\left[4\eta+(1-\beta^2)\epsilon+\left(\frac{\beta^2}{4}-1\right)\epsilon^2\right]\,, \\ f_3 &= -\frac{5Ha^3\epsilon}{3}\left[4\eta+2(\beta^2-1)\epsilon+\left(\frac{\beta^2}{4}-1\right)\beta^2\epsilon^2\right]\,. \end{aligned} \tag{5.38}$$

The last remaining difficulty lies with the early time behaviour of the integrand. At very early times ($N_0 \to -\infty, a \to 0, A \to \infty$) ζ oscillates very rapidly and has a growing amplitude, but the $f_{\rm NL}$integral formally converges. At early times the integrand becomes proportional to

$$\int_{-\infty}^{N} dN\, f(H, \epsilon, \dots) \left(\frac{k}{aH}\right)^n e^{-i(2+\beta)\frac{k}{aH}}\,, \tag{5.39}$$

for some integer n. By rotating slightly into the imaginary plane, $(k/aH) \to (1 - i\delta)(k/aH)$ one can obtain a finite answer independent of the cut-off time. Numerically one cannot integrate to infinity and in it's present form the integral does not converge numerically. To resolve this one can add a damping factor to the integrand (similar to the above procedure) however this tends to systematically underestimate the final integrals and the optimum damping factor δ differs from mode to mode [128, 129].

A better method is to use the early time approximation for ζ and then integrate by parts. We are interested in calculating an integral of the form

$$I = \int_{-\infty}^{N} dN\, f(N)\, \zeta^2 \zeta_\beta\,. \tag{5.40}$$

Using (5.17) we can write $\zeta^2 \zeta_\beta$ at early times as

$$\zeta^2 \zeta_\beta \to \frac{1}{\Gamma}\frac{\mathrm{d}}{\mathrm{d}N}(\zeta^2 \zeta_\beta)\,, \tag{5.41}$$

where

$$\Gamma = -\left[i(2+\beta)\frac{k}{aH} + 3(1 + \epsilon - \eta)\right]. \tag{5.42}$$

Inserting this into (5.40) and integrating by parts yields

$$I \to \left[\frac{f(N)}{\Gamma}\zeta^2\zeta_\beta\right]_{-\infty}^{N} - \int_{-\infty}^{N} dN\, \frac{\mathrm{d}}{\mathrm{d}N}\left(\frac{f(N)}{\Gamma}\right)\zeta^2\zeta_\beta\,. \tag{5.43}$$

The resulting integral is now more convergent than before as $1/\Gamma \to aH/k$. One can repeat the process until the final integrand converges in the limit $a \to 0$ and all divergences are transferred to the boundary term. These divergences can be removed by using the same contour as before, but now the terms vanish for any finite δ. The boundary term evaluated at $N = -\infty$ can then be safely ignored.

To apply this procedure to the calculation of $f_{\rm NL}$we first split the integral into two parts

$$\int_{N_0}^{N_2} dN = \int_{N_0}^{N_1} dN + \int_{N_1}^{N_2} dN\,, \tag{5.44}$$

where N_0 and N_2 are times when $k = A\,aH$ and $k = B\,aH$ respectively with $A \gg 1$ and $B \ll 1$. N_1 is any time when (5.17) is a good approximation for both modes. The late time contribution remains unchanged and we perform the "approximate then integrate by parts" procedure to the early time contribution. The early time contribution, E, then takes the form

$$\begin{aligned} E &= \frac{5Ha^3\epsilon}{3(2+\beta)^3}\left[B_1\Gamma + \cdots + \frac{B_{-4}}{\Gamma^4}\right]\zeta^2\zeta_\beta\Bigg|_{N_1} - \\ &\int_{N_0}^{N_1} dN\,\frac{5Ha^3\epsilon}{12(2+\beta)^3}\left[\frac{A_{-2}}{\Gamma^2} + \cdots + \frac{A_{-6}}{\Gamma^6}\right]\zeta^2\zeta_\beta\,, \end{aligned} \tag{5.45}$$

where A_i and B_i are polynomials of the HSR parameters and β. For example

$$\begin{aligned} B_1 &= (2+\beta)^2\left[(4+\beta(2\beta-3))\,\epsilon - \right. \\ &\left. 2(2+\beta)\eta + \beta\left(1-\frac{\beta^2}{4}\right)\epsilon^2\right]. \end{aligned} \tag{5.46}$$

We omit the full list of the complicated polynomials for brevity. The second term in (5.45) gives a completely negligible contribution to the final value of $f_{\rm NL}$ as it is roughly a factor of Γ^3 smaller and we are in the regime where $\Gamma >> 1$. The early time contribution is therefore given completely by the boundary term in (5.45).

This method was first used in [129]. However the authors choose to focus on particular inflation models such as those with a feature whereas this paper takes a much more general approach. Dealing with the late time divergence from $\zeta^2\zeta'$ also received little attention. The best explanation on how to deal with this is in [130] where the authors demonstrate a fortunate cancellation between the troublesome term and the field redefinition.

Here we explicitly keep all terms to all orders in slow-roll. Most of the computational effort is spent dealing with the oscillatory nature of ζ so not much is gained by a slow-roll approximation. This allows a much broader range of models to be analysed which in turn leads to Monte Carlo treatment in the next section. We do drop the early time integration in (5.45) but this is an approximation relying on the behaviour of ζ in the limit $k \gg aH$, not an explicit slow-roll approximation. Finally, to our knowledge, this is the first time the third order action has been presented in the form of (5.33) and used in a calculation. This form provides a much more efficient way to perform the numerical calculation without having to rely on fortuitous cancellations of terms after the integration.

In summary $f_{\rm NL}$, to a good approximation with respect to the early time oscillatory integral, is given by the following expression

$$\begin{aligned} f_{\rm NL} &= \left[|\zeta|^2\left(|\zeta|^2+2|\zeta_\beta|^2\right)\big|_{N_2}\right]^{-1}\times \\ &\quad \mathcal{I}\left[\zeta^{*2}\zeta^*_\beta\big|_{N_2}\int_{N_1}^{N_2}dN\,\left(f_1\zeta^2\zeta_\beta+f_2\zeta\zeta'\zeta'_\beta+f_3\zeta_\beta\zeta'^2\right)\right. \\ &\quad \left.+\,\zeta^{*2}\zeta^*_\beta\big|_{N_2}\frac{5Ha^3\epsilon}{3(2+\beta)^3}\left[B_1\Gamma+\cdots+\frac{B_{-4}}{\Gamma^4}\right]\zeta^2\zeta_\beta\bigg|_{N_1}\right]. \end{aligned} \tag{5.47}$$

5.4. Results

As a check of our method we have verified that our results converge on super-horizon scales and with respect to early-time integration limits. The first condition is illustrated in Figure 5.1 for a typical random trajectory drawn from the ensemble generated by our method using the end-of-inflation random boundary conditions on the HSRs. A typical trajectory in these ensembles will be deep in the slow-roll regime when modes of interest cross the horizon. The green line is the real part of ζ while the red and blue lines represent the real and imaginary parts of $f_{\rm NL}$as a function of N. $f_{\rm NL}$ oscillates roughly three times quicker than ζ as it is proportional to ζ^3. The real part diverges due to the $k^2a\zeta^3/H$ term discussed previously however it does not contribute to the amplitude of the correlator in the in-in formalism and can be safely ignored. The imaginary part (the value of interest) converges when the mode exits the horizon. The results shown in figure 5.1 does not include the contribution of the boundary term in (5.47) as it contributes only a constant.

The next step is to verify our results do not depend sensitively on the early time cut-off. Figure 5.2 shows the dependence of $f_{\rm NL}$ as the integration is started at earlier and earlier times. The color represents the value of β, our shape parameter for the $\mathbf{k}_1+\mathbf{k}_2+\mathbf{k}_3$ triangle. The value of $f_{\rm NL}$ converges for all shapes when the parameter A, which sets how much smaller than the horizon the mode with the *smallest* k in the triangle $\mathbf{k}_1+\mathbf{k}_2+\mathbf{k}_3$ has to be at the start of integration, is approximately 400. This is larger than what would be required for an accurate calculation of the corresponding power spectrum statistic due to the diverging oscillatory behaviour of the terms contributing to the $f_{\rm NL}$ integration.

It is also important to verify convergence with respect to the choice of integration split point N_1, or cut-off time, introduced in (5.44).The choice is parametrised by the variable X defined by $X = k/aH$, again this condition is imposed on the *smallest* k in the triangle $\mathbf{k}_1+\mathbf{k}_2+\mathbf{k}_3$. $f_{\rm NL}$ as a function of X is shown in figure 5.3. If X is too small, the split point is too close to the time of horizon exit and the early time approximation used in (5.41) will not be valid. If $X \sim A \to \infty$, this is equivalent to (5.37) i.e. doing no regularisation procedure at all. Therefore if X is too large relative to A one would expect the early time contribution to be unable to compensate for the increasingly divergent integral. This is the origin of the noise seen in figure 5.3. There is an optimal region for the value of X which minimises the combined contribution from both sources of numerical error. From figure 5.3 it can be seen that $\ln X \approx 4 - 5$ is a good choice for "folded" shapes $\beta \to 2$ (left-panel). There optimal position for the split-point is somewhat shape dependent as shown in the right-panel of figure 5.3 which shows ten "squeezed" cases for the same HSR trajectory but in both cases for ln $\sim$ 4 the inaccuracies are very small ($\ll 1\%$). For the following we chose the values $\ln A = 6$, $\ln X = 5$, and B, the parameter that sets the required size of the largest k in the $\mathbf{k}_1+\mathbf{k}_2+\mathbf{k}_3$ triangle with respect to the horizon at the end of the integration, is set to 0.01.

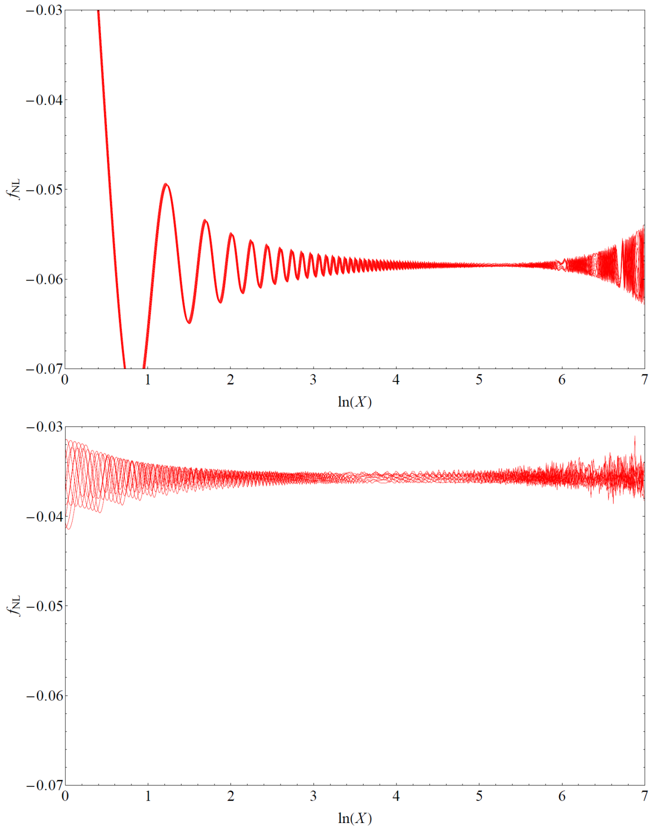

Figure 5.3.: Top Panel: Dependence of $f_{\rm NL}$ on the position of the integral split point parameter X. The ten lines are for $f_{\rm NL}$ from 10 "equilateral" shape configurations ($\beta = [0.95, 1.05]$) for the same HSR trajectory. If the split point is too late, $X = k/aH \to 1$ then the WKB approximation used to calculate the early contribution from the diverging, oscillating integrand breaks down. If the split point is too early then inaccuracies in the numerical integration of the oscillatory function start to dominate. The optimal value of the split point is found to be $\ln X = 4 \to 5$ where the total noise is $\ll 1\%$. Bottom panel: same but for the ten most "squeezed" triangles (i.e. with $\beta = [0.1 - 0.2]$). The optimal value for X is slightly lower in this case but still small for the choice $\ln X = 4 \to 5$.

We generate ensembles of trajectories for two different HSR boundary conditions. The first is the "end-of-inflation" setup where the HSR are drawn from uniform distributions with a given range at the end of inflation defined by the time when $\epsilon = 1$. The second, "early-time" case is one where the HSR, including ϵ in this case, are drawn from uniform distributions at the time when the largest scale of interest is crossing the horizon. For this case ϵ is drawn from the range $[0, 0.4]$ and the system is evolved *back* $\ln A = 6$ e-folds to the start of the mode integration and then forward for the required number of total e-folds to cover horizon exit of all observables scales.

For both cases we used $l_{\rm max} = 4$ and $s = 1.5$ as defined in (5.13) to impose a hierarchical prior. For the "end-of-inflation" ensemble this choice is wide enough to give a proposal distributions in the observables n_s, r, etc. that are wider than the current, parametric constraints obtained from the recent Planck analysis [15]. For each trajectory the number of $e-$folds was chosen from a uniform distribution in the range be $N_{\rm tot} = [60, 80] + \ln A$. The factor of $\ln A$ is important to maintain convergence in the limit of $A \to \infty$ as discussed previously. Each ensemble includes some $\mathcal{O}(10^5)$ trajectories.

In figure 5.4 we show $f_{\rm NL}$ as a function of shape parameter β and overall scale k for a selection 30 trajectories from the "end-of-inflation" ensemble. For this ensemble we expect that at the time when observable quantities are evaluated the HSRs are going to be in the deep slow-roll limit with ${}^i\lambda \ll 1$. This is due to the fact that the system is evolved back from the wide proposal at the end of inflation towards a slow-roll attractor at early times when the observable scales are exiting the horizon. The results for this ensemble should therefore agree with the slow-roll approximations and consistency conditions. Figure 5.4 shows that the scale dependence is very mild and that for trajectories where there is shape dependence $|f_{\rm NL}|$ peaks close to the equilateral configuration $\beta = 1$. It is also known that $f_{\rm NL}$ should be near scale-invariant in the slow-roll limit and peak in the equilateral configuration. In addition, $f_{\rm NL}$ must also satisfy the well known consistency condition in the squeezed limit given by $f_{\rm NL} \approx (5/12)(n_s - 1)$ [70, 95].

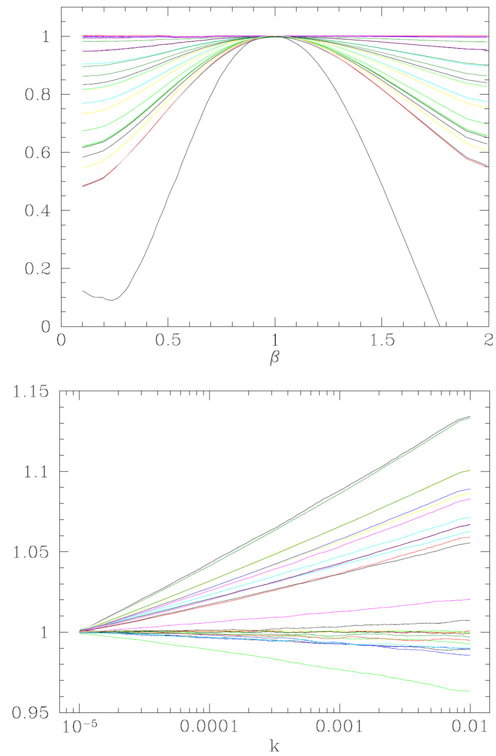

Figure 5.4.: Shape (top) and scale (bottom) dependence of f_{NL} for a selection of trajectories from the "end-of-inflation" boundary condition ensemble. The curves have been normalised with respect to their value at $\beta = 1$ and $k_\star = 10^{-5}(\mathrm{Mpc})^{-1}$ respectively.

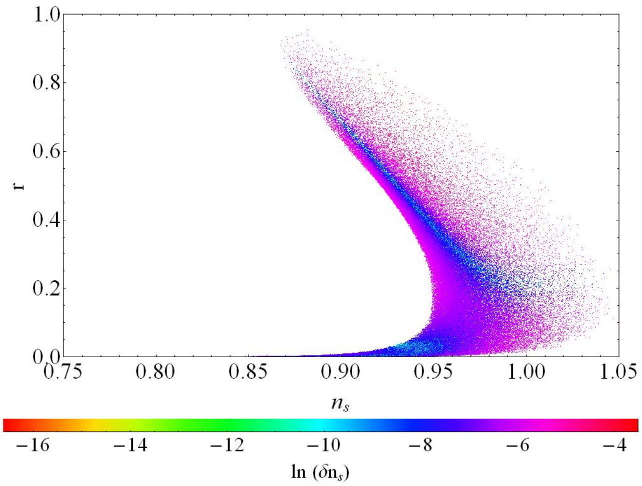

Figure 5.5.: r *vs* n_s scatter plot for 10^5 trajectories generated as part of the HSR ensemble. Colour represents relative difference from the second order slow-roll formula for n_s. $k_* = 10^{-5}(\mathrm{Mpc})^{-1}$. The distribution clearly shows the typical inflationary "attractor" for trajectories with $r > 0$.

As a consistency check we also make scatter plots for the ensembles in the n_s *vs* r and n_s *vs* f_{NL} planes. We do this by plotting the values of n_s, r, and f_{NL} from the *largest* scale for each trajectory in the ensembles. In the slow-roll limit the n_s *vs* r plane should show a clear "inflationary" attractor [77, 78]. The f_{NL} consistency condition should also appear as a strong attractor in the squeezed $\beta \sim 0$ shape case.

Figure 5.5 shows the "end-of-inflation" ensemble scatter plot for n_s *vs* r. The inflationary attractor is clearly visible. The colour coding in the figure depicts the difference between the numerical n_s and second order slow-roll approximation $\bar{n}_s$ given by (5.10) and defined $\delta n_s = |(n_s - \bar{n}_s)/n_s|$. This shows that the numerical and slow-roll results for n_s agree very well when the trajectory lies close to the attractor.

The equivalent of the slow-roll expressions (5.10)-(5.12) for f_{NL} is

$$\bar{f}_{\mathrm{NL}} = \frac{5}{12}\left(\bar{n}_s - 1 + f(\beta)\,\bar{n}_t\right)\,, \tag{5.48}$$

where $\bar{n}_t$ is the slow-roll approximation for the tensor spectral index and $f(\beta)$ is a function of the shape with $f(\beta) \to 0$ as $\beta \to 0$ and $f(\beta) = 5/6$

when $\beta = 1$. Even though this formula was derived only at first order in ϵ, η we used the second order formulae for n_s and n_t. Figure 5.6 shows the trajectories in the n_s *vs* $f_{\rm NL}$ plane for both the squeezed and equilateral. The $5/12\, n_s$ dependence is clear in both cases but the equilateral case has an additional dependence on n_t which dominates when $n_s \to 1$ in analogy with Figure 5.5. The figure also shows the difference between the slow-roll approximation for $f_{\rm NL}$ and the value obtained numerically. The two agree to within a few percent except when $f_{\rm NL} \ll 10^{-2}$.

Figure 5.7 shows what happens to the equilateral $f_{\rm NL}$ distributions in the case where the trajectories are generated using the "early-time" priors on the HSR parameters. In this case, if the proposal ranges for the HSR are wide enough, the largest scales considered will be crossing the horizon when the trajectory is typically still in the out-of-slow-roll regime. At later times the trajectory will typically end up in a slow-roll attractor and the situation will revert to a picture much closer to that seen in figure 5.6. The squeezed distribution remains unchanged but the equilateral case can have $f_{\rm NL}$ values much larger than that allowed by the $5/12\, n_s$ scaling. Typically the value of n_s for the scale where we are sampling $f_{\rm NL}$ is also large but we have filtered the trajectories to include only ones where $0.946 < n_s < 0.976$ at the *smaller* scale $k = 10^{-2}(\mathrm{Mpc})^{-1}$ where observational constraints are much tighter. The filter imposes a severe cut on the trajectories with only a fraction $\sim 10^{-3}$ of trajectories satisfying the constraint on n_s on smaller scales. For this subset of trajectories the power spectrum, on the largest scales, has a strong scale dependence. This may be preferred by observations of the CMB where there are indications of lower than expected power on the largest scales.

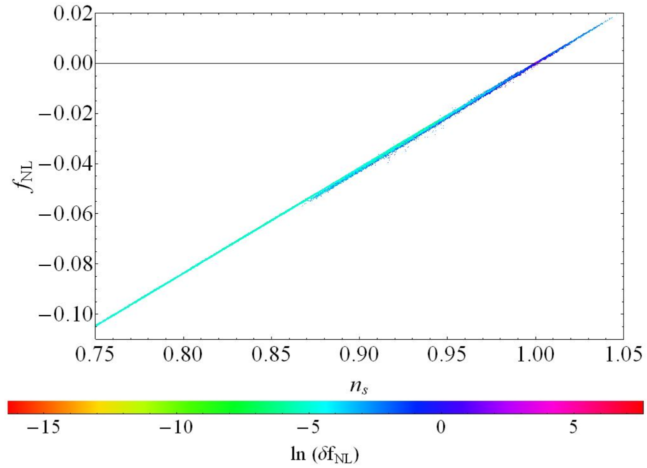

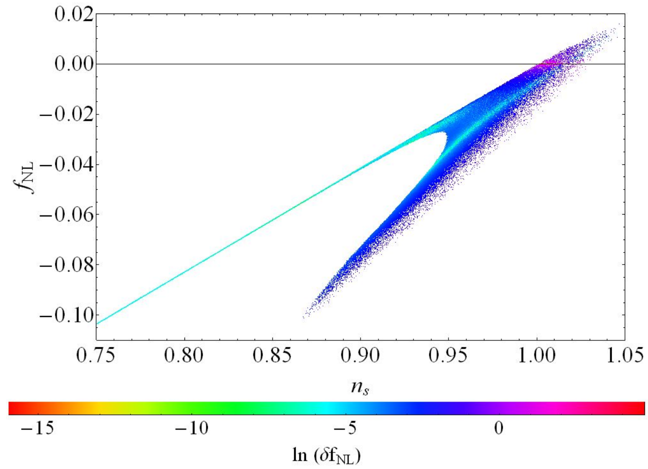

Figure 5.6.: n_s vs $f_{\rm NL}$ scatter plot for 10^5 trajectories generated with "end-of-inflation" priors. The top panel is for the squeezed limit $\beta = 0.1$ and the bottom panel is for the equilateral case $\beta = 1$. The colour scale represents the ln of the relative difference from the slow-roll approximation for $f_{\rm NL}$. The values of n_s and $f_{\rm NL}$ are sampled for a scale corresponding to $k_\star = 10^{-5}(\text{Mpc})^{-1}$.

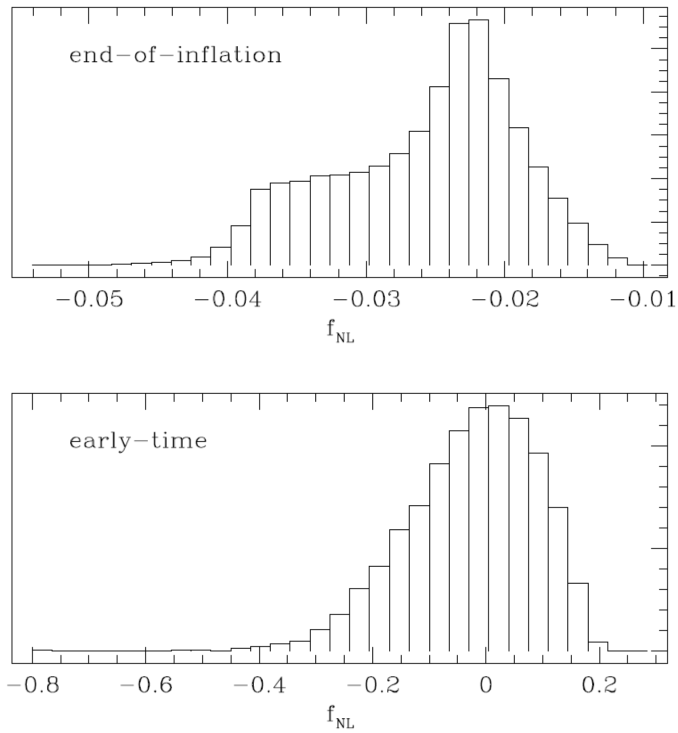

Figure 5.7.: Histogram of $f_{\rm NL}$ values equilateral bispectra for the large scale mode $k_\star = 10^{-5}(\mathrm{Mpc})^{-1}$ in both "end-of-inflation" (top) and "early-time" (bottom) ensembles. Both ensembles have been filtered such that all trajectories have $0.946 < n_s < 0.976$ at the *smaller* scale $k = 10^{-2}(\mathrm{Mpc})^{-1}$ in order to agree roughly with observations at the 2σ level. The "early-time" proposal of HSR parameters allows for significant variation in the parameters while the largest scales are crossing the horizon leading to $f_{\rm NL}$ about an order of magnitude larger than in the other case.

5.5. Discussion

We have outlined a full numerical calculation of the bispectrum of primordial curvature perturbations arising from generalised inflationary trajectories. The bispectrum has been evaluated in terms of a scale dependent $f_{\rm NL}(\mathbf{k}_1, \mathbf{k}_2, \mathbf{k}_3)$. The calculation is valid in the out-of-slow-roll regime as long as the weak coupling limit is maintained. This is of interest in models where there is significant evolution of slow-roll parameters during inflation that can lead to observational features in both power spectrum and bispectrum.

We have explored the generation of inflationary ensembles via the HJ formalism using HSR parameters and calculated the distribution of the bispectrum $f_{\rm NL}$ for various configurations of the $\mathbf{k}_1 + \mathbf{k}_2 + \mathbf{k}_3$ triangle. In doing so we have verified the consistency relation for the squeezed limit and the equilateral configurations in the slow-roll regime. We have shown that, in the out-of-slow-roll limit, $f_{\rm NL}$ equilateral has a much wider distribution due to the scale dependence of the perturbations and has values that are typically an order of magnitude larger than in the slow-roll limit. These types of trajectories can be viable with respect to observations since on smaller scales the perturbations become near scale invariant due to the HSR asymptoting to small values.

The generation of inflationary ensembles including the calculation of the bispectrum will be useful for HSR parameter explorations using future data. $f_{\rm NL}$ observational constraints are currently far from the regime where they can affect the shape of trajectories and consequently add to our knowledge of the shape of the inflaton potential. However future observations may probe a regime that could constrain any out-of-slow-roll features in the trajectories. This would in turn constrain any significant feature in the single field inflation scenario. Even if features do not exist, probing $f_{\rm NL}$ to $\mathcal{O}(10^{-2})$ by a combination of future LSS observations would be a powerful probe of inflationary physics, particularly in scenarios where no tensor perturbations are detected.

6. BICEP's Bispectrum

6.1. Introduction

The recent results from BICEP2 [20], hinting at a detection of primordial B-mode power in the Cosmic Microwave Background (CMB) polarisation, place the inflationary paradigm on much firmer footing. This result, in combination with the PLANCK total intensity measurement [13], imply that primordial perturbations are generated from an almost de-Sitter like phase of expansion early in the Universe's history before the standard big bang scenario.

At first glance there is potential tension between the polarisation measurements made by BICEP2 and PLANCK's total intensity measurements. PLANCK's power spectrum is lower than the best-fit ΛCDM models at multipoles $\ell \lesssim 40$ and BICEP2's high B-mode measurement exacerbates this since tensor modes also contribute to the total intensity. The tension is indicated by the difference in the $r \sim 0.2$ value implied by BICEP2's measurements and the 95% limit of $r < 0.1$ implied by the PLANCK data for ΛCDM models. Many authors have pointed out how the tension can be alleviated by going beyond the primordial power-law, ΛCDM paradigm by allowing running of the spectral indices, enhanced neutrino contributions (see for examples [23–26]) or more exotic scenarios [27]. However the simplest explanation, that also fits the data best, is one where there is a slight change in acceleration trajectory during the inflationary phase when the largest modes were exiting the horizon. This was shown by [24] where a specific model was used to generate a slightly faster rolling trajectory at early times. The effect of such a "slow-to-slow-roll" transition is to result in a slightly suppressed primordial, scalar power spectrum that fits the PLANCK data despite the large tensor contribution required by BICEP2. In [155] the author analyses generalised accelerating, or inflating, trajectories that fit the combination of BICEP2 and PLANCK data and conclude that the suppression is required at a significant level and the best-fit trajectories are all of the form where the acceleration has a slight enhancement at early times.

An alternative explanation is that the B-mode power observed by BICEP2 is not due to foregrounds and is not primordial. This possibility has been discussed by various authors [21,22] who point out that more measurements on the frequency dependence of the signal are required to definitively state whether we have detected the signature of primordial tensor modes. These measurements will be provided in part by the PLANCK polarisation analysis and BICEP2's cross-correlation with further KECK data [20].

If the BICEP2 result stands the test of time then the signal we point out in the analysis below is expected to be present if the simplest models of inflation driven by a single, slow-rolling scalar field are the explanation behind the measurements. In this case a measurement of tensor mode amplitude, or r, is a direct measurement of the background acceleration since $r \sim 16\epsilon$ and the tension between BICEP2 polarisation and PLANCK total intensity measurements implies a change in the acceleration at early times. In turn, the change in acceleration enhances the non-Gaussianity on scales that were exiting the horizon while the acceleration was changing.

In this *paper* we construct a simple toy-model inspired by the best fitting trajectories found in [155] and calculate its bispectrum numerically. At small scales, as one would expect, the non-Gaussianity is small $\mathcal{O}(10^{-2})$ [70, 95] but at large scales, where the scalar power spectrum is suppressed, the non-Gaussianity can be significantly larger, $\mathcal{O}(10^{-1})$. The results are compared against the slow-roll approximation in the equilateral configuration and the squeezed limit consistency relation. Whilst at small scales there is exceptional agreement with the slow-roll approximation, at large scales the results can deviate by up to 10%.

This *paper* is organised as follows. We outline the calculation of the scalar and tensor power spectra in Section 6.2 and summarise the calculation of the bispectrum in Section 8.16. Our results are presented in Section 7.4 and we discuss their implications in Section 7.5.

6.2. Computation of the scalar power spectrum

The calculation is best performed in a gauge where all the scalar perturbations are absorbed into the metric such that $g_{ij} = a^2\,(t)e^{2\zeta(t,\mathbf{x})}\delta_{ij}$ and the inflaton perturbation $\delta\phi(t, \mathbf{x}) = 0$. The primordial power spectrum is then simply given by:

$$\langle \zeta_{k_1} \zeta^{\star}_{k_2} \rangle = (2\pi)^3 \delta^{(3)}(\mathbf{k}_1 + \mathbf{k}_2) P_\zeta(k_1) \,, \tag{6.1}$$

where $\mathbf{k}$ is the Fourier wavevector and $k \equiv |\mathbf{k}|$. The mode $\zeta_k(t)$ satisfies the Mukhanov-Sasaki equation [71, 72]

$$\frac{\mathrm{d}^2 \zeta_k}{\mathrm{d}N^2} + (3 + \epsilon - 2\eta)\frac{\mathrm{d}\zeta_k}{\mathrm{d}N} + \frac{k^2}{a^2 H^2}\zeta_k = 0 \,. \tag{6.2}$$

In the above N is the number of $e-$folds which increases with time or alternatively

$$H = \frac{\dot{a}}{a} = \frac{dN}{dt} \,, \tag{6.3}$$

and ϵ and η are the usual slow-roll variables defined by

$$\epsilon = -\frac{\dot{H}}{H^2}, \qquad \eta = \epsilon - \frac{1}{2H}\frac{d\ln\epsilon}{dt} \,. \tag{6.4}$$

Outside the horizon ζ_k quickly goes to a constant and the power spectrum is then related to the freeze-out value of ζ_k on scales $k \ll aH$

$$P_\zeta(k) = |\zeta_{k \ll aH}|^2 \,. \tag{6.5}$$

The initial conditions for the solutions to (6.2) can be set when the mode is much smaller than the horizon $k \gg aH$ and takes on the Bunch-Davies form [73]

$$\zeta_k \to \frac{1}{M_{\mathrm{pl}}} \frac{e^{-ik\tau}}{2a\sqrt{k\epsilon}} \,, \tag{6.6}$$

where τ is conformal time defined by $\mathrm{d}N/\mathrm{d}\tau = aH$.

An identical calculation can be performed for the tensor power spectrum $P_h(k) = |h_{k \ll aH}|^2$ with h_k satisfying the following differential equation

$$\frac{\mathrm{d}^2 h_k}{\mathrm{d}N^2} + (3 - \epsilon)\frac{\mathrm{d}h_k}{\mathrm{d}N} + \frac{k^2}{a^2 H^2} h_k = 0 \,, \tag{6.7}$$

with initial condition

$$h_k \to \frac{1}{M_{\mathrm{pl}}} \frac{e^{-ik\tau}}{a\sqrt{2k}} \,, \tag{6.8}$$

in the limit where $k \gg aH$. Solving for $P_\zeta(k)$ and $P_h(k)$ numerically we can calculate n_s, r and n_t directly from their definitions:

$$
\begin{aligned}
n_s(k_\star) &= 1 + \left.\frac{\mathrm{d}\ln\left[k^3 P_\zeta(k)\right]}{\mathrm{d}\ln k}\right|_{k=k_\star} \\
r(k_\star) &= 8\,\frac{P_h(k_\star)}{P_\zeta(k_\star)} \\
n_t(k_\star) &= \left.\frac{\mathrm{d}\ln\left[k^3 P_h(k)\right]}{\mathrm{d}\ln k}\right|_{k=k_\star}
\end{aligned}
\tag{6.9}
$$

The factor of 8 comes from how the tensor perturbations are normalised in the second order action.

The above procedure outlines the general calculation of the primordial power spectrum from inflation. In this work we are interested in specifying a background model favoured by the recent Bicep2 + Planck data. In particular we choose a function for ϵ, then η and H are easily obtained by its derivative and integral respectively.

Instead of a direct function of time or N though we specify $\epsilon(x)$ where $x = \ln(k'/k_{\min})$. k' is the mode crossing the horizon at $e-$foldings N ($k' = aH$) and $k_{\min} \sim 10^{-5}(\mathrm{Mpc})^{-1}$ is the largest scale observable today. In addition to being proportional to r this condition allows one to easily specify how the background should evolve in our observational window. For concreteness we require ϵ to be relatively large, but still satisfying the slow-roll limit, at large scales and then to flatten out into another slow-roll regime with a smaller value. To this end we adopt a simple toy-model for ϵ as a function of x

$$
\epsilon = \{\epsilon_1 \tanh\left[(x - x_0)\right] + \epsilon_2\}\,(1 + mx)\ , \tag{6.10}
$$

where the coefficients ϵ_1, ϵ_2, m, and x_0 are chosen to give a final power spectrum with the required suppression and position ($\sim 26\%$ and 1.5×10^{-3} Mpc^{-1} respectively [24]) and $n_s \sim 0.96$ on small scales. Fig. 6.1 shows ϵ and η as a function of N for this toy-model and the resulting power spectra are shown in Fig. 8.9.

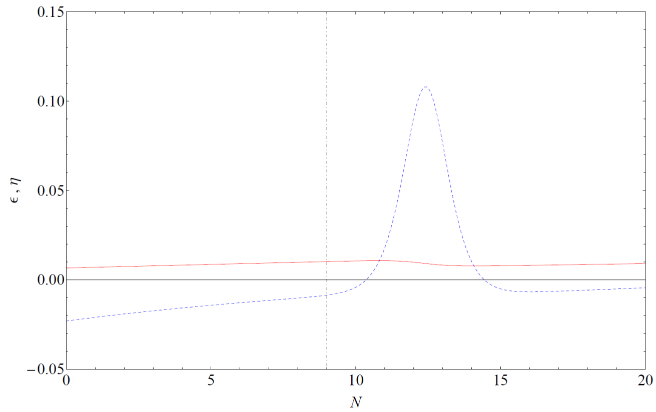

Figure 6.1.: Background functions ϵ (red, solid) and η (blue, dashed) of our toy-model plotted as a function of $e-$folds N. The grey vertical line indicates roughly the time when the first observable mode crosses the horizon.

6.3. Computation of the bispectrum

The largest contribution to primordial non-Gaussianity will come from the bispectrum of the curvature perturbation

$$\langle \zeta_{k_1} \zeta_{k_2} \zeta_{k_3} \rangle = (2\pi)^3 \delta^{(3)}(\mathbf{k}_1 + \mathbf{k}_2 + \mathbf{k}_3) B(k_1, k_2, k_3) \,. \tag{6.11}$$

The quantity that is often quoted in observational constraints is the dimensionless, reduced bispectrum

$$\begin{aligned} f_{\rm NL}(k_1, k_2, k_3) \quad &= \quad \frac{5}{6} B(k_1, k_2, k_3) / \left(|\zeta_{k_1}|^2 |\zeta_{k_2}|^2 + \right. \\ & \qquad \left. |\zeta_{k_1}|^2 |\zeta_{k_3}|^2 + |\zeta_{k_2}|^2 |\zeta_{k_3}|^2 \right) \,, \end{aligned} \tag{6.12}$$

The analytical calculation is much simpler if we consider the equilateral configuration $f_{\rm NL}(k, k, k)$ however this is not a directly observed quantity as the estimator requires $B(k_1, k_2, k_3)$ to be factorizable [97]. This is not true for the general case, which we are considering. However the overall amplitude of the reduced bispectrum gives a good indication of the size of the expected observable $f_{\rm NL}$.

All theories of inflation will produce a non-zero bispectrum. This is simply because gravity coupled to a scalar field is a non-linear theory and will

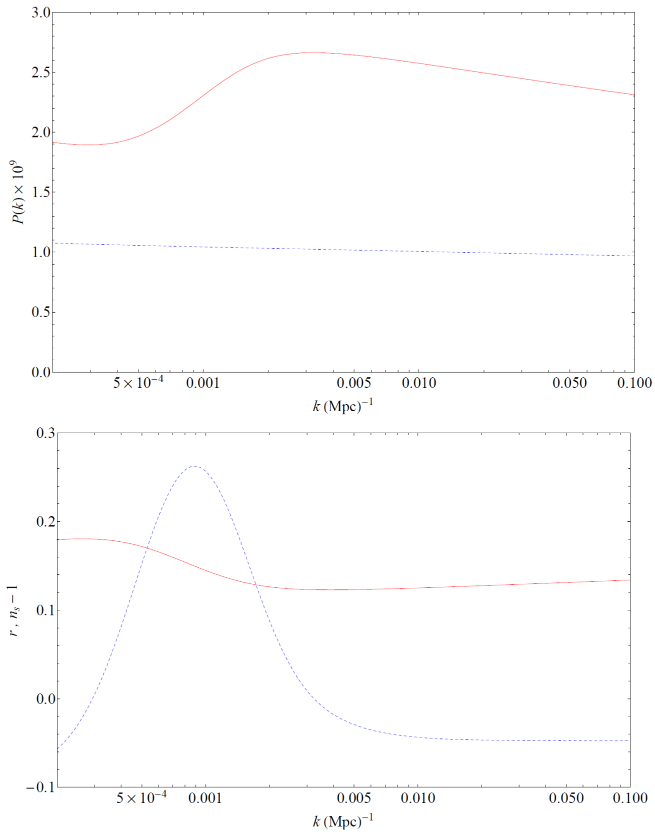

Figure 6.2.: Top: Scalar (red, solid) and tensor (blue, dashed) dimensionless power-spectra. The tensors have been multiplied by a factor of 25 for comparison. Bottom: r (red, solid) and $n_s - 1$ as functions of k. The parameters in the toy-model were chosen to give a good match to the Planck and Bicep2 data.

contain interaction terms for the primordial curvature perturbation $\zeta(t, \mathbf{x})$. These interaction terms will source the bispectrum with the largest contributors coming from tree-level diagrams associated with the cubic interaction terms. The bispectrum can then be calculated using the "in-in" formalism [70, 103, 115], which to tree level becomes

$$\langle \zeta^3(t) \rangle = -i \int_{-\infty}^{t} \mathrm{d}t' \langle \left[\zeta^3(t), H_{\mathrm{int}}(t') \right] \rangle \,, \tag{6.13}$$

where H_{int} is the interaction Hamiltonian associated with the following third order action

$$
\begin{aligned}
S_3 &= \int d^4x\, a^3\epsilon \left[(2\eta-\epsilon)\,\zeta\dot{\zeta}^2 + \frac{1}{a^2}\epsilon\zeta(\partial\zeta)^2 \right. \\
&\quad -(\epsilon-\eta)\zeta^2\partial^2\zeta - 2\epsilon\left(1-\frac{\epsilon}{4}\right)\dot{\zeta}\partial_i\zeta\partial_i\partial^{-2}\dot{\zeta} \\
&\quad \left. +\frac{\epsilon^2}{4}\partial^2\zeta\partial_i\partial^{-2}\dot{\zeta}\partial_i\partial^{-2}\dot{\zeta}\right] ,
\end{aligned} \tag{6.14}
$$

The numerical calculation of the bispectrum is technically challenging and is described in more detail in [1]. Briefly, for the equilateral configuration it requires the calculation of the following integral

$$
f_{\rm NL} = \frac{1}{3|\zeta|^4} \times \mathcal{I}\left[\zeta^{*3}\int_{N_0}^{N_1} dN\,(f_1\zeta^3 + f_2\zeta\zeta'^2)\right] , \tag{6.15}
$$

where $\zeta = \zeta_k$, $\zeta' = \mathrm{d}\zeta/\mathrm{d}N$, and $\mathcal{I}$ represents the imaginary part. The background functions f_i are given by

$$
\begin{aligned}
f_1 &= \frac{5k^2a\epsilon}{H}(2\eta-3\epsilon) , \\
f_2 &= -5Ha^3\epsilon\left(4\eta-\frac{3}{4}\epsilon^2\right) .
\end{aligned} \tag{6.16}
$$

The times N_0 and N_1 correspond to when the mode is sufficiently sub- and super-horizon respectively. For calculating the shape dependence we restrict ourselves to the case of isosceles triangles so we parametrise our modes in the following way. $|\mathbf{k}_1| = |\mathbf{k}_2| = k, |\mathbf{k}_3| = \beta k$. This covers most configurations of interest ($\beta = 0$ is squeezed, $\beta = 1$ is equilateral, $\beta = 2$ is folded) and is simple to interpret.

6.4. Results

For the toy-model given in (6.10) the non-Gaussianity amplitude is plotted in Fig. 6.3. For comparison, as well as a consistency check, we plot the full-numerical calculation (blue-dashed) as well as the the slow-roll approximation (red-solid) which, in the equilateral limit, is given by [70]

$$
f_{\rm NL}(k) = \frac{5}{12}\left(n_s(k) - 1 + \frac{5}{6}n_t(k)\right) . \tag{6.17}
$$

In applying this formula we used the exact values of n_s and n_t given by equations (6.9). As can be seen from Fig. 6.3, if values close to $r \sim 0.2$ are confirmed from polarisation measurements, the non-Gaussianity on large scales are likely to be an order of magnitude larger than expected. This is simply because $r \propto \epsilon$ but on smaller scales ϵ is constrained to be lower by the total intensity measurements. The only way to reconcile the two regimes is by having ϵ change to a lower value at later times and this results in an enhancement of non-Gaussianity being generated as the value is changing. Fig. 6.3 also shows that, even with strong scale dependence, there is remarkable agreement between the full numerical results and the Maldacena formula, with deviations only occurring at the largest scales. Fig. 6.4 shows the complete scale and shape dependence of $f_{\rm NL}$.

6.5. Discussion

Models of inflation that contain a feature causing the background acceleration to change can reconcile Planck and Bicep2 observations of the CMB total intensity and polarisation power spectra. We have shown that these models result in enhanced non-Gaussianity at scales corresponding to the size of the horizon at the time when the acceleration is changing. The level of non-Gaussianity at these scales is an order of magnitude larger than what is expected in the standard case with no feature and is strongly scale dependent.

Whilst the effect was illustrated using a simple toy-model of the background evolution $H(t), \epsilon(t)$, etc, we expect the non-Gaussian enhancement to be present in any model where the acceleration changes relatively quickly in order to fit the Planck and Bicep2 combination. The exact form of non-Gaussianity will obviously be model dependent.

It is not clear that this level of non-Gaussianity will be observable since it corresponds to scales $\ell \sim 2 \to 80$ where there may not be a sufficient number of CMB modes on the sky to ever constrain $f_{\rm NL}$to $\mathcal{O}(10^{-1})$. However cross-correlation with other surveys of large scale structure may help to constrain non-Gaussianity on these scales. In particular it may be possible to detect any anomalous correlation of modes induced by the non-Gaussianity.

The biggest question at this time however is whether or not the claimed detection of primordial tensor modes by Bicep2 is correct. This will be addressed in the near future as the polarisation signal is observed at more frequencies at the same signal-to-noise levels reached by the BICEP2 experiment.

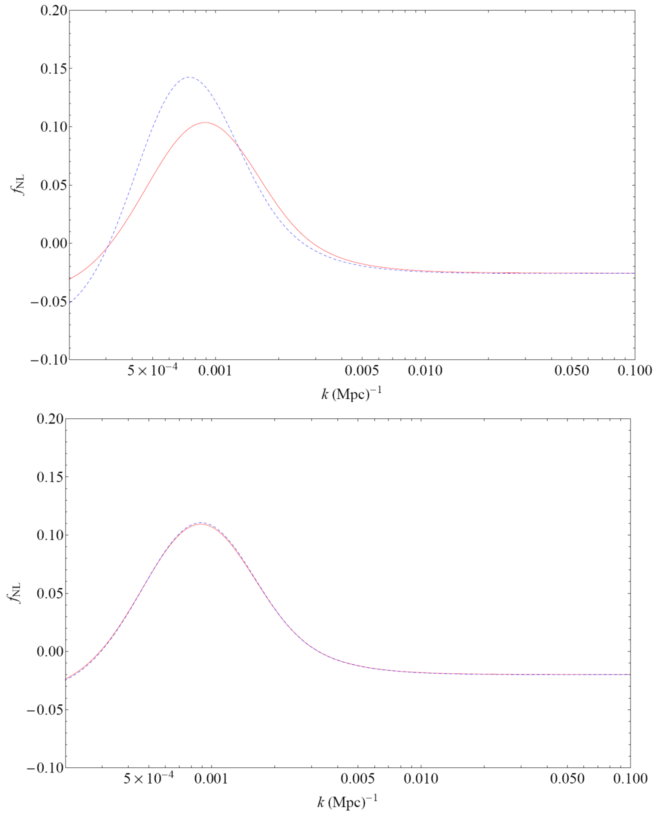

Figure 6.3.: f_{NL}as a function of k for equilateral (top) and squeezed (bottom) configurations. The blue (dashed) curves represents the numerical calculation. The red curves represent the slow roll approximation (6.17) (top) and the consistency condition $5/12(n_s - 1)$ (bottom). It is not possible to calculate the exact squeezed configuration numerically so a configuration with $\beta = 0.1$ was used to approximate the squeezed limit.

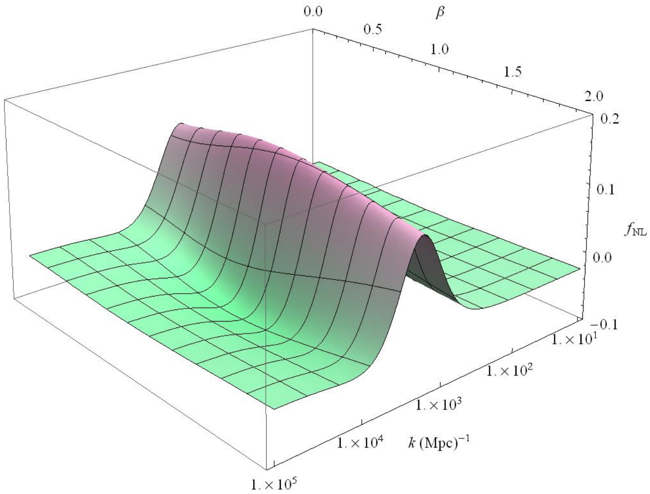

Figure 6.4.: $f_{\rm NL}$as a function of scale k and shape β. There is a mild peak in the equilateral limit, $\beta = 1$. For all shapes the non-Gaussianity peaks around the scales corresponding to the size of the horizon at the time when the background acceleration is changing.

7. Sound-Speed Non-Gaussianity

7.1. Introduction

Current observations of the universe suggest that its density perturbations, to a good approximation, can be considered as a realisation of a correlated Gaussian statistic and are very close to but not exactly scale independent [13, 15, 18, 19]. This scale dependence is characterised by the measurement of the scalar spectral index $n_s = 0.968 \pm 0.006$ [18] which agrees well with the framework of the early universe undergoing a phase of quasi-de Sitter expansion that resulted in correlated, super-horizon scaled curvature perturbations to the background metric. The standard, and the most commonly accepted, explanation for both the origin of the perturbations and the reason for the quasi-de Sitter expansion is the presence of a scalar field known as the inflaton whose potential energy dominates the Hubble equation and whose spatial fluctuations seed the curvature perturbations that later drive all structure formation [29–32, 71, 139–145].

One of the main issues facing efforts aimed at understanding the nature and origin of the inflaton is that many classes of different inflationary models predict observables such as n_s and r that are in broad agreement with observations (see for example [53–55, 60, 61, 105]). With the final analysis of Planck data imminent and the combined Planck-BICEPII/Keck analysis [28] confirming that r was in fact *not* detected in the BICEPII data [20] this situation may become the *status quo* for the foreseeable future. This will be the case unless tensor modes, in the form of $r \neq 0$, are detected by the next generation of sub-orbital Cosmic Microwave Background (CMB) experiments, or, non-Gaussianity is measured. In the former case, discernment between different inflationary models may also require the measurement of the spectral tilt of tensor modes n_t which is challenging due to the cosmic variance effect on the largest scales where the tensor mode signal is clearest.

A detection of non-Gaussianity, in the form of a non-zero bispectrum

[46, 91] or un-connected contributions to higher order moments, may then provide the key to uncovering the origin of the inflaton. Non-Gaussianity is necessarily present in the universe since general relativity is a non-linear theory and even if the inflation were driven by a single, free, scalar field it would still interact with gravity giving rise to a non-zero bispectrum. In general, the non-Gaussianity of less standard models of inflation, particularly ones that predict low tensor contributions with $r \to 0$, tends to be large and potentially measurable in the near future.

The bispectrum is the third-order moment of the curvature perturbation in Fourier space and is expected to be the easiest non-Gaussian signal to measure as it is both the lowest order component in the perturbation and has no Gaussian counterpart. Observational bounds are often quoted in terms of the scale-free amplitude f_{NL} [45], a dimensionless quantity which is typically of order the Slow-Roll (SR) parameter $\epsilon \sim 10^{-2}$ for simple inflationary models [70, 76]. For more complicated models, it is possible to generate a larger f_{NL} while maintaining $n_s \approx 1$ and much effort has been spent constructing such models in the hope that a large non-Gaussianity is detected (see [46, 60, 61, 103, 105, 112] for some examples).

Within the context of single field models, there are a couple of possibilities. One is to break the slow-roll approximation temporarily by introducing a feature [128,129], such as a bump, in the inflaton potential $V(\phi)$. A second is to use a non-canonical kinetic term for the scalar field [60, 103, 112, 156]. This involves adding extra derivatives $\partial_\mu \phi$ as interactions for the field. One physical consequence of this is that the scalar perturbations typically propagate at a new sound speed $c_s < 1$ and it is these models that will be considering in this work.

In this work, for simplicity, we restrict ourselves to the case of a constant $c_s \neq 1$, reserving arbitrary time-dependent sound speeds for future work. We calculate the bispectrum of these models numerically, allowing for high values of $c_s^{-2} - 1$ and combine this with a Monte Carlo approach for sampling inflationary models. We analyse in detail the exact scale and shape dependence of such models, verifying our results by demonstrating the squeezed-limit consistency relation for very small sound speeds and large SR parameters.

This *paper* is organised as follows; In Section 7.2 we summarise the framework and parameters required for the calculation of the bispectrum and briefly discuss the Monte Carlo generation of inflationary trajectories using the Hamilton-Jacobi formalism discussed in more detail in [1]. In Section 7.3.1 we give an overview of the numerical calculation of the power spectrum before proceeding to the calculation of the bispectrum in Section 7.3.2. We summarise our results and consistency checks in Section 7.4 before finally concluding in Section 7.5.

7.2. Monte-Carlo approach to sampling trajectories

This Hamilton-Jacobi (HJ) formalism [77, 78, 149, 150], and its role in numerical inflation was discussed at length in [1] and we refer the reader to that work for an extended discussion. Here we summarise the method. In the HJ formalism the dynamics of an inflating cosmology can be captured entirely by considering the Hubble parameter, $H(\phi)$ as a function of the inflaton field value ϕ and by considering a hierarchy of Hubble Slow-Roll (HSR) parameters defining the hierarchy if derivatives of H with respect to ϕ.

We extend this formalism by introducing an arbitrary, but constant sound speed $c_s \neq 1$. Following [103, 112, 132] we consider actions of the form

$$
\begin{aligned}
S &= \int \mathrm{d}^4x\sqrt{-g}\,\mathcal{L}\,, &(7.1)\\
\mathcal{L} &= \frac{M_{pl}^2}{2}R + P(X,\phi)\,, &(7.2)\\
X &= \frac{1}{2}g^{\mu\nu}\partial_\mu\phi\partial_\nu\phi\,, &(7.3)
\end{aligned}
$$

where M_{pl} is the Planck mass, R is the Ricci scalar, and $g^{\mu\nu}$ is the inverse space-time metric. The Lagrangian density $\mathcal{L}$ in the action above describes a perfect fluid with pressure $P(X,\phi)$ and energy density $\rho = 2XP_X - P$ where $P_X = \partial P/\partial X$. The speed of sound, c_s, is defined as

$$
c_s^2 = \frac{P_X}{\rho_X} = \frac{P_X}{P_X + 2XP_{XX}}\,. \tag{7.4}
$$

For constant c_s this can be treated as a differential equation for $P(X,\phi)$.

Using the initial condition $P(X,\phi) = X - V(\phi)$ when $c_s = 1$ one obtains

$$P(X,\phi) = \frac{2c_s^2}{1+c_s^2} X^{\frac{1}{2}(1+\frac{1}{c_s^2})} - V(\phi)\,. \tag{7.5}$$

The equation of motion for ϕ differs from the canonical case so the original definitions of the HSR parameters in the HJ formalism should be altered accordingly. However, one can still define $e-$foldings N, the Hubble rate $H(t)$ and its *time* derivatives independently of the dynamics of the inflation. That is

$$\begin{aligned} a(N) &= e^N\,, && (7.6)\\ H(N) &= \frac{\dot{a}}{a} = \frac{\mathrm{d}N}{\mathrm{d}t}\,, && (7.7)\\ \epsilon(N) &= -\frac{\mathrm{d}\ln H}{\mathrm{d}N}\,, && (7.8) \end{aligned}$$

where a is the scale factor and overdots denote differentiation with respect to cosmic time t. The HSR parameters can now be defined so that they correspond to the HJ formalism HSR parameters in the limit where $c_s = 1$

$$\frac{\mathrm{d}^l\lambda}{\mathrm{d}N} = [l\epsilon + (1-l)\eta]\ {}^l\lambda - {}^{l+1}\lambda\,, \tag{7.9}$$

where ${}^1\lambda = \eta$, ${}^2\lambda = \xi$.

The values of ${}^l\lambda$ at the end of inflation at $N = N_{tot}$ can be drawn randomly to sample the distribution of consistent inflationary trajectories as described in [1]. The sound speed will not affect the time dependence of these parameters so it will not play an explicit role in the sampling of trajectories . In practice the random sampling is achieved by drawing the following set of parameters with uniform distributions (flat prior) in the intervals

$$ {}^l\lambda = [-1,1]xe^{-sl} \tag{7.10}$$

$$N_{tot} = [60,80] + \ln A\,, \tag{7.11}$$

where $l > 0$. In addition since we draw samples at the end of inflation we fix the value of the $l = 0$ HSR parameter ${}^0\lambda \equiv \epsilon(N_{tot}) = 1$.

In (7.10), x and s are parameters that specify the scaling of the uniform prior range with l and can be used to investigate the dependence of our final results on the assumed priors. The random sampling of N_{tot} represents the uncertainty in the total duration of the post-inflationary reheating phase and the constant A is related to the normalisation of H which will be discussed shortly. Formally one would need to evolve an infinite number of ${}^l\lambda$ parameters to sample the space of all possible $H(N)$ functions. In practice this is not possible and one must truncate the series at some finite order $L_{\max}$. We define $L_{\max}$ such that $L_{\max}$ HSR parameters includes $\epsilon(N)$ e.g. $L_{\max} = 2$ corresponds to $\epsilon(N)$ and $\eta(N)$ with all other ${}^l\lambda = 0$ identically. Once random values of ${}^l\lambda$ have been drawn the entire inflationary trajectory can be obtained by integrating the background equations of motion sufficiently far back in the past to cover the required number of e-foldings given by N_{tot}.

7.3. Computational method

The calculation of the bispectrum relies on the same basic building blocks as the calculation of the primordial power spectrum. In addition the bispectrum is often compared to the spectral tilt of the power spectrum and the squeezed limit consistency condition is a valuable tool for checking the numerical method. We therefore give a brief review the calculation of the power spectrum as the first step in the numerical calculation of the bispectrum.

7.3.1. Computation of the power spectrum

We choose a gauge where the inflaton perturbation $\delta\phi(t, \mathbf{x}) = 0$ and the spatial metric is given by $g_{ij} = a^2(t)e^{2\zeta(t,\mathbf{x})}\delta_{ij}$. This defines the comoving curvature perturbation $\zeta(t, \mathbf{x})$. The primordial power spectrum of the curvature perturbation is then

$$\langle\zeta_{k_1}\zeta^*_{k_2}\rangle = (2\pi)^3\delta^{(3)}(\mathbf{k}_1 + \mathbf{k}_2)P_\zeta(k_1)\,, \tag{7.12}$$

where $\mathbf{k}$ is the wavevector of the Fourier mode and $k = |\mathbf{k}|$. These modes satisfy the Mukhanov-Sasaki equation [71, 72] which, with our choice of variables becomes

$$\frac{\mathrm{d}^2\zeta_k}{\mathrm{d}N^2} + (3+\epsilon-2\eta)\frac{\mathrm{d}\zeta_k}{\mathrm{d}N} + \left(\frac{c_s k}{aH}\right)^2 \zeta_k = 0\,. \tag{7.13}$$

To obtain the power spectrum we simply require the freeze-out value of ζ_k when the mode crosses the sound-horizon, i.e.

$$P_\zeta(k) = |\zeta|^2\big|_{c_s k \ll aH} \tag{7.14}$$

notice that for theories where the speed of sound and light are not equivalent the horizon set by the speed of sound is the relevant scale beyond which freeze-out occurs.

We apply the usual Bunch-Davies initial conditions [73] when the mode is deep inside the sound-horizon

$$\zeta_k \to \frac{1}{2M_{pl}a}\sqrt{\frac{c_s}{k\epsilon}}e^{-ic_s k\tau}\,, \tag{7.15}$$

where τ is conformal time defined through $\mathrm{d}N/\mathrm{d}\tau = aH$.

We impose initial conditions (7.15) at different e-folds for each mode k. This ensures all modes are sufficiently deep inside the sound-horizon at the start of the forward integration of (7.13). The starting e-folds, N_k, for mode with wavenumber k is set by requiring that $c_s k = A\,aH(N_k)$ where $A \gg 1$. In practice this means that the integration is started at successively later times as k increases. This avoids unnecessary computational steps at smaller scales.

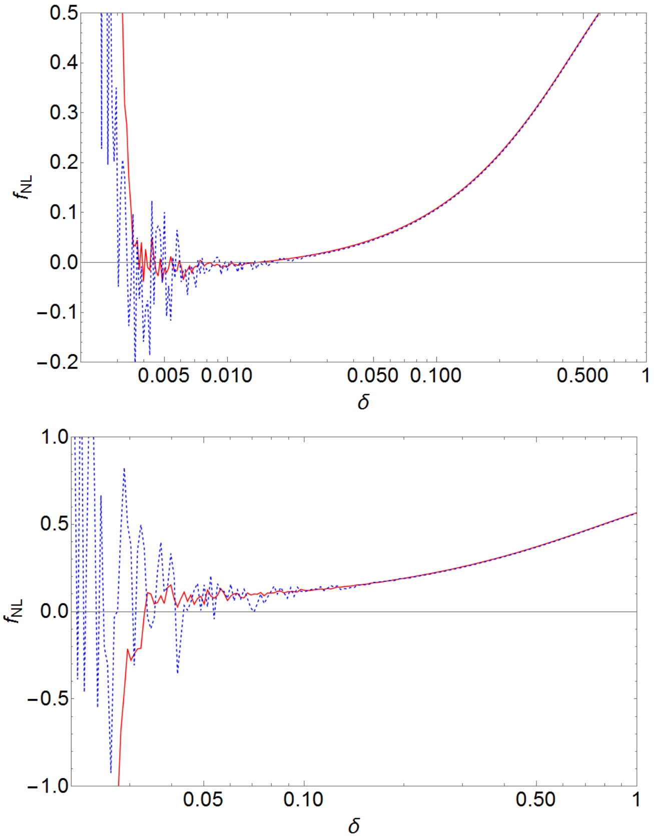

Figure 7.1.: Dependence of f_{NL} on the damping factor δ when $n = 1$ for squeezed (top) and folded (bottom) configurations. For this trajectory $c_s^{-2} = 3$. The red-solid and blue-dashed lines show $k_{min} = 10^{-5}\,(\mathrm{Mpc})^{-1}$ and $k_{max} = 10^{-2}\,(\mathrm{Mpc})^{-1}$ respectively. For large δ the damping factor is too large affecting the horizon crossing behaviour and the oscillations provide no contribution, producing a smooth curve. For small δ the oscillations are not sufficiently suppressed producing noise. Ideally f_{NL} should converge with decreasing δ in some sense to its true value before the noise begins to dominate. There is an indication of this in the right panel at $\delta \sim 0.1$. Unfortunately for the squeezed limit, the amplitude of f_{NL} is too small relative to the noise to extract any reasonable result. To make matters worse, depending on the shape the optimum δ changes by an order of magnitude. Also note noise begins at larger δ for larger k.

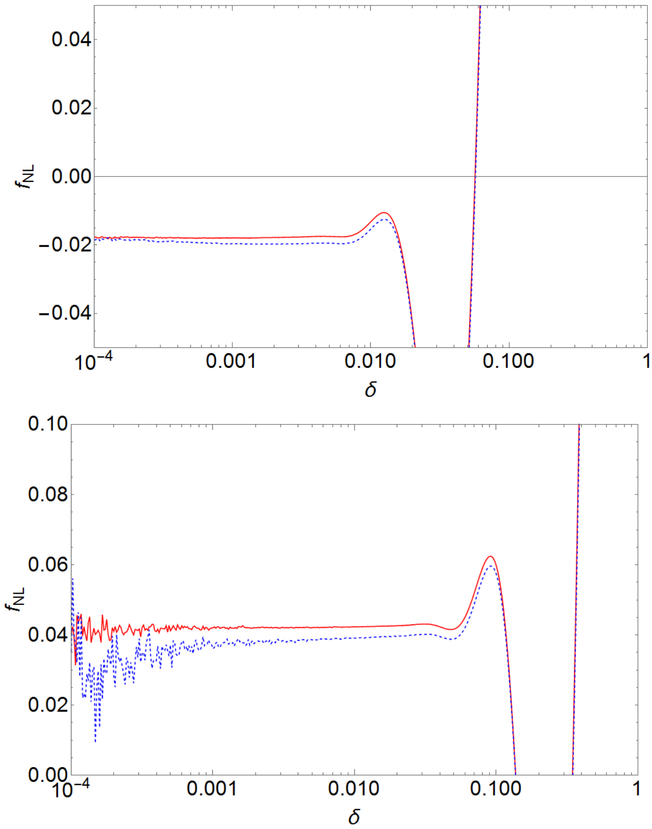

Figure 7.2.: Dependence of $f_{\rm NL}$ on the damping factor δ when $n = 3$ for squeezed (top) and folded (bottom) configurations. For this trajectory $c_s^{-2} = 3$. The red-solid and blue-dashed lines show $k_{min} = 10^{-5}\,(\mathrm{Mpc})^{-1}$ and $k_{max} = 10^{-2}\,(\mathrm{Mpc})^{-1}$ respectively. By choosing $n > 1$ the suppression is weighted more towards the early time oscillations and less on the horizon crossing time. Practically this pushes the noise back to very small values of δ allowing $f_{\rm NL}$ to converge to its true value. The acceptable range of δ is also much wider solving the shape dependence problem. One could choose $n \gg 1$ but most of the time $c_s k/aH > 1$. Therefore to prevent damping at horizon crossing δ must be reduced to compensate and this method can only be pushed so far. In practice we found $n = 3$ to be sufficient. Note for large k the noise still arises at larger δ.

Assuming $H(N)$ varies slowly enough, each mode will evolve for roughly $\ln A$ e-folds before they cross the sound-horizon and freeze out. The earliest mode of interest to freeze out will be $k_{\rm min}$ so we choose $N_{k_{\rm min}} = 0$, i.e. $N = 0$ is defined such that $c_s k_{\rm min} = A\, aH(N = 0)$ and we then apply (7.15) to this mode. This means the $k_{\rm min}$ mode will cross the sound-horizon at $N_c \approx \ln A$ and we can then use the standard analytical result relating H to the amplitude of the power spectrum to normalise H. In practice, during the backwards integration of the HSR parameters, we apply a normalisation condition on H such that

$$H(N_c) = 2\pi\sqrt{2\, c_s \epsilon(N_c)} A_s M_{pl}\,, \tag{7.16}$$

where A_s is conventional the normalisation of the dimensionless primordial curvature power spectrum. In the usual power law convention for the form of the power spectrum A_s is employed as

$$k^3 P_\zeta(k) = A_s^2 \left(\frac{k}{k_{min}}\right)^{n_s - 1} . \tag{7.17}$$

A similar procedure can be carried out for the calculation of the gravitational wave spectrum which is unaffected by c_s. The analogues of (7.13) and (7.15) are are identical to the standard case with $c_s = 1$

$$\frac{\mathrm{d}^2 h_k}{\mathrm{d}N^2} + (3-\epsilon)\frac{\mathrm{d}h_k}{\mathrm{d}N} + \left(\frac{k}{aH}\right)^2 h_k = 0\,, \tag{7.18}$$

$$h_k \to \frac{1}{M_{pl}}\frac{e^{-ik\tau}}{a\sqrt{2k}}\,. \tag{7.19}$$

A complication that arises due to the sound and light horizon not being the same is that scalar and tensor modes freeze out at different times so one must be sure that the Bunch-Davies conditions are applied when both modes are sufficiently deep inside their respective horizons. In principle the power spectrum must converge in the limit $A \to \infty$ therefore the answer should not depend on whether the Bunch-Davies conditions are applied earlier to one mode with respect to another as long as both modes are sufficiently deep inside their respective horizons. In practice this means nothing needs to be changed. If $c_s k = A\, aH$ then we know $k \geq A\, aH$ as $c_s \leq 1$ so the tensor mode is even deeper inside its respective horizon than the scalar mode is. The only concern is a penalty to computational efficiency as the modes become highly oscillatory when they deep within their horizon.

With all the integration constants fixed, the full set of differential equations (7.6)-(7.9), (7.13) and (7.18) can be integrated until both the scalar and tensor modes are well outside the sound and light horizons respectively. This requirement can be parametrised by a constant $B \ll 1$. Following the same argument, if $k = B\,aH$, we have $c_s k \leq B\,aH$ as $c_s \leq 1$. In summary we integrate the mode equations from a time such that $c_s k = A\,aH$ until $k = B\,aH$ with $A \gg 1$ and $B \ll 1$. When calculating the bispectrum (for isosceles triangles) we have a third horizon to consider for the squeezed/folded mode. Similar arguments can be made and one should take care to ensure all relevant modes exit their horizons and satisfy the relevant initial conditions. we have We found the bispectrum to converge when $A \sim 400$ and $B \sim 1/100$. Higher values of A significantly increased the computation time due to the oscillatory nature of the mode functions while providing no real benefit. Smaller values of B did not affect the accuracy or computation time.

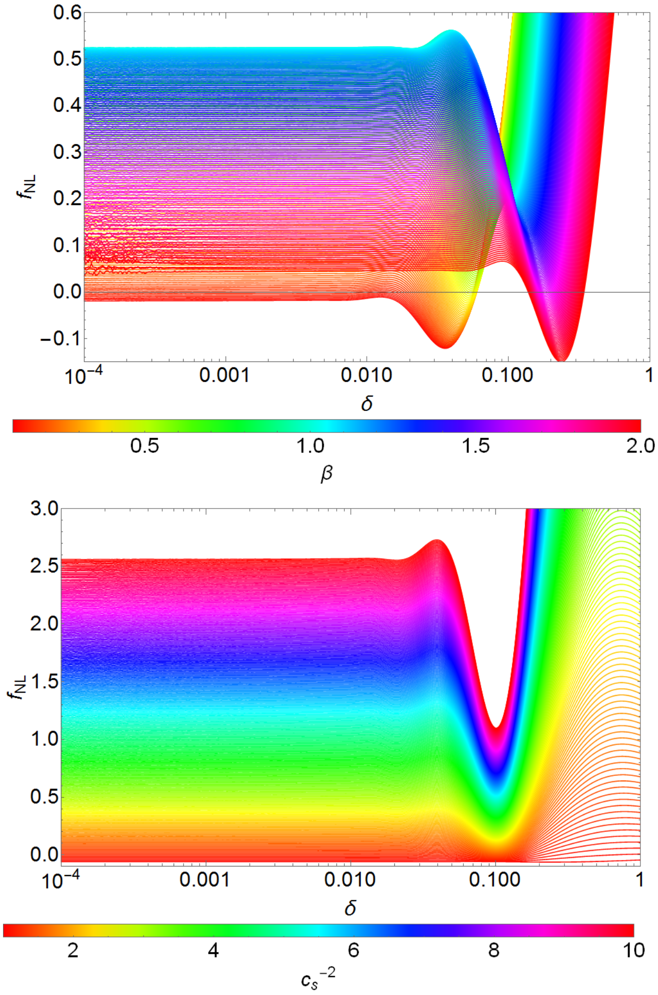

Figure 7.3.: Dependence of $f_{\rm NL}$ on δ on shape and sound speed for the smallest scale $k = k_{\rm max} = 10^{-2}\,({\rm Mpc})^{-1}$. The optimum delta occurs when the relevant curve has converged. The top panel shows how the δ dependence varies for each shape evaluated at $c_s^{-2} = 3$. There is a mild shape dependence in the optimum δ where squeezed triangles require smaller δ values. As a consequence, noise from folded configurations occurs at larger values of δ so the optimum δ must lie between these two cases. The bottom panel shows how the δ dependence varies with sound speed dependence evaluated in the equilateral limit. There is remarkably little dependence on c_s even at very small sound speeds.

With the scalar and tensor power spectra in hand, the observables n_s and r can be calculated directly following their definitions, either as a function of scale k or at a specific "pivot" scale $k_\star$ for comparison with conventional models

$$
\begin{aligned}
n_s(k_\star) &= 1 + \left.\frac{\mathrm{d}\ln\left(k^3 P_\zeta(k)\right)}{\mathrm{d}\ln k}\right|_{k=k_\star}, \qquad (7.20)\\
r(k_\star) &= 8\frac{P_h(k_\star)}{P_\zeta(k_\star)}, \qquad (7.21)
\end{aligned}
$$

where the factor of 8 in the definition of r arise from the definition of the tensor perturbations and from the fact that two independent polarisations contribute to the total power.

7.3.2. Computation of the bispectrum

The bispectrum of ζ is the simplest, lowest-order moment, where we expect to see deviations from a pure Gaussian statistic. It corresponds to a tree-level three-point vertex for an interacting quantum field and will be the most dominant form of non-Gaussianity as higher order moments are expected to be suppressed by higher order terms in both the HSR parameters and level of curvature perturbations with $A_s^{1/2} \sim 10^{-5}$. In the isotropic limit it reduces to a function of three variables, the magnitudes of the wavevectors $\mathbf{k}_1$, $\mathbf{k}_2$, and $\mathbf{k}_3$ making up the allowed, closed triangles in Fourier space

$$
\langle \zeta_{k_1}\zeta_{k_2}\zeta_{k_3}\rangle = (2\pi)^3\delta^{(3)}(\mathbf{k}_1+\mathbf{k}_2+\mathbf{k}_3)B(k_1,k_2,k_3)\,, \qquad (7.22)
$$

where the delta function imposes the closed triangle condition due to isotropy. We define the reduced, dimensionless, scale and shape dependent bispectrum as

$$
\begin{aligned}
f_{\mathrm{NL}}(k_1,k_2,k_3) = 5B(k_1,k_2,k_3)/\\
6\left(|\zeta_{k_1}|^2|\zeta_{k_2}|^2 + |\zeta_{k_1}|^2|\zeta_{k_3}|^2 + |\zeta_{k_2}|^2|\zeta_{k_3}|^2\right)\,, \qquad (7.23)
\end{aligned}
$$

This is different to the usual f_{NL}, scale free, amplitude for the bispectrum quoted in the literature [45].

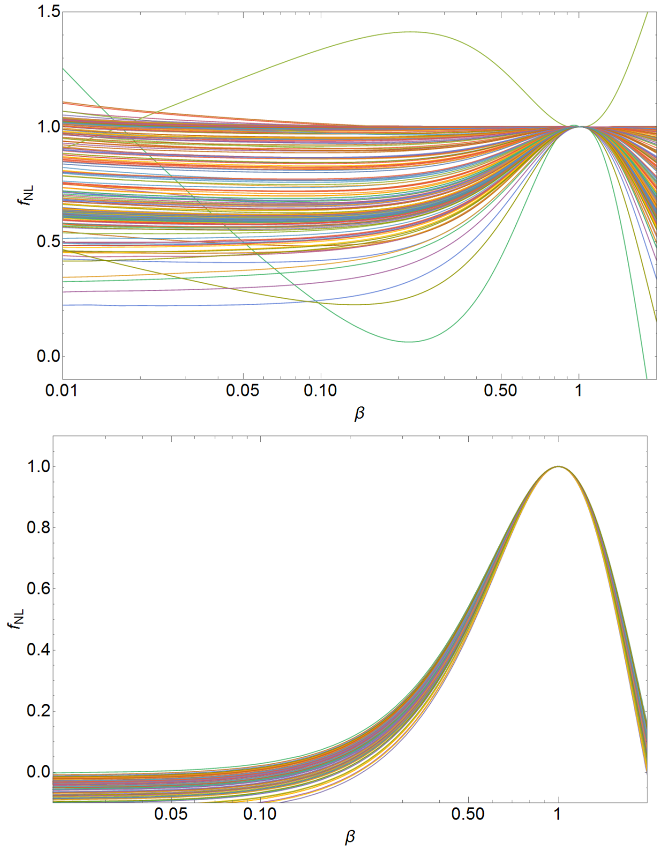

Figure 7.4.: Shape dependence of $f_{\rm NL}$ for several trajectories evaluated at $c_s^{-2} = 1$ (top) and $c_s^{-2} = 3$ (bottom). All values of $f_{\rm NL}$ are normalised to their value at $\beta = 1$. Single field inflation models generically peak in the equilateral limit but because they must follow the consistency relation in the limit $\beta \to 0$ their β dependence is much sharper.

The weighting introduced in the definition of $f_{\rm NL}$ (7.23) is known as the "local" weighting. Other definitions are used in the literature depending on the expected shape dependence of the signal. When observational constraints are obtained from data, such as with Planck [19] the various choices of weighting are used to define limits on *different* types of $f_{\rm NL}$. These include equilateral and orthogonal weightings. The limits reported in [19] are $f_{\rm NL}^{\rm local} = 0.8 \pm 5.0$, $f_{\rm NL}^{\rm equil} = -4 \pm 43$, $f_{\rm NL}^{\rm ortho} = -26 \pm 21$.

The most dominant contribution to the bispectrum comes from (7.1) expanded to third order in ζ. Following [103, 112] the third-order action for single field inflation with a constant sound speed c_s is

$$
\begin{aligned}
S_3 \;=\; & M_{pl}^2 \int \mathrm{d}^4x \left[\frac{2a^3\epsilon}{3Hc_s^2}\left(\frac{1}{c_s^2} - 1\right)\dot{\zeta}^3 \right. \\
& + \frac{a^3\epsilon}{c_s^2}\left(\frac{2\eta - \epsilon}{c_s^2} + 3\left(1 - \frac{1}{c_s^2}\right)\right)\zeta\dot{\zeta}^2 \\
& + \frac{a\epsilon}{c_s^2}(\epsilon + 1 - c_s^2)\zeta(\partial\zeta)^2 + \frac{a\epsilon}{c_s^2}(\eta - \epsilon)\zeta^2\partial^2\zeta \\
& \left. - \frac{2a^3\epsilon^2}{c_s^4}\left(1 - \frac{\epsilon}{4}\right)\dot{\zeta}\partial_i\zeta\partial_i\partial^{-2}\dot{\zeta} + \frac{a^3\epsilon^3}{4c_s^4}\partial^2\zeta\partial_i\partial^{-2}\dot{\zeta}\partial_i\partial^{-2}\dot{\zeta}\right] .
\end{aligned}
\tag{7.24}
$$

Section III.B of [1] discussed why the action is written in the form (7.24) in order to deal with apparent divergences and we refer the reader to that work for further detail. A $c_s \neq 1$, and indeed, an arbitrary time-dependant c_s provides no further complications in dealing with the third-order action.

The "In-In formalism" [70, 103, 112] is used to calculate the bispectrum and ultimately $f_{\rm NL}$. Using (7.24) to define an interaction Hamiltonian and treating $\zeta(t, \mathbf{x})$ as a scalar field with canonical commutation relations, the bispectrum can be reduced to a single integral over N.

$$
B(k_1, k_2, k_3) = \mathcal{I}\left[\zeta_1^\star\zeta_2^\star\zeta_3^\star \int_{N_0}^{N_1} \mathrm{d}N \; Z(N)\right] . \tag{7.25}
$$

Here $\mathcal{I}[z]$ denotes the imaginary part of the imaginary number z. N_0 and N_1 represent times when the largest and smallest scales are sufficiently deep inside and far outside the sound-horizon respectively, using the same A and B parameters as described above. $Z(N)$ implicitly depends on the shape and scale of the triangle but the function arguments have been omitted for brevity.

We now specialise to the case where $k_1 = k_2 = k$ and $k_3 = \beta k$ where $0 < \beta \leq 2$. This simple parametrisation covers many cases of interest. The squeezed, equilateral, and folded limits correspond to $\beta = 0, 1$ and 2 respectively. $Z(N)$ then takes on the following form:

$$\begin{aligned}
Z(N) &= \frac{5Ha^3\epsilon}{3c_s^2}\left(f_1\zeta'^2\zeta'_\beta + f_2\zeta^2\zeta_\beta + f_3\zeta\zeta'\zeta'_\beta + f_4\zeta'^2\zeta_\beta\right)\,, \\
f_1 &= 4u\,, \\
f_2 &= \left(2+\beta^2\right)\left(\frac{c_s k}{aH}\right)^2\left(u + \frac{1}{c_s^2}(2\eta - 3\epsilon)\right)\,, \\
f_3 &= 12u - \frac{2}{c_s^2}\left(4\eta + (1-\beta^2)\epsilon + \left(\frac{\beta^2}{4} - 1\right)\epsilon^2\right)\,, \\
f_4 &= 6u - \frac{1}{c_s^2}\left(4\eta + 2(\beta^2 - 1)\epsilon + \left(\frac{\beta^2}{4} - 1\right)\beta^2\epsilon^2\right)\,,
\end{aligned} \tag{7.26}$$

where $\zeta = \zeta_k$, $\zeta' = \mathrm{d}\zeta/\mathrm{d}N$, $\zeta_\beta = \zeta_{\beta k}$ and $u = 1 - c_s^{-2}$. At early times in the limit $A \to \infty$, $|Z(N)| \to \infty$. However we deform the integration contour by a small, imaginary component $i\delta$ so that the oscillations arising from (7.15) become exponentially suppressed. This is the usual choice of contour one makes when calculating interacting correlation functions. In this limit (7.15) becomes

$$\zeta_k \to \lim_{\delta\to 0}\frac{1}{2M_{pl}a}\sqrt{\frac{c_s}{k\epsilon}}e^{-ic_s k(1+i\delta)\tau}\,, \tag{7.27}$$

as $\tau \to -\infty$ and the integral converges at very early times.

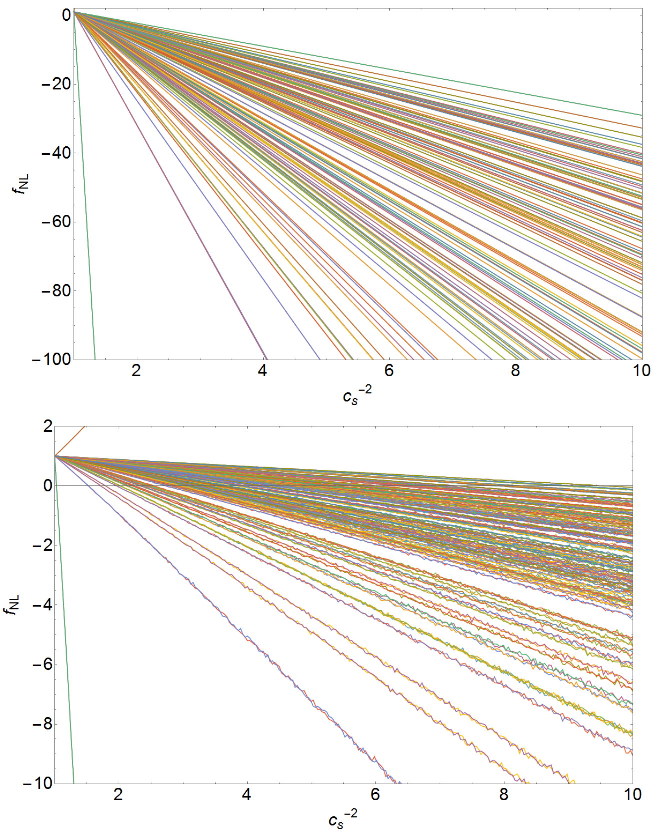

Figure 7.5.: c_s dependence of $f_{\rm NL}$ for several trajectories evaluated at $\beta = 1$ (top) and $\beta = 0.1$ (bottom). All values of $f_{\rm NL}$ are normalised to their value at $\beta = 1$. For equilateral triangles the β dependence is much stronger. In the squeezed limit the c_s dependence becomes much smaller but remains non-zero.

Regulating the integral

To calculate the bispectrum we integrate (7.25) numerically. Analytically, after performing the integral, one could take the limit $\delta \to 0$ to obtain an answer that is well behaved. Unfortunately this is not possible numerically and gives rise to large errors. We cannot integrate over an infinite range in time, i.e. from $A = \infty$, $a(N) = 0$ or $N = -\infty$, so there will always be a sharp integration cutoff at very early times. Because of this sharp cutoff, the oscillations in the integrand result in large fluctuations in the final answer even though they should cancel out if the integration constant is formally extended to $-\infty$.

A solution o this problem is to add an exponential damping factor similarly to the one introduced in (7.27). This was the first approach taken by Chen *et. al.* in [128]. However there are some issues with this method. Firstly the amplitude of the integrals tend to be suppressed resulting in an underestimation of the bispectrum. In addition, the optimal value for the damping factor δ needs to be fine tuned for each scale considered [128].

An alternative method exists which which does not suffer from these issues. It was first used in [129] and then expanded on in [1]. We refer the reader to [1] for the details. The method splits the integral into two parts at an arbitrary split point defined by $c_s k = XaH$. X needs to be large enough for (7.15) to be a good approximation for all three modes. Some integration by parts is performed then X is chosen to minimise the error on the bispectrum. Unfortunately this method does not work for $c_s \neq 1$ because of the new ζ'^3 term. The method still prevents the contributions from the oscillations at early times from diverging but the ζ'^3 term still introduces a large oscillatory signature to the final integral. We therefore adopted the first method employing an improved exponential damping factor

$$Z(N) \to Z(N) e^{-\delta\left(\frac{c_s k}{aH}\right)^n}, \tag{7.28}$$

in the numerical integration.

Fig. 7.1 shows the dependence of f_{NL} on the suppression factor δ for $n = 1$ in both the squeezed and folded limits. For this figure, and all the other δ dependence figures, a random trajectory was taken with $s = 1.5$, $x = 1$ and $L_{\max} = 4$, as defined in (7.10). We see that if δ is too small, the early time oscillations are not sufficiently suppressed producing a large amount of noise. This noise is exaggerated for large values of k. Secondly, if δ is too large, the damping factor will interfere with the time dependence around the time of horizon crossing. This is the most dominant contribution to the integral so it will no longer be a good approximation to the bispectrum. For this choice of $n = 1$ it is hard to justify an optimal value of δ where f_{NL} has converged.

Another issue is that the optimal δ depends on the shape of the triangle. Indeed, between the folded and squeezed cases the optimal δ drops by an order of magnitude. This dependence can be reduced by adjusting the value of n. $c_s k/aH$ is very large at early times and of order 1 during horizon crossing. Therefore increasing n will give stronger weighting to the damping factor at early times, while interfering less with the horizon crossing time. We found $n = 3$ to give the best results. The δ dependence for $n = 3$ is shown in Fig. 7.2.

Most of the residual noise arises from large k modes, particularly in the folded configuration. In contrast most results calculated in the equilateral configuration are relatively clean. Fig. 7.3 shows how the δ dependence varies with shape factor β and c_s in the equilateral configuration. Fig. 7.2 motivates a choice of $\delta \approx 0.005$ and we use this suppression factor along with $n = 3$ for the remainder of our calculations.

Figure 7.6.: Monte Carlo plots for $c_s = 1$ (left) and $c_s^{-2} = 3$ (right). From top to bottom the shape configurations are evaluated in the squeezed, equilateral and folded limits respectively. The red-dashed line represents the consistency relation $5(n_s - 1)/12$. The colour of each trajectory illustrates the scale dependence of the bispectrum, $n_{f_{\rm NL}}$. For squeezed $c_s^{-2} = 3$ (top-right) it was necessary to reduce $\beta = 0.02$ to recover the squeezed limit as opposed to $\beta = 0.1$ for the $c_s = 1$ case. This increased computation time by roughly an order of magnitude.

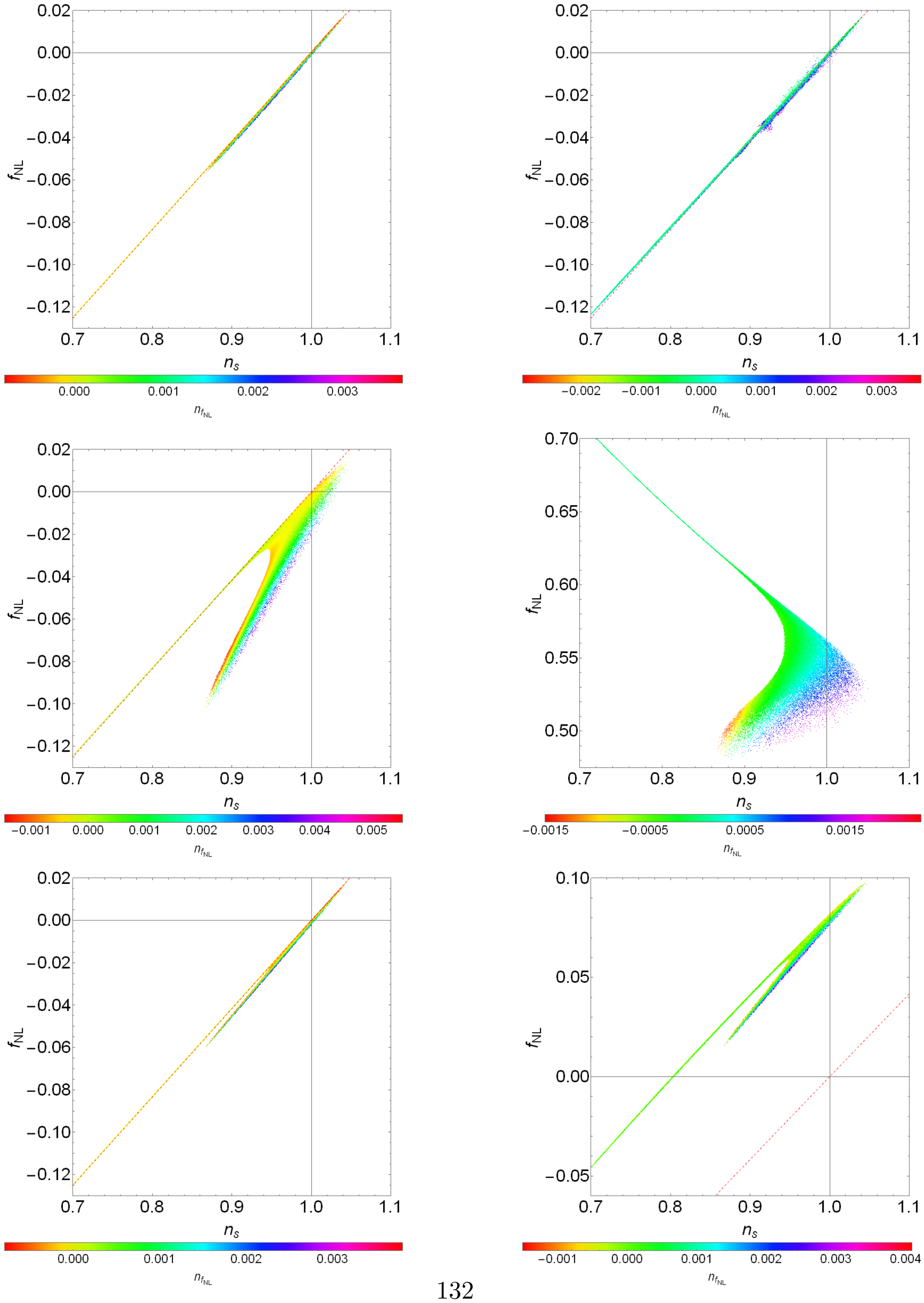

7.4. Results

One way to test our numerical results for robustness and consistency is by comparison with the the squeezed limit consistency relation [70, 95]. For *any* single field inflation model the following limit must hold

$$\lim_{k_3 \ll k_1, k_2} -\langle \zeta_{k_1} \zeta_{k_2} \zeta_{k_3} \rangle \to (2\pi)^3 \delta^{(3)}(\mathbf{k}_1 + \mathbf{k}_2 + \mathbf{k}_3)\,(n_s - 1)\, P_{k_1} P_{k_3} \tag{7.29}$$

or in our notation

$$\lim_{\beta \to 0} f_{\mathrm{NL}} \to \frac{5}{12}\,(n_s - 1)\ . \tag{7.30}$$

It is important to emphasise here that this holds for all single field models independent of the value of c_s or the prior we choose for the initial conditions of the background trajectories. However increasing the value of c_s or the HSR parameters typically increases the amplitude of f_{NL} therefore we don't necessarily expect all models to tend to the squeezed limit at the same rate. For example $\beta = 0.1$ might be "squeezed enough" for low values of c_s but not for higher values. We first analyse the shape and sound speed dependence of the trajectories, elaborating on the consistency relation in section 7.4.3. Unless stated otherwise, the trajectories are taken from a prior with $x = 1, s = 1.5$ and $L_{\max} = 4$.

7.4.1. Shape dependence

Fig. 7.4 compares the shape dependence of trajectories evaluated at $k_{\min} = 10^{-5}\,(\mathrm{Mpc})^{-1}$ normalised to their equilateral values. As expected, for trajectories with shape dependence $|f_{\mathrm{NL}}|$ peaks in the equilateral configuration. As c_s reduces, the amplitude of $|f_{\mathrm{NL}}|$ typically increases but the trajectories must still obey the squeezed limit consistency relation where $|f_{\mathrm{NL}}| \sim 10^{-2}$. This exaggerates the shape dependence of all the trajectories, even those which appear flat when $c_s = 1$.

It is worth noting that in the squeezed limit, the shape dependence is curved in comparison to the roughly linear dependence in the folded limit. This is in agreement with [96] where the authors show that corrections linear in β drop out. Any terms linear in $\mathbf{k}_3$ must contract symmetrically with the remaining two modes. As they have equal magnitudes in opposite directions they will cancel out leaving only quadratic corrections in k_3. In the folded limit this cancellation does not occur producing the linear dependence shown in Fig. 7.4.

7.4.2. c_s dependence

Fig. 7.5 compares the dependence of $f_{\rm NL}$ on c_s for equilateral and squeezed triangles. These values are normalised to their values at $c_s = 1$. To a good approximation the dependence is linear in c_s^{-2} and much stronger for equilateral triangles. This shows that for fixed $\beta = 0.1$ one can still obtain large $f_{\rm NL}$ by choosing an arbitrarily small c_s. At $c_s = 1$, $f_{\rm NL}$ is typically small and negative so as $c_s \to 0$ $f_{\rm NL}$ becomes large and positive. The close linear dependence on c_s^{-2} is not surprising and it clearly arises from the functions f_i in (7.26).

7.4.3. Monte Carlo Plots

The scale dependence is linear to a good approximation and can easily be analysed. To this end we define $n_{f_{\rm NL}}$ as

$$n_{f_{\rm NL}}(k_\star, \beta) = \left.\frac{{\rm d} f_{\rm NL}(k,\beta)}{{\rm d}\ln k}\right|_{k=k_\star} . \tag{7.31}$$

As discussed in [106, 157, 158] it is possible to define a scale dependence as long as the shape of the triangle is kept fixed. Our definition is different to the usual definition of $n_{f_{\rm NL}}$ which is the derivative of $|\ln f_{\rm NL}|$ and this is simply to avoid difficulties arising when $f_{\rm NL} \approx 0$. Recall, reducing c_s often in induces a sign change as can be seen in Fig. 7.5.

Fig. 7.6 shows numerous Monte Carlo plots for various sound speeds and shapes. Each plot consists of 2^{18} trajectories with their colour representing $n_{f_{\rm NL}}$. The top two figures show that all trajectories tend towards the squeezed limit consistency relation even for small sounds speeds $c_s < 1$. The consistency relation $5(n_s - 1)/12$ is shown by the red-dashed line. To reach the consistency relation in the $c_s^{-2} = 3$ case, a much smaller β was required (and consequently the value of δ had to be lowered, recall Fig. 7.2).

In the equilateral case one can see clearly how a small sound speed deforms the inflationary attractor. For example in the $c_s = 1$ case, the consistency relation acts as a firm upper limit for $f_{\rm NL}$. The deviation from the consistency relation is simply proportional to $\epsilon > 0$ and $f(k) > 0$ defined in [70]. A small $c_s < 1$ clearly violates this relation deforming the distribution significantly, resulting in a large positive $f_{\rm NL}$. In the folded limit, the distribution is reduced back again to be parallel with the consistency relation, although this time with a positive,c_s dependent offset.

To illustrate the flexibility of the method Fig. 7.7 shows a distribution with $c_s^{-2} = 100$ with colour of the trajectories now representing the third slow roll parameter $\xi = {}^2\lambda$ evaluated shortly after horizon crossing and the tensor-to-scalar ratio r. The dashed lines represent the current Planck constraints on $n_s = 0.968 \pm 0.006$ [18]. Planck also constrains $f_{\rm NL}^{\rm equil} = -4 \pm 43$ [19] although it is important to remember that there is not an exact one-to-one correspondence between our $f_{\rm NL}$ calculated here and the one constrained by Planck [19] due to assumptions on scale-invariance.

For example in power law inflation $\xi = \epsilon^2$ and is often assumed to be vanishingly small. However at these sound speeds, one can see that a small variation in ξ can lead to an appreciable change in $f_{\rm NL}$ even though it is likely to be neglected.

From the right panel in Fig. 7.7 one can also see that for small c_s tighter constraints on r require larger $|f_{\rm NL}|$. From one perspective this is not surprising as, to leading order, $r \approx 16\, c_s \epsilon$ [132] so smaller sounds speeds naturally induce smaller r. However one has to remember that the right panel in Fig. 7.7 shows trajectories for *fixed* $c_s = 0.1$. The changes in $f_{\rm NL}$ and r can *only* be induced by the slow-roll parameters (and H). More concretely smaller values of ϵ are thus expected to produce *more* non-Gaussianity. This is in contrast to the $c_s = 1$ case where *larger* values in ϵ produce more non-Gaussianity. Indeed it is often quoted that $f_{\rm NL} \sim \epsilon$. From the plots this is fairly easy to explain. Increasing ϵ always contributes negatively to $f_{\rm NL}$. It just so happens that at $c_s = 1$, $f_{\rm NL}$ is small and negative so they add constructively. On the other hand reducing c_s always contributes positively to $f_{\rm NL}$ eventually inducing a sign change. As soon as $f_{\rm NL}$ changes sign, increasing ϵ reduces the amount of non-Gaussianity.

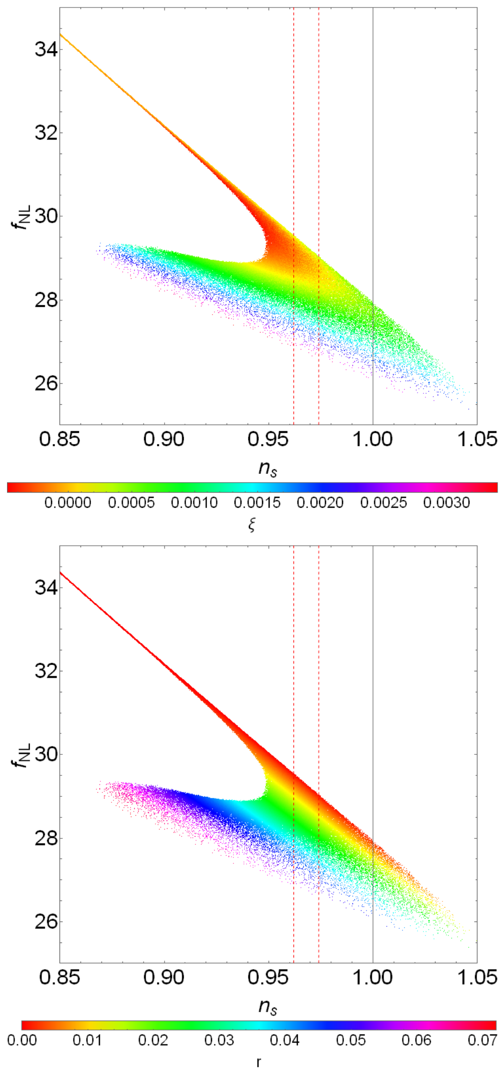

Figure 7.7.: Monte Carlo plot for a very small sound speed $c_s^{-2} = 100$ evaluated in the equilateral limit. The red-dashed lines represent the recent Planck constraints on n_s [18]. The top panel shows how small variations in ξ can change $f_{\rm NL}$. The bottom panel shows the corresponding tensor-to-scalar ratio r for each trajectory.

7.5. Discussion

We have outlined a full, numerical calculation of the bispectrum with a particular emphasis on single field models of inflation with non-canonical speed of sound. The calculation is challenging due to the oscillatory nature of the integrands involved which is exacerbated for the case with $c_s \neq 1$ and we have shown how regularising the integrals can lead to stable results with the correct choice of numerical damping terms. The methods explored in this work can be used to investigate the scale and shape dependence of the bispectrum signal produced by an epoch of inflation.

For convenience we have adopted a more general description of bispectrum signal than that normally quoted in the literature by re-defining a scale and shape dependent $f_{\rm NL}$, which always tends to $5(n_s - 1)/12$ as the shape parameter $\beta \to 0$. For lower values of c_s, $|f_{\rm NL}|$ is typically much greater and thus requires much smaller values of β to recover the squeezed limit consistency relation.

If future observational surveys of the CMB or large scale structure become accurate enough to constrain any scale dependence of the non-Gaussian signal then our work could be applied to the calculation of accurate model of the bispectrum to be used in likelihood evaluations of the data. This is not currently possible as the strongest limit on non-Gaussianity come from an ad-hoc analysis of Planck CMB maps assuming a scale-independent and fixed shape templates for the bispectrum leading to constraints on a single amplitude parameter. Whilst these results may be consistent with the simplest model of inflation, if a non-zero amplitude for $f_{\rm NL}$ were ever to be measured, more accurate parametrisations of the non-Gaussianity will be useful to try to gain a better understanding of the nature of the inflaton and its connection with extensions to the standard model of particle physics. This will particularly become a priority if primordial tensor modes are not discovered at levels $r \sim 0.01 - 0.1$.

8. Planck and WMAP constraints on generalised Hubble flow inflationary trajectories

8.1. Introduction

Recent Planck results [13] have confirmed, with the highest precision to date, the existence of a spectrum of primordial curvature perturbations on super-horizon scales with a power law with a spectral index close to but not equal to unity. This picture has now been verified over roughly three decades of scales probed by primary Cosmic Microwave Background (CMB) anisotropies that can be related to the primordial curvature perturbations on super-horizon scales via a well defined set of photon perturbation transfer functions. The quoted value for the scalar spectral index of $n_s = 0.9603 \pm 0.0073$ seems to be in good agreement with many models of cosmological inflation [15]. The fact that n_s is not compatible with unity is also interpreted by many to support the actual *existence* of an inflationary epoch in the very early universe.

The interpretation of the result, in the context of inflationary model selection, is complicated by the large number of inflationary models that are compatible with the CMB observations (see for example section 2 of [15] for a review of the landscape of models). The models range from the simplest chaotic model with a single scalar field to massively, multi-field models inspired by dimensional compactification in string theory. A typical discriminatory approach is to analyse the consistency of a particular model in the space of parameters such as n_s and tensor-to-scalar ratio r constrained directly by the data. However it becomes readily apparent that this combination does not refine the space of possible models to an extent at which conclusions about the fundamental nature of the inflaton can be made. Including higher-order parameters (in either slow-roll approximation or perturbation expansion) such as running of the spectral index with wavenumber k $dn_s/d\ln k$ or non-Gaussianity amplitude $f_{\rm NL}$ greatly enhances the ability to reject or falsify models. However the data has not reached the sensitivity to detect the expected higher-order signals.

An alternative method adopted here is known as the Hubble flow equation method. This method [150–153] assumes inflation was driven by a single scalar field and employs the Hamilton-Jacobi framework [77] to define a hierarchy of differential equations that can be used to generate inflationary trajectories consistent with *any* inflationary potential up to a certain order in derivatives of the Hubble rate H with respect to the inflaton field value ϕ. Within this framework one can dispense with proposing a *single* model consisting of a parametrised potential and constrain directly the space of allowed inflationary trajectories described by the evolution of the Hubble parameter $H \equiv \dot{a}/a$.

This approach allows one to compare all possible inflationary trajectories with a given complexity with no loss of accuracy. This is because, for a given truncation of the hierarchy of differential equations, the value of the Hubble rate during the inflationary epoch can be evaluated to arbitrary precision. Once the history of H has been obtained it is then possible to calculate all observable quantities to the desired precision irrespective of whether the trajectory satisfies slow-roll conditions.

One can then use the hierarchy of Hubble flow parameters as the base parameters being constrained. This has two advantages. Firstly, the space of Hubble flow parameters explores the space of all inflationary potentials allowed at a certain order consistently. Secondly, Bayesian model comparison is simplified for a given Hubble flow order since there is a *single* model proposition which reduces the selection to a comparison of likelihood values for two different points in the Hubble parameter space with no need to calculate Bayesian evidence.

In the work reported here Planck total intensity results, together with WMAP polarisation results [159] are used to directly constrain the space of Hubble flow parameters with priors given by the set of Assumptions 1-4. The constrained space of Hubble flow parameters can then be related to "conventional" parameters including n_s, r, $dn_s/d\ln k$, and $f_{\rm NL}$ without the need to redefine the model from a Bayesian perspective. The definition of *detections* of the conventional parameters $n_s - 1$, r, $dn_s/d\ln k$, and $f_{\rm NL}$ has no meaning within this analysis and the constraints can be viewed as ranges *allowed* by the observations i.e. *predictions* given the underlying set of assumptions.

This *paper* is organised as follows. In section 8.2 we review the Hubble flow formalism and describe how to obtain observables to compare with data in section 8.3. In section 8.4 we show the results obtained by constraining Hubble flow trajectories using the latest CMB data. We also describe the derived constraints on primordial spectral parameters and on the inflaton potential. In section 8.5 we discuss our results and future extensions.

8.2. Hubble flow equations

The Hamilton-Jacobi approach to analysing the dynamics of inflation consists of changing the independent variable in the Friedmann equations from cosmological time t to the value of the inflaton scalar field ϕ. The only assumption required for this change of variable is that ϕ is a monotonic function of t. The Friedmann equation and the inflaton's equation of motion then take on the following form

$$\begin{aligned} \dot{\phi} &= -2M_{pl}^2 H'(\phi)\,, &(8.1)\\ \left[H'(\phi)\right]^2 - \frac{3}{2M_{pl}^2}H(\phi)^2 &= -\frac{1}{2M_{pl}^4}V(\phi)\,, &(8.2)\end{aligned}$$

where dot denotes a derivative with respect to t, prime denotes a derivative with respect to ϕ, $H \equiv \dot{a}/a$ is the Hubble rate for the FRW scale factor $a(t)$, M_{pl} is the Planck mass and $V(\phi)$ is the inflaton potential. One of the advantages of performing this change of of variables is that one can merely pick a function $H(\phi)$ and this will correspond to an exact solution of a corresponding potential $V(\phi)$ in (8.2).

The system can be further simplified by introducing an infinite hierarchy of Hubble flow parameters [1]

$$^{\ell}\lambda = \left(2M_{pl}^2\right)^{\ell}\frac{(H')^{\ell-1}}{H^{\ell}}\frac{d^{(\ell+1)}H}{d\phi^{(\ell+1)}}\,. \qquad (8.3)$$

[1] Sometimes called Hubble-Slow-Roll (HSR) parameters to contrast with the Potential-Slow-Roll (PSR) parameters.

The first of these parameters, ${}^0\lambda \equiv \epsilon$, is a proxy for the acceleration of the scale factor and it is straightforward to verify that the relation

$$\epsilon = 2M_{pl}^2 \left(\frac{H'(\phi)}{H(\phi)}\right)^2 = \frac{-\dot{H}}{H^2} = \frac{\dot{\phi}^2}{2M_{pl}^2 H^2} < 1\,, \tag{8.4}$$

is a necessary and sufficient condition for the universe to be undergoing inflation with $\ddot{a}/a > 0$ [2]. The $\ell = 1$ and 2 flow parameters can also be identified with the usual slow roll parameter $\eta = {}^1\lambda = -(\ddot{\phi}/H\dot{\phi})$ and $\xi = {}^3\lambda$.

A further change of variable can be introduced by using the relation between the rate of change in e-folds $N = \ln(a/a_i)$, where a_i is the value of the scale factor at the beginning of inflation, and cosmological time t with $dN/dt = H$. The entire system can then be re-cast as an infinite hierarchy of differential "Hubble flow" equations with N as the independent variable

$$\frac{\mathrm{d}H}{\mathrm{d}N} = -\epsilon\, H\,, \tag{8.5}$$

$$\frac{\mathrm{d}\epsilon}{\mathrm{d}N} = 2\,\epsilon\,(\epsilon - \eta)\,, \tag{8.6}$$

$$\frac{\mathrm{d}{}^\ell\lambda}{\mathrm{d}N} = [\ell\,\epsilon - (\ell - 1)\,\eta]\;{}^\ell\lambda - {}^{\ell+1}\lambda\,, \tag{8.7}$$

with solutions $H(N)$ and ${}^\ell\lambda(N)$.

This is the most natural set of variables to use when constructing single field inflationary trajectories and the solution of the infinite system provides a *complete* set of exact solutions for the background evolution that are consistent with single field inflation and monotonic time evolution of ϕ. Truncating the hierarchy at $\ell_{\max}$ provides an *incomplete* set of solutions that are nonetheless still *exact*.

In practice a set of solutions for a given $\ell_{\max}$ is obtained by integrating the system with a set of random initial conditions for H and ${}^\ell\lambda$ for $\ell = 0, 1, ..., \ell_{\max}$. The system can be integrated forward or backwards to obtain an exact solution describing the dynamics of the background within a required window in e-foldings N.

[2] This is in contrast to the the PSR ϵ_V for which $\epsilon_V < 1$ is only an *approximate* condition for inflation.

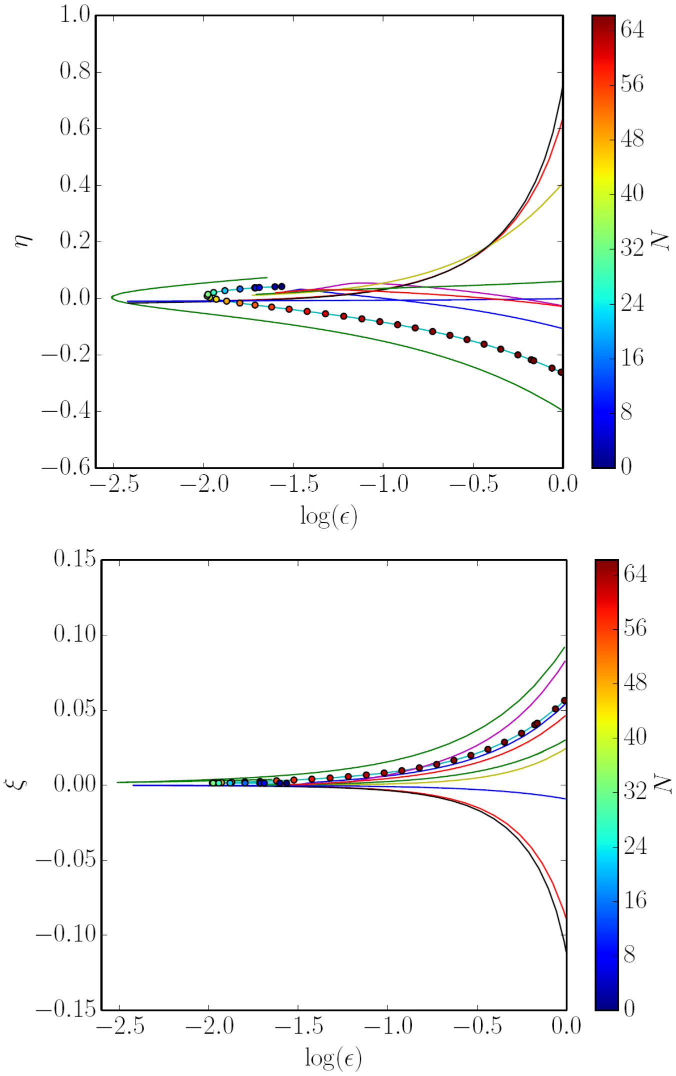

Figure 8.1.: Ten random trajectories drawn using the scheme described in 8.1. The evolution of η (top) and ξ (bottom) are plotted against $\log(\epsilon)$ from the end of inflation ($\epsilon = 1$) back to a time when the largest scale of interest $k_\star$ was a few order of magnitude smaller than the horizon scale. One of the trajectories also shows points colour coded by e-folding number N as points colour coded with respect to e-fold N. $N = 0$ corresponds a few e-folds before the $k_\star$ exits the horizon. All trajectories are evolving away (as N increases) from a "slow-roll" attractor with $\epsilon \ll 1$, $\eta \ll 1$, and $\xi \ll 1$. For most trajectories observable scales exit the horizon, when $N \sim \mathcal{O}(1) \to \mathcal{O}(10)$ and the flow parameters are well within the slow-roll limit. Trajectories with larger, negative final η values are ones where the trajectory is furthest from the slow-roll regime at early times.

8.2.1. Hubble flow measure

The Hubble flow method of generating random inflationary trajectories has a well known measure problem due to the seemingly arbitrary choice of proposal density and location for the initial conditions in H and ${}^{\ell}\lambda$. The existence of attractors in the phase space of the ${}^{\ell}\lambda$ complicates the interpretation of the imposed measure and the nature of trajectories obtained.

A number of choices have been made in the literature [150–153]. These include starting at arbitrary points and integrating forward or backwards to select trajectories with enough e-folds. Different choices have been made with regards to the encounters with fixed points in the HSR phase space where ϵ asymptotes to a constant and ${}^{\lambda}\ell \to 0$ for $\lambda > 1$. These can be interpreted as eternally inflating solutions that can be allowed or discarded if only trajectories where inflation ends are to be allowed. In all cases the proposal densities for the HSR have been uniform and the random draws have been made *wherever* each trajectory's integration was started.

In this work the simplest possible assumptions compatible with the data are made to define the choice of location for the initial conditions

Assumption 1 *A phase of accelerated expansion (inflation) with $\ddot{a} > 0$ occurred before the radiation dominated, decelerating phase of the standard big bang model.*

Assumption 2 *Inflation lasted a minimum number of e-folds such that all scales that are sub-horizon sized today were super-horizon by the end of inflation.*

Assumption 3 *Inflation ended when the universe stopped accelerating i.e. $\ddot{a}$ switched sign.*

Assumption 4 *Inflation was driven by a single scalar field ϕ.*

In line with these assumptions the initial conditions are drawn at the *end* of inflation i.e. a fixed point where $\epsilon = 1$. Only the remaining flow parameters for $\ell = 1, .., \ell_{\max}$ are then drawn from uniform distributions with fixed ranges. A value for N_0 is drawn from a uniform distribution and the system (8.5) is integrated *backwards* a total number of e-folds N_0. The e-folding N_0 is interpreted as the e-folding where the largest mode k_0

in the observable window is sufficiently smaller than the horizon to allow normalisation using the Bunch-Davies adiabatic limit [73]. This ensures that the system is integrated far back enough for the calculation of all observables required for comparison with data. In all cases considered in this work N_0 is drawn with a uniform distribution in the range $N_0 = [60, 70]$, this allows for the uncertainty in the total number of e-folds that occurred after the end of inflation due to the details of reheating. The uncertainty impacts our ability to connect a given scale exiting the horizon at a given time during inflation with a physically observable scale that subsequently re-entered the horizon during the decelerating epoch (see e.g. equation (24) of [15]).

8.2.2. Potential reconstruction

Each trajectory generated in this manner corresponds to a realisation of inflation with particular initial conditions and potential $V(\phi)$. Given a trajectory one can reconstruct the potential function probed during the evolution as the solution to the Hubble flow system is equivalent to selecting a solution by specifying a potential $V(\phi)$ and initial conditions for ϕ and $\dot{\phi}$.

For example if ${}^{\ell}\lambda = 0$ for all $\ell > 0$ then the only remaining non-zero parameter is ϵ. This implies $H(\phi)$ is a linear function and hence $V(\phi)$ is quadratic. The solutions for $\epsilon(N)$ and therefore $H(N)$ and $\phi(N)$ can then be obtained easily. The potential is obtained by combining (8.2) and (8.4) to get

$$V[\phi(N)] = 3M_{pl}^2 H^2(N) \left[1 - \frac{\epsilon(N)}{3}\right] . \tag{8.8}$$

8.3. Calculation of observables

8.3.1. Power spectrum

The evolution of background, homogeneous quantities during inflation is fully determined by the Hubble flow trajectory. Background also determines the evolution of the inflaton perturbations that end up as super-horizon primordial curvature perturbations that seed structure formation after inflation. The power spectrum of primordial curvature perturbations can be calculated numerically for any given Fourier wavenumber $k \equiv |\boldsymbol{k}|$. This is done by integrating the Mukhanov-Sasaki [72, 141] equation for the Fourier

Figure 8.2.: Hubble flow proposal densities projected into the space of derived parameters n_s, r, and f_{NL}. The derived parameters are obtained from numerical calculation of scalar and tensor power spectra and $f_{\mathrm{NL}}$and evaluated at the pivot scale $k_\star = 0.05\ \mathrm{Mpc}^{-1}$. The contours indicate the 68% and 95% confidence regions in the n_s-r plane from the PLANCKr reference fits [160]. Each point represents the derived quantities at the pivot scale obtained for each of ~ 10000 random Hubble flow trajectories generated using the uniform sampling described in section (8.2.1). The points are colour coded according to the random values η, ξ, and N_0 used to generate the trajectory. The inflationary attractor and the level of its correlation to the underlying flow parameters is clearly visible in both n_s-r and n_s-f_{NL}planes. The f_{NL}attractor follows a consistency relation given by $f_{\mathrm{NL}} \sim \frac{5}{12}(n_s - 1)$ [1,137]shown as the solid (magenta) line.

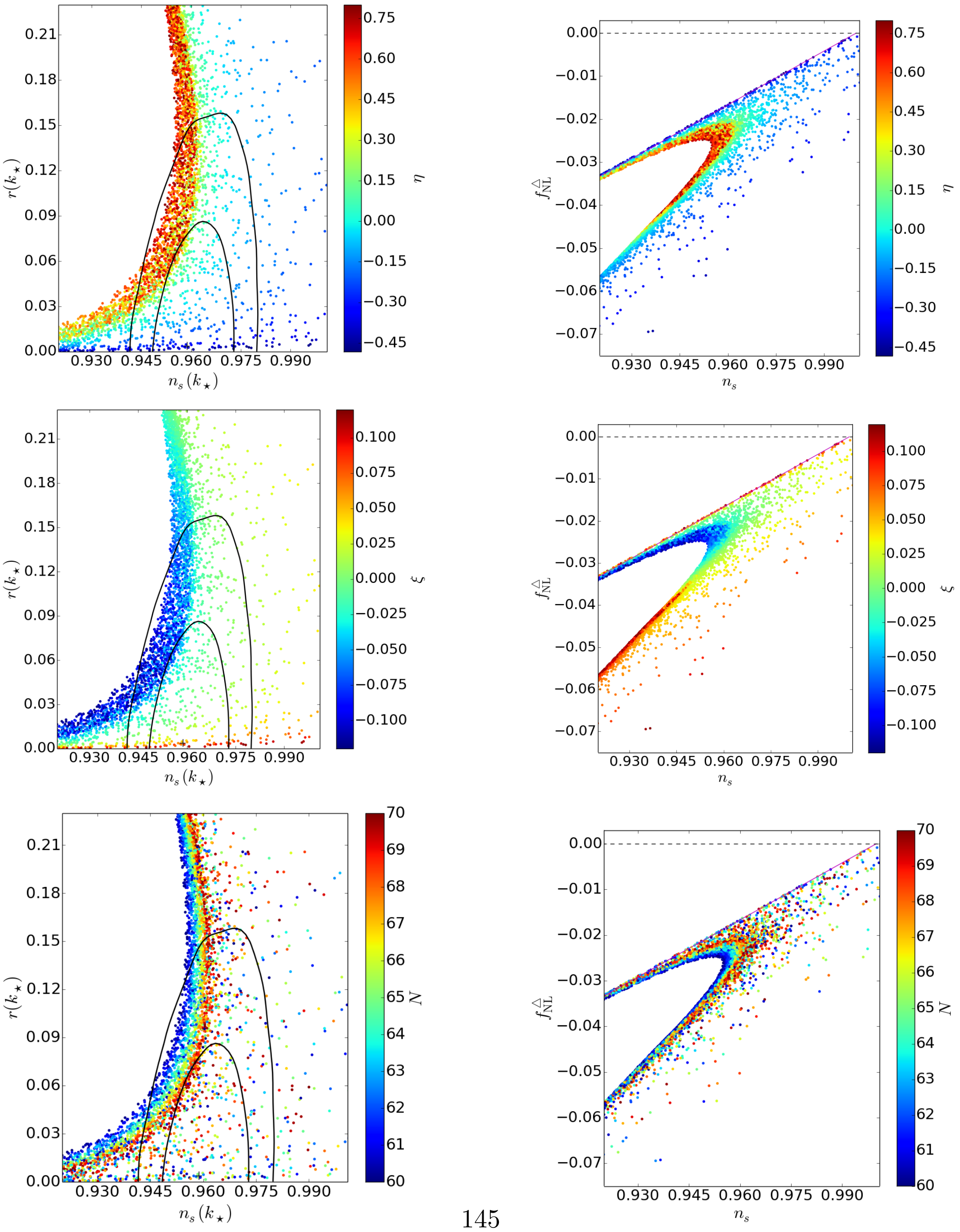

Table 8.1.: Uniform MCMC priors for cosmological parameters and a short description of each parameter. PLANCK Nuisance parameters are not listed here but are included with the same prior settings as used in [160]. The second block are derived parameters that are not used to randomly sample trajectories.

Parameter	Prior range	Definition
$\omega_b \equiv \Omega_b\, h^2$	[0.005,0.1]	Baryon density today
$\omega_c \equiv \Omega_c\, h^2$	[0.001,0.99]	Cold dark matter density today
τ	[0.01,0.8]	Optical depth to reionisation
$100\,\theta_{MC}$	[0.5,10.0]	100 $\times$ `CosmoMC` sound horizon to angular diameter distance ratio approximation
$\ln(\tilde{H}_{\rm inf})$	[2.5,3.5]	Log of rescaled Hubble rate at time of Horizon exit of scale $k_\star$
N_0	[60,70]	Number of e-folds for which trajectory is integrated back from end of inflation
${}^0\lambda \equiv \epsilon$	1.0	Flow parameter value at end of inflation
${}^1\lambda \equiv \eta$	[-1.0,1.0]	Flow parameter value at end of inflation
${}^2\lambda \equiv \xi$	[-0.2,0.2]	Flow parameter value at end of inflation
$n_s(k_\star)$	...	Scalar spectral index measured from trajectory spectrum at scale $k_\star = 0.05$ Mpc^{-1}
$r(k_\star)$	...	Tensor-to-scalar ratio measured from trajectory spectra at scale $k_\star = 0.05$ Mpc^{-1}
$n_t(k_\star)$	...	Tensor spectral index measured from trajectory spectrum at scale $k_\star = 0.05$ Mpc^{-1}
$f_{\rm NL}(k_\star)$	...	Equilateral non-Gaussianity amplitude at scale $k_\star = 0.05$ Mpc^{-1}
$\epsilon(k_\star)$	...	Flow parameter value shortly after mode $k_\star$ exits the horizon
$\eta(k_\star)$	...	Flow parameter value shortly after mode $k_\star$ exits the horizon
$\xi(k_\star)$	...	Flow parameter value shortly after mode $k_\star$ exits the horizon

expanded comoving curvature perturbation $\zeta(\boldsymbol{k})$. The isotropic power spectrum is defines the variance of the curvature perturbations as

$$\begin{aligned}\langle\zeta(\boldsymbol{k})\zeta(\boldsymbol{k}')\rangle &= (2\pi)^3\delta^{(3)}(\boldsymbol{k}+\boldsymbol{k}')P_\zeta(k) \\ &\equiv (2\pi)^3\delta^{(3)}(\boldsymbol{k}+\boldsymbol{k}')|\zeta(k)|^2_{k\ll aH}\,, \end{aligned} \tag{8.9}$$

and is evaluated at a time when the amplitude of the mode has converged on superhorizon scales ($k \ll aH$).

Expressed in terms of N the Mukhanov-Sasaki equation becomes

$$\frac{\mathrm{d}^2\zeta(k)}{\mathrm{d}N^2} + (3+\epsilon-2\eta)\frac{\mathrm{d}\zeta(k)}{\mathrm{d}N} + \frac{k^2}{a^2H^2}\zeta_k = 0\,, \tag{8.10}$$

from which it can also be seen that the amplitude of $\zeta(k)$ is conserved on superhorizon scales.

The initial condition for integration of (8.10) is set when $k \gg aH$ for each mode being solved for in which case the adiabatic Bunch-Davies conditions can be assumed and the mode asymptotes to the form

$$\zeta(k) \to \frac{e^{-ik\tau}}{2a\sqrt{k\epsilon}}\,, \tag{8.11}$$

with τ the conformal time defined by $\mathrm{d}N/\mathrm{d}\tau = aH$. The phase of $\zeta(k)$ is irrelevant and only the rate of change for the initial condition on $\mathrm{d}\zeta_k/\mathrm{d}N$ is required such that the value of τ at when the mode is normalised need never be evaluated explicitly.

In the following (8.10) is integrated for a range of modes of interest for observational comparison; $10^{-5} < k < 10^{-1}$ in units of Mpc^{-1}. This is done for each flow trajectory drawn at random in order to compare the resulting power spectrum to observations via calculation of CMB angular power spectrum

$$C_L = \int k^2\, dk\, P_\zeta(k)\, |\Delta_L(k)|^2\,, \tag{8.12}$$

where L here is the angular multipole and $\Delta_L(k,\eta_0)$ is the multipole expanded radiation transfer function for the mode k integrated to the present. The CMB angular power spectrum is evaluated using modified version of `CAMB` [89] where $P_\zeta(k|^\ell\lambda)$ is used as input to (8.12) instead of the conventional assumption

$$k^3\, P_\zeta(k) = A_s \left(\frac{k}{k_\star}\right)^{n_s(k_\star) + \frac{1}{2}\frac{dn_s}{d\ln k}\ln\left(\frac{k}{k_\star}\right) + \dots}, \tag{8.13}$$

i.e. a power law with amplitude A_s and spectral index given by n_s and higher derivative contributions . The power spectrum of tensor modes $P_h(k|^\ell\lambda)$ is calculated in a similar fashion for the same range of wavenumbers and the tensor contribution to the CMB angular power spectrum is also calculated. In this case the full functional form of $P_h(k|^\ell\lambda)$ replaces the parametrisation in terms of the tensor-to-scalar ratio r and tensor spectral index n_t.

It is important to note that the numerical integration of mode evolution provides *exact* solutions (within numerical tolerances) without use of any "slow-roll" assumptions. The results obtained are therefore valid also in the case when the flow parameters are not small as long as other necessary conditions of weak coupling and linearity are satisfied[3].

The remaining stochastic parameter is the initial condition for H. This value only affects the overall amplitude of the perturbation spectra and does not modify the solution for the flow parameters. There is therefore more freedom in choosing where to impose a normalisation. For this work a value for $\ln(\tilde{H}_{\rm inf})$ is drawn from a uniform distribution and used to normalise the Hubble rate of the trajectory at a time when a chosen pivot scale $k_\star$ has been outside the horizon for a few e-foldings i.e. when it's amplitude has converged as

$$H|_{k_\star \sim aH} = \frac{10^6}{4\pi\sqrt{2\pi}}\, \tilde{H}_{\rm inf}\,. \tag{8.14}$$

The value of $\tilde{H}_{\rm inf}$ is then related linearly to the final amplitude of the curvature power spectrum.

$$H(N_c) = 4\pi\sqrt{2\pi\epsilon(N_c)} M_{pl} A_s \tag{8.15}$$

8.3.2. Non-Gaussianity

The bispectrum is defined as

$$\langle\zeta(\boldsymbol{k})\zeta(\boldsymbol{k}')\zeta(\boldsymbol{k}'')\rangle = (2\pi)^3\delta^{(3)}(\boldsymbol{k}+\boldsymbol{k}'+\boldsymbol{k}'')B(k,k',k'')\,, \tag{8.16}$$

[3]For further details of our numerical integration scheme see [1]

where momentum conservation forces $\boldsymbol{k}$, $\boldsymbol{k}'$, $\boldsymbol{k}''$ to form a closed triangle and isotropy implies $B(k,k',k'')$ only depends on their magnitudes. It is convenient to work with a dimensionless bispectrum, which is independent of the power spectrum amplitude, often denoted as

$$f_{\rm NL}(k,k',k'') \equiv \frac{5}{6}B(k,k',k'')/ \\ \left[P_\zeta(k)P_\zeta(k') + P_\zeta(k)P_\zeta(k'') + P_\zeta(k')P_\zeta(k'')\right] . \tag{8.17}$$

There are many "type" of $f_{\rm NL}$ with different weightings to $P_\zeta(k)$ in the denominator while the above definition is frequently called $f_{\rm NL}^{local}$. The calculation of the bispectrum relies on the "in-in" formalism to calculate correlation-functions in time-dependent backgrounds for interacting quantum fields.

$$\langle\zeta^3(t)\rangle = -i\int_{-\infty}^{t} {\rm d}t'\langle\left[\zeta^3(t), H_{\rm int}(t')\right]\rangle\,, \tag{8.18}$$

Just as in flat space when we express our fields as a sum of plane waves (solutions to Klein-Gordon equation, Dirac equation etc.), here we express ζ as a sum of solutions of (8.10).

$$\zeta(t,\mathbf{x}) = \int\frac{{\rm d}^3\mathbf{p}}{(2\pi)^3}\left(\zeta_{\mathbf{p}}(t)\,a_{\mathbf{p}} + \zeta^*_{-\mathbf{p}}(t)\,a^\dagger_{-\mathbf{p}}\right)e^{i\mathbf{p}\cdot\mathbf{x}}\,. \tag{8.19}$$

$\zeta_{\mathbf{p}}(t)$ by definition satisfies equation (8.10) with initial condition (8.11). The interaction Hamiltonian $H_{\rm int}(t')$ is obtained from expanding the action for ζ to third order which produces cubic interactions with time-dependent coupling constants [1, 70, 103, 130, 148].

$$\begin{aligned} S_3 \;=\; & \int d^4x\,a^3\epsilon\left[(2\eta-\epsilon)\,\zeta\dot\zeta^2 + \frac{1}{a^2}\epsilon\zeta(\partial\zeta)^2\right. \\ & -(\epsilon-\eta)\zeta^2\partial^2\zeta - 2\epsilon\left(1-\frac{\epsilon}{4}\right)\dot\zeta\partial_i\zeta\partial_i\partial^{-2}\dot\zeta \\ & \left.+\frac{\epsilon^2}{4}\partial^2\zeta\partial_i\partial^{-2}\dot\zeta\partial_i\partial^{-2}\dot\zeta\right]\,, \end{aligned} \tag{8.20}$$

Using this expression for $H_{\rm int}(t')$ in (8.18)) produces the following expression for $f_{\rm NL}$

$$\begin{aligned} f_{\rm NL} &= \frac{1}{3|\zeta|^4} \times \\ & \mathcal{I}\left[\zeta^{*3}\int_{N_0}^{N_2} dN\, f_1\zeta^3 + f_2\zeta\zeta'^2\right] , \end{aligned} \tag{8.21}$$

where $\zeta = \zeta_k, \zeta_\beta = \zeta_{\beta k}$ and $\zeta' = {\rm d}\zeta/{\rm d}N$. The functions f_i are given by

$$\begin{aligned} f_1 &= \frac{5k^2 a\epsilon}{H}(2\eta - 3\epsilon) , \\ f_2 &= -5Ha^3\epsilon\left(4\eta - \frac{3}{4}\epsilon^2\right) , \end{aligned} \tag{8.22}$$

N_0 and N_2 are e-folds when ζ_k is deep inside and far outside the horizon respectively. The subtleties involved for dealing with this integral numerically are fully explored in [1].

8.4. Constraints on Hubble Flow trajectories

8.4.1. Base parameters

Having defined a measure for generating random Hubble flow trajectories one can now ask whether the resulting observables i.e. scalar and tensor power spectra are compatible with observations and/or gain constraints on the allowed space of flow parameters. To do this the set of parameters defining the random trajectory N_0, $H_{\rm inf}$, and ${}^1\lambda$, ${}^2\lambda$, ..., ${}^{\ell_{\rm max}}\lambda$ can be used as base parameters in an MCMC exploration of the likelihood of CMB observations. In this case the set of flow parameters replaces the conventional parametrisation of scalar and tensor primordial power i.e. A_s, n_s, $dn_s/d\ln k$, etc., and r, n_t, $dn_t/d\ln k$, etc.

Here, the `CosmoMC` [154] code is used, together with a modified version of `CAMB`, to explore the likelihood of the Hubble flow parameters with respect to CMB observations. The parameter set used in the exploration in this case is the combination of radiation transfer parameters ω_b, the physical density of baryons, ω_c, the physical density of cold dark matter, $\theta_M C$, the angular diameter distance parameter used by `CosmoMC` [160], and τ, the optical depth parameter, and the set of flow parameters N_0, $H_{\rm inf}$, and ${}^0\lambda$, ${}^1\lambda$, ..., ${}^{\ell_{\rm max}}\lambda$. The flow parameters only affect the primordial scalar and tensor spectra

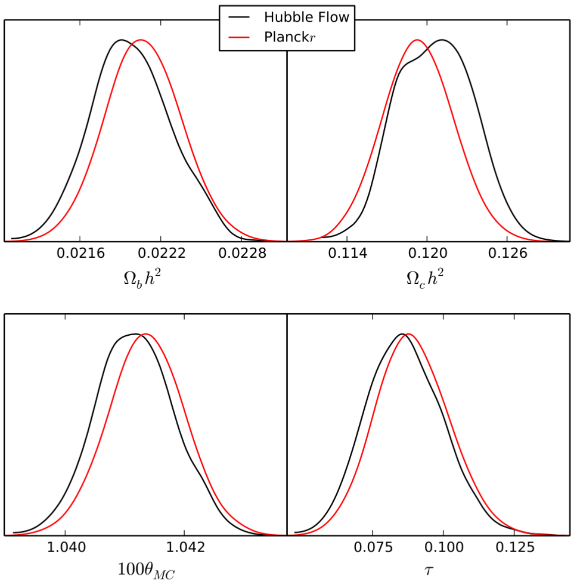

Figure 8.3.: Comparison of 1d marginalised posteriors in the overlapping parameters between the reference PLANCKr run and the Hubble flow case with $\ell_{\max} = 2$. There is no significant changes in the constraints as expected. The PLANCK nuisance parameters are not shown but also show no significant change in constraints.

and are therefore probed as *fast* parameters in `CosmoMC` runs. In practice at each step in the MCMC we compute the trajectory resulting from the set of proposed flow parameters and then numerically evaluate the corresponding scalar and tensor power spectra. We also evaluate numerically the value of $f_{\rm NL}$, the dimensionless amplitude of the bispectrum in the equilateral configuration, for the pivot scale.

For CMB observations, the latest PLANCK temperature only results [14] are used together with WMAP polarisation measurements. In all the runs described in this work the PLANCK likelihood settings and nuisance parameters are set as in the standard "PLANCK+WP" combination (see [160] for details). The PLANCK+WP "`base r planck lowl lowLike`" (abbreviated to PLANCKr in the following) MCMC chains [154] using the conventional parametrisation A_s, n_s for the primordial scalar spectrum with a tensor extension parametrised solely by r can be used as a reference run to compare with the results reported below[4].

[4]For the tensor spectral index the inflationary consistency relation is used to treat it is

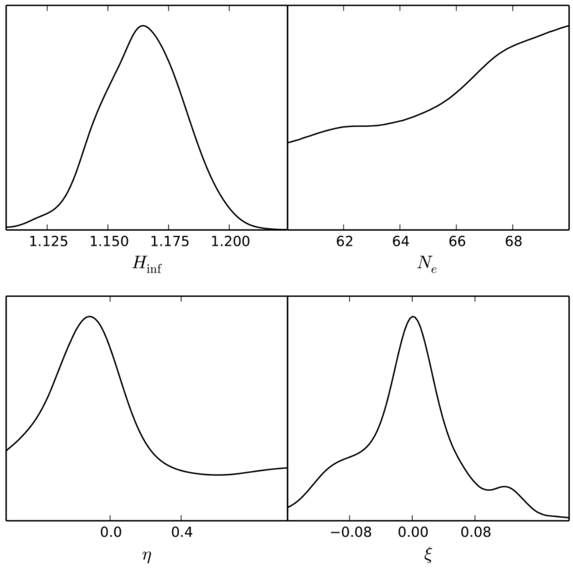

Figure 8.4.: 1d marginalised posteriors for the Hubble flow parameters. These parameters replace the conventional A_s, n_s, r, n_t, $dn_s/d\ln k$, etc. $H_{\rm inf}$ is equivalent to the scalar amplitude parameter A_s and is well constrained, as expected, whereas the e-folds parameter N_e is unconstrained. This is also expected since there is little sensitivity in the observable to the *total* duration of inflation and N_e can be regarded as an additional nuisance parameter. The flow parameters have posteriors peaked around 0.

The conventional parameters A_s, n_s, r, etc., can be calculated directly from the power spectra obtained by numerical integration of the mode equations and can then be treated as *derived* parameters for each accepted flow trajectory in the MCMC chains. $f_{\rm NL}$can also be treated as a *derived* parameter to gain insight into the level of non-Gaussianity preferred by the current data in the context of random Hubble flow proposal. It is instructive to visualise how the Hubble flow proposal density used here projects into the space of derived parameters. Figure 8.2 shows the scatter of trajectories in the n_s-r and n_s-$f_{\rm NL}$planes. The derived quantities are evaluated from the numerically obtained spectra at a pivot scale $k_\star = 0.05$ Mpc^{-1}. The points are also colour coded according to the random value of η, ξ, and N_0 used to generate the trajectory. The value of the random flow parameters is

as a function of n_s.

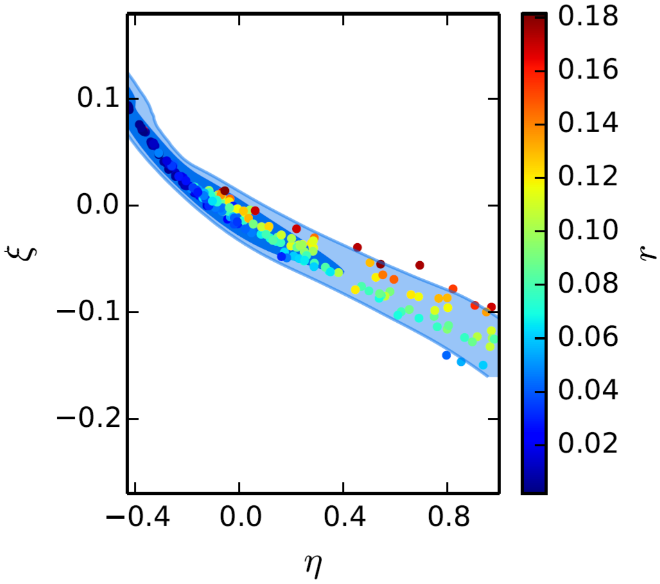

Figure 8.5.: The 2d marginalised posterior for ξ and η, the base flow parameters for the Hubble flow $\ell_{\mathrm{max}} = 2$ run. The contours are denote the 68% and 95% significance levels. The coloured scatter plot indicates the value of $r \sim 16\,\epsilon(k_\star)$ for each sample in the chain. The two base parameters are highly correlated and the unconstrained, large positive η tail is correlated with larger values of r.

highly correlated with the resulting values of n_s, r, and $f_{\mathrm{NL}}$and the scatter shows a strong "inflationary" attractor [150–153]. The attractor overlaps the PLANCKr constraints for the n_s-r combination in a corner of the region between the 68% and 95% contours.

We consider a Hubble flow system with $\ell_{\mathrm{max}} = 2$ (i.e. including ϵ, η, and ξ) for the MCMC exploration. This allows potentials that include up to order 6 polynomials in ϕ. The uniform priors chosen for this run are shown in Table 8.1 together with a description of each base and derived parameter. The run uses seven base parameters which is the same number used for the conventional PLANCKr run. The Planck nuisance parameters are omitted for brevity.

The chains are run until the R^{-1} convergence parameter [154] falls below 0.1. Figure 8.3 shows the resulting 1-dimensional marginalised posterior distribution for the conventional parameters that determine the form of the

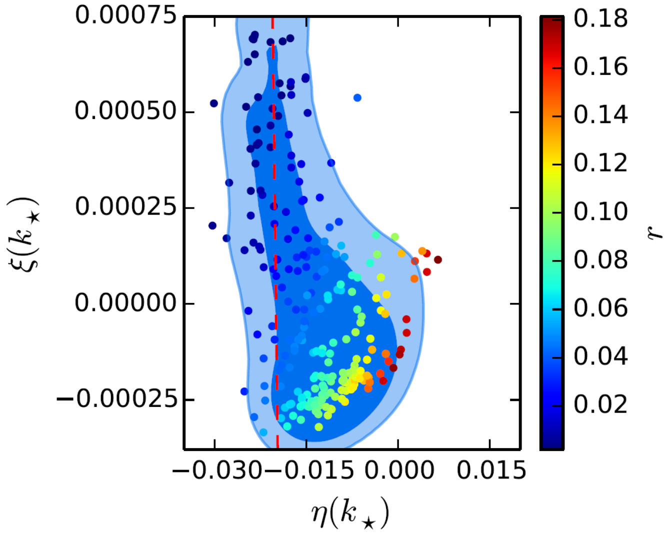

Figure 8.6.: Same as Figure 8.5 but for ξ and η values at the observationally relevant scale $k_\star$. The red (dashed) line indicates the expected value of η as $r \to 0$ as given by the second order slow-roll approximation.

radiation perturbation transfer functions. These shared by both PLANCKr and the Hubble flow runs. The marginalised posteriors are very similar between the two runs indicating that there is no *tension* in the transfer parameters with respect to how the primordial perturbation spectrum is sampled.

Figure 8.4 shows the marginalised posteriors for the flow parameters that do not have counterparts in the conventional runs. The overall amplitude is tightly constrained as expected - it takes the same role as the conventional amplitude A_s. The total number of e-folds is unconstrained and acts an an extra nuisance parameter which is marginalised in the given interval. The two flow parameters whose values are allowed to vary at the end of inflation, η and ξ have posteriors that are peaked around zero. The ξ parameter is also well constrained with respect to its uniform prior. Positive values of η are unconstrained and the posterior approaches a uniform distribution that extends to the $\eta = 1$ limit of the uniform prior.

The two Hubble flow parameters are highly correlated as seen in Figure 8.5. The large η, negative ξ tail however is correlated with larger values of $r \sim 16\,\epsilon(k_\star)$ and therefore lower upper limits on the tensor-to-scalar ratio

Table 8.2.: Parameter constraints from the marginalised posteriors for both Hubble flow $\ell_{\max} = 2$ and PLANCKr runs. Parameters marked with † are derived ones in the Hubble flow run. Upper limits are 95% significance values.

	Hubble Flow	PLANCK r
$\Omega_b h^2$	$0.02198^{+0.00028}_{0.00032}$	$0.02207^{+0.00028}_{-0.00028}$
$\Omega_b h^2$	$0.1206^{+0.0028}_{-0.0031}$	$0.1193^{+0.0026}_{-0.0026}$
$100\theta_{MC}$	$1.04117^{+0.00063}_{-0.00069}$	$1.04137^{+0.00063}_{-0.00063}$
τ	$0.087^{+0.013}_{-0.015}$	$0.089^{+0.012}_{-0.014}$
$H_{\rm inf}$	$1.164^{+0.017}_{-0.017}$	-
$\log(10^{10} A_s)$	-	$3.09^{+0.024}_{-0.027}$
$^\dagger n_s$	$0.9579^{+0.0072}_{-0.0090}$	$0.9623^{+0.0075}_{-0.0075}$
$^\dagger r$	< 0.143	< 0.126
$^\dagger\ f_{\rm NL}$	$-0.0205^{+0.0037}_{-0.0057}$	-

will help in eliminating the large η tail and break the degeneracy. The resulting 2d posterior for the Hubble flow parameters at observable scales can be seen in Figure 8.6 that also includes a line indicating the consistency of η and ξ with the slow-roll limit expression in the limit that $r \sim 16\,\epsilon(k_\star) \to 0$ and $n_s - 1 \to -0.04$.

Trajectories with positive η values, and hence positive derivative in ϵ at the end of inflation approach the slow–roll limit very quickly as they are evolved backwards towards the observable window. These therefore almost always result in acceptable values for e.g. n_s, r, etc. Negative values of η are cutoff by the data at $\eta \sim -0.42$. The reason for this strong cutoff can be seen in Figure 8.1 where trajectories with larger negative values of η at the end of inflation approach the slow-roll limit much slower, giving values of $|n_s - 1|$ that are typically larger and therefore in disagreement with observations.

The best-fit sample in the chain for the $\ell_{\max} = 2$ Hubble flow run has a

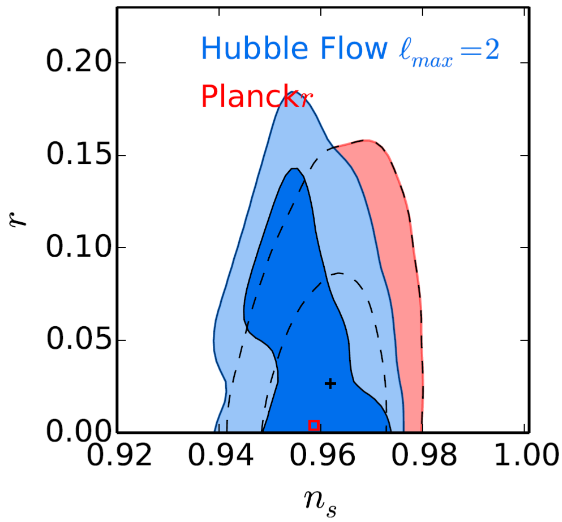

Figure 8.7.: The 2d marginalised posterior for n_s and r. These are derived at the pivot scale $k_\star$ in the Hubble flow case. The same contours for the PLANCKr run are shown for comparison. The cross and square indicate the position of the best-fit sample for the Hubble flow and PLANCKr run respectively. The Hubble flow case prefers higher values of r due to the proposal density peaking at $r \sim 0.075$ for acceptable values of n_s.

negative log-likelihood $-\ln L \equiv \mathcal{L} = 4903.2521$ compared to the PLANCKr one of $\mathcal{L} = 4904.3370$ giving a better fit by $\Delta\mathcal{L} = 1.085$. The two runs have a comparable number of degrees of freedom since the N_e can be considered as an additional nuisance parameter. The marginalised constraints on parameters in both Hubble flow and PLANCKr run are compared in Table 8.1.

8.4.2. Derived parameters

It is useful to compare the marginalised posteriors in the derived r and n_s parameters between the Hubble flow run and the conventional PLANCKr case. Figure 8.7 shows the 2d marginalised constraints for this combination together with their respective best-fit sample location. The Hubble flow case prefers higher values of r due to the proposal density peaking at $r \sim 0.075$ for acceptable values of n_s. Constraints on n_s are similar in both cases although the Hubble flow constraints disfavour relatively large values of n_s compared to PLANCKr.

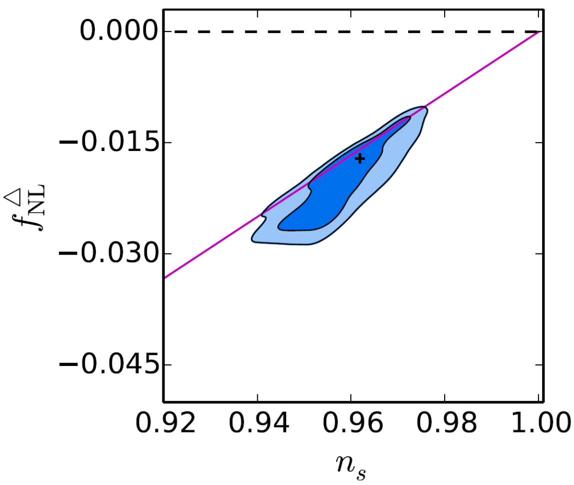

Figure 8.8.: The 2d marginalised posterior for n_s and $f_{\rm NL}$at the picot scale $k_\star$. The cross indicates the location of $f_{\rm NL}$of the best-fit sample. The line shows the slow-roll consistency condition $f_{\rm NL}\approx 5(n_s - 1)/12$.

A novel feature of this method is that existing data *already* constrains the possible values of $f_{\rm NL}$. This is simply due to the fact that each trajectory has a non-vanishing bispectrum and there fore the data will constrain this degree of freedom too. Figure 8.8 shows the 2d marginalised constraints in the n_s *vs* $f_{\rm NL}$plane. Since most of the trajectories are in the slow–roll regime when the pivot scale $k_\star$ is leaving the horizon the posterior for $f_{\rm NL}$agree well with the limiting consistency condition $f_{\rm NL}\approx 5(n_s - 1)/12$ [1, 70]. This result, of course, should not be interpreted as a detection of non-Gaussianity but rather as an indication of what amplitudes of the bispectrum are consistent with the general single field inflationary solutions for a Hubble flow system with $\ell_{\rm max}$. If measurements of primordial non-Gaussianity ever reach the sensitivity to constrain the level of $f_{\rm NL}\sim 10^{-2}$ then the measurement will provide a fundamental consistency check for single field inflation.

In Figure 8.9 we also show the approximately 200 best-fit power spectra in the chains. The spectra are coloured and weighted by their $\Delta\mathcal{L}$ with respect to the best-fit sample to emphasise the best fitting curves. The best-fitting spectra are very close to power laws with respect to $\ln k$. The best fitting spectra have very similar normalisations at the pivot scale $k_\star = 0.05h$ Mpc^{-1} as the normalisation of the primordial spectrum is one of the best

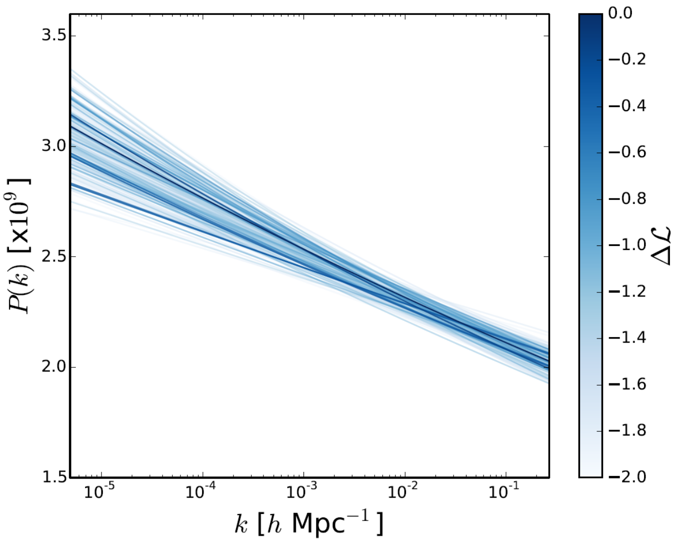

Figure 8.9.: The primordial curvature power spectra for all samples within $\Delta\mathcal{L} = 2$ of the best-fit sample. This is an indication of all spectra allowed within the 95% significance level. Each spectrum is coloured and weighted on a scale given by $\Delta\mathcal{L}$ and $1/(1 - \Delta\mathcal{L})$ respectively in order to emphasise the best-fitting spectra.

constrained parameters.

8.4.3. Inflaton potential

Each trajectory in the MCMC chain yields an individual potential and we can therefore translate directly the constraints on our base parameters into the space of allowed potentials using (8.8). For the $\ell_{\max} = 2$ Hubble flow run the best-fit potential is one given by $\eta \sim \xi \sim 0$ i.e. with small curvature. Figure 8.10 shows all the potentials in the MCMC chain that have $\Delta\mathcal{L} = 2$ with respect to the best-fit sample. There are some 200 samples within this range. Each potential is weighted by its $\Delta\mathcal{L}$ value so the darkest curves are the most likely.

The range in η probed by the sample is large and extends from $\eta \sim -0.4$ to $\eta \sim 1$. This translates to potentials that are both convex and concave, and those that include an inflection point. This is simply a feature of the degeneracy in the contribution from both ϵ and η to the scalar tilt n_s, the only shape spectral parameter, aside from amplitude, that has been constrained so far. If r were to be detected in future it would help to constrain the sign of the curvature of the potential in the observable regime ($\Delta\phi \sim 0$).

An n^{th}-order polynomial fit to the best-fit sample potential converges for $n = 5$ and gives a potential $V(\varphi)$

$$V(\varphi) = V_0 \left(1 + \sum_{n=1}^{n=4} \lambda_n \, \varphi^n \right) , \tag{8.23}$$

with $\varphi = \Delta\phi$, and $V_0 = 1.50 \times 10^{-12}$, $\lambda_1 = 2.20$, $\lambda_2 = 0.66$, $\lambda_3 = -6.00 \times 10^{-2}$, $\lambda_4 = 1.78 \times 10^{-3}$, and $\lambda_5 = -1.98 \times 10^{-5}$. The best-fit sample potential and the polynomial fit are shown in the left panel of Figure 8.10. The coefficients λ_n for $n \leq 4$ converge for higher order fits with $n > 4$ and the potential does not change appreciably in the interval $\varphi = 0 \to \mathcal{O}(10)$. Note that given (8.8) an $\ell_{\text{max}} = 2$ flow system allows for potentials that include terms up to ϕ^6.

8.5. Discussion

We have obtained constraints on generalised, single field inflation trajectories using the Hamilton-Jacobi formalism. The Hubble flow system was used as base parameters in an MCMC exploration of the likelihood with respect to the latest CMB data. This allowed us to obtain marginalised posteriors on the flow parameters that define the evolution of the Hubble parameter $H(N)$ as a function of e-folds N during inflation. Alternatively, the constraints can be viewed as a selection in the space of inflaton potentials $V(\phi)$.

Our method also includes the numerical calculation of primordial bispectra and we obtained *predictions* based on current data of consistent bispectrum amplitude f_{NL} for the equilateral case.

Further exploration will be left for future work. In particular it will be of interest to extend the system to higher ℓ_{max} to allow for more structure in the trajectories. This is currently limited by the fact that the highly correlated space of HSR parameters result in a very inefficient MCMC exploration. More work to explore the likelihood more efficiently or defining new sets of HSR parameters may help in extending this line of work to systems with higher ℓ_{max}.

Future data from CMB and also large scale structure will also provide deeper probes of non-Gaussianity which will provide tighter constraints in the space of trajectories. This will be particularly important if the discovery and characterisation of tensor modes will turn out to elude future CMB polarisation measurements due to foreground contamination. In that case non-Gaussianity measurements will possibly provide the only way to break shape degeneracies and reveal the precise form of the inflaton potential over the range of scales accessible to observations.

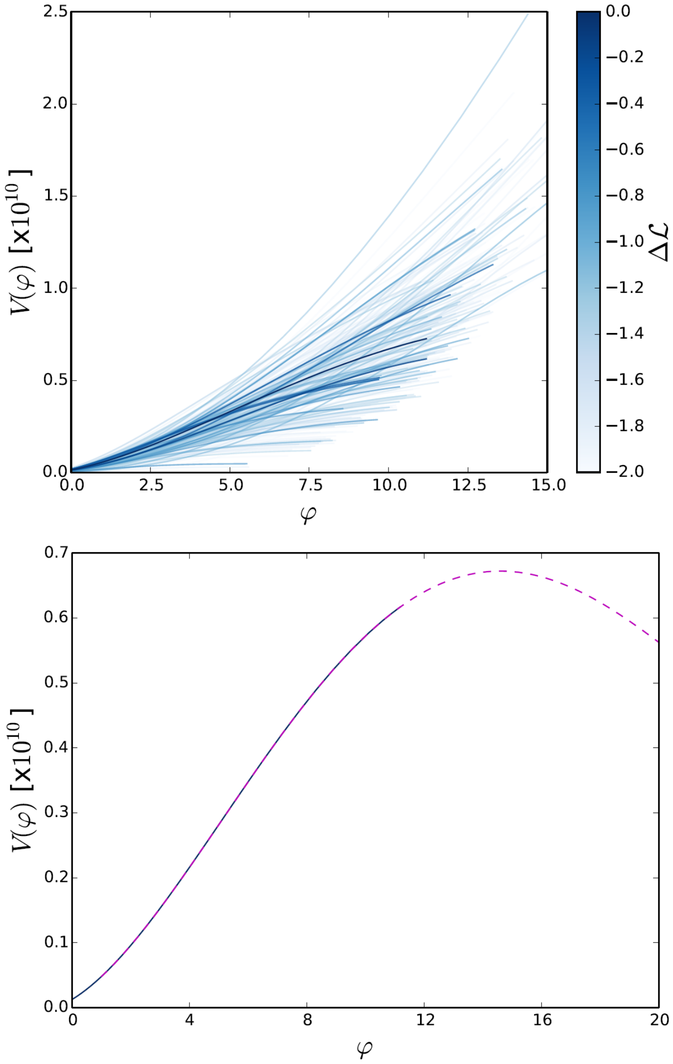

Figure 8.10.: *Top*: All sampled potentials within $\Delta\mathcal{L} = 2$ of the best-fit sample. This is an indication of all potential shapes and normalisations allowed with the 95% significance level. The x-axis shows the change in ϕ from the final value where inflation ends ($\varphi \equiv \Delta\phi = 0$). Both ϕ and V are in units of $M_{\rm pl} = 1$. The weighting of curves is the same as in Figure 8.9. *Bottom*: The best-fit sample potential (solid) and its 4$^{\rm th}$-order polynomial fit (dashed).

9. Conclusion

In this thesis, the numerical calculation of the bispectrum from inflation was performed for a variety of different cases. With the recent Planck results [18, 19], the constraints on inflationary models are being pushed to new limits meaning an accurate and fast calculation of the primordial bispectrum will continue to become more important. Even though current measurements of f_{NL} are still consistent with 0, placing stronger limits on bispectrum will continue to rule out models and possibilities.

It was shown how the calculation can be applied to with features which are difficult to include in the Monte Carlo sampling. The calculation was further expanded to include more complex non-canonical models of inflation where the perturbations propagate with slow sound speed $c_s \neq 1$. Finally it was shown how the bispectrum calculation can be naturally included when one reconstructs the inflaton potential by comparing the numerical power spectrum directly to data.

In Chapter 5 a detailed overview was given, combining the calculation with Monte Carlo sampling of inflationary trajectories and reproducing known consistency relations. We chose to specialise to equilateral triangles, covering most shapes of interest with a single parameter. It was shown that by considering different priors in the sampling of the slow-roll parameters, it is possible generate larger levels of non-Gaussianity. However these models are highly suppressed probabilistically when a simple cut in n_s-space is imposed, making it difficult for these models to agree with observations.

Chapter 6 marks a unique point in the history of Cosmology when the field was on the edge of a landmark discovery. Unfortunately the detection of primordial B-mode polarisation by BICEP2 [20] was ultimately invalidated [28] but the paper Chapter 6 was based on was written in the intermediate months. Had the BICEP2 result been verified, inflation models with a sudden change in acceleration would have been placed on much firmer footing. These models predict a large peak in the bispectrum at large scales where the power is suppressed. Unfortunately it may not be possible to constrain the bispectrum at these scales using CMB data alone but large scale structure surveys provide better constraints.

Chapter 7 generalised results of Chapter 5 to more complex single field inflation models, easily generating large amounts of non-Gaussianity. The squeezed limit consistency relation was shown to hold for these more general models and in the equilateral limit it was found that even small variations of the slow-roll parameters could significantly change f_{NL}. This further justifies the need for a precise calculation of the bispectrum as observations place tighter constraints on non-Gaussianity.

Combining the bispectrum calculation with data was done performed in Chapter 8, where instead of sampling over n_s, A_s, etc. one treats the slow-roll parameters and H as fundamental parameters. Quantities such as n_s, r, f_{NL}, etc. are then derived parameters and can be easily calculated. In the very recent 2015 Planck results [18] a similar procedure was performed where the authors sampled over the Hubble slow-roll parameters.

Since its introduction in the 1980s, inflation has been a huge topic in Theoretical Physics and Cosmology. Now, as experiments are reaching unprecedented levels of precision, and with the hope that large scale structure surveys will shed even more light on primordial non-Gaussianity [161], we may be finally getting close to understanding what happened at the beginning of time.

A. Appendix

A.1. More details for perturbing the ADM formalism

After inserting the first order expressions for N and N_i some useful quantities are:

$$
\begin{aligned}
\Gamma^k{}_{ij} &= 2\delta^k{}_{(i}\partial_{j)}\zeta - \delta_{ij}\delta^{kl}\partial_l\zeta && \text{(A.1)}\\
E_{ij} &= \left(H + \dot{\zeta}\right) h_{ij} - \partial_i\partial_j\psi + 2\partial_{(i}\psi\partial_{j)}\zeta - \delta_{ij}\partial_k\zeta\partial_k\psi && \text{(A.2)}\\
E_{ij}E^{ij} - E^2 &= -6(H+\dot{\zeta})^2 + 4(H+\dot{\zeta})\left(\partial^2\psi + \partial_i\psi\partial_i\zeta\right)\frac{e^{-2\zeta}}{a^2} && \text{(A.3)}\\
&\quad + h^{ik}h^{jl}\partial_i\partial_j\psi\left(\partial_k\partial_l\psi - 4\partial_{(k}\psi\partial_{l)}\zeta\right) && \text{(A.4)}\\
R^{(3)} &= -\frac{2}{a^2}\left(2\partial^2\zeta + (\partial\zeta)^2\right)e^{-2\zeta} && \text{(A.5)}
\end{aligned}
$$

Simply inserting these expressions into the action gives:

$$
\begin{aligned}
S = \frac{1}{2}\int \mathrm{d}^4x \Bigg[-2ae^{\zeta}\left(1 + \frac{\dot{\zeta}}{H}\right)\left(M_{pl}^2\left(2\partial^2\zeta + (\partial\zeta)^2\right) + Va^2e^{2\zeta}\right) \\
+ \frac{M_{pl}^2}{1 + \frac{\dot{\zeta}}{H}}\left(E^{ij}E_{ij} - E^2 + \frac{\dot{\phi}^2}{M_{pl}^2}\right)a^3\zeta^{3\zeta}\Bigg]
\end{aligned}
\qquad \text{(A.6)}
$$

When performing these manipulations it is helpful to maintain the exponential factors e^{ζ} for as long as possible as they are easier to keep track of then the series expansion. For example the most complicated term above is

$$\frac{a^3 e^{3\zeta}}{1+\frac{\dot\zeta}{H}}(E_{ij}E^{ij}-E^2) = -6\left(1+\frac{\dot\zeta}{H}\right)a^3e^{3\zeta} + 4Ha\left(\partial^2\psi+\partial_i\zeta\partial_i\psi\right)e^{\zeta}$$
$$+\frac{1}{a\left(1+\frac{\dot\zeta}{H}\right)}\left[\partial_i\left((\partial_j\psi\partial_i\partial_j\psi-\partial_i\psi\partial^2\psi)e^{-4\zeta}\right)e^{3\zeta}-4\partial_i\zeta\partial_i\psi\partial^2\psi e^{-\zeta}\right] \tag{A.7}$$

To arrive at this expression a 4th order term, which won't contribute to anything in this thesis, was dropped. Even though currently we are only concerned with terms up to second order, we left the final third order term here as it will be needed later. It can be safely dropped.

From now on the task is a combination of finding total derivatives, using the zeroth order equations of motion and dropping higher order terms. In a lot of cases it pays off dropping terms later rather than earlier. For example the first line contains a total spatial derivative to all orders which can be safely ignored.

$$4Ha\left(\partial^2\psi+\partial_i\zeta\partial_i\psi\right)e^{\zeta} = 4Ha\partial_i\left(\partial_i\psi e^{\zeta}\right) \tag{A.8}$$

To second order then the final line is also a total derivative

$$a^3\partial_i\left(\partial_i\psi\partial_i\partial_j\psi-\partial_i\psi\partial^2\psi\right). \tag{A.9}$$

This drastically simplifies our action to a more manageable form

$$S=\frac{1}{2}\int \mathrm{d}^4x\left[-2ae^{\zeta}\left(1+\frac{\dot\zeta}{H}\right)\left(M_{pl}^2\left(2\partial^2\zeta+(\partial\zeta)^2\right)+Va^2e^{2\zeta}\right)\right.$$
$$\left.-6M_{pl}^2H^2\left(1+\frac{\dot\zeta}{H}\right)a^3e^{3\zeta}+\frac{\dot\phi^2}{1+\frac{\dot\zeta}{H}}a^3e^{3\zeta}\right] \tag{A.10}$$

Replacing $V(\phi)$ with the Friedmann equation we find

$$S = \int \mathrm{d}^4x \left[-M_{pl}^2 a e^{\zeta} \left(1 + \frac{\dot{\zeta}}{H}\right) \left(2\partial^2\zeta + (\partial\zeta)^2\right) \right.$$
$$+ \left(\dot{\phi}^2 - 6M_{pl}^2 H^2\right) a^3 e^{3\zeta} - 6M_{pl}^2 H \dot{\zeta} a^3 e^{3\zeta} \tag{A.11}$$
$$\left. + \frac{\dot{\phi}^2}{2H^2} \frac{\dot{\zeta}^2}{1 + \frac{\dot{\zeta}}{H}} a^3 e^{3\zeta} \right].$$

For the middle line, integrating the $\dot{\zeta}$ term by parts and using the equation of motion $\dot{\phi}^2 + 2M_{pl}^2 \dot{H} = 0$ leaves the following total time derivative which can be dropped.

$$-2M_{pl}^2 \frac{\mathrm{d}}{\mathrm{d}t} \left(H a^3 e^{3\zeta}\right) \tag{A.12}$$

The final term proportional to ae^{ζ} is the least obvious but it can be shown to be a combination of time and spacial total derivatives.

$$\begin{aligned}
&-a\left(1 + \frac{\dot{\zeta}}{H}\right) e^{\zeta} \left(2\partial^2\zeta - (\partial\zeta)^2\right) \\
&\quad = -\frac{1}{H}\frac{\mathrm{d}}{\mathrm{d}t}\left(ae^{\zeta}\right)\left(2\partial^2\zeta + (\partial\zeta)^2\right) \\
&\quad = +\frac{\mathrm{d}}{\mathrm{d}t}\left(\frac{1}{H}\right) ae^{\zeta}\left(2\partial^2\zeta + (\partial\zeta)^2\right) - \frac{\mathrm{d}}{\mathrm{d}t}\left(\frac{ae^{\zeta}}{H}\right)\left(2\partial^2\zeta + (\partial\zeta)^2\right) \\
&\quad = a\epsilon\left(-(\partial\zeta)^2 + \partial_i\left(\partial_i\zeta e^{\zeta}\right)\right) - \frac{\mathrm{d}}{\mathrm{d}t}\left(\frac{ae^{\zeta}}{H}\right)\left(2\partial^2\zeta + (\partial\zeta)^2\right) \\
&\quad = -a\epsilon\left(\partial\zeta\right)^2 e^{\zeta} + a\epsilon\partial_i\left(\partial_i\zeta e^{\zeta}\right) \\
&\qquad\qquad - \frac{\mathrm{d}}{\mathrm{d}t}\left(\frac{ae^{\zeta}}{H}\left(2\partial^2\zeta + (\partial\zeta)^2\right)\right) + 2\frac{a}{H}\partial_i\left(\partial_i\dot{\zeta}e^{\zeta}\right)
\end{aligned} \tag{A.13}$$

These total derivatives can be dropped leaving us with the final action

$$S = M_{pl}^2 \int \mathrm{d}^4x \, a\epsilon \, e^{\zeta} \left(a^2\dot{\zeta}^2 \frac{e^{2\zeta}}{1 + \frac{\dot{\zeta}}{H}} - (\partial\zeta)^2\right), \tag{A.14}$$

which is trivial to truncate to second order.

Bibliography

[1] Jonathan S. Horner and Carlo R. Contaldi. Non-Gaussian signatures of general inflationary trajectories. 2013.

[2] Jonathan S. Horner and Carlo R. Contaldi. BICEP's bispectrum. 2014.

[3] Jonathan S. Horner and Carlo R. Contaldi. The bispectrum of single-field inflationary trajectories with $c_s \neq 1$. 2015.

[4] Carlo R. Contaldi and Jonathan S. Horner. Planck and WMAP constraints on generalised Hubble flow inflationary trajectories. *JCAP*, 1408:050, 2014.

[5] Jaswant Yadav, Somnath Bharadwaj, Biswajit Pandey, and T.R. Seshadri. Testing homogeneity on large scales in the Sloan Digital Sky Survey Data Release One. *Mon.Not.Roy.Astron.Soc.*, 364:601–606, 2005.

[6] R. Adam et al. Planck 2015 results. I. Overview of products and scientific results. 2015.

[7] D. J. Fixsen. The Temperature of the Cosmic Microwave Background. *Astrophys.J.*, 707:916–920, December 2009.

[8] R. A. Alpher, H. Bethe, and G. Gamow. The Origin of Chemical Elements. *Physical Review*, 73:803–804, April 1948.

[9] R. A. Alpher and R. C. Herman. Theory of the Origin and Relative Abundance Distribution of the Elements. *Reviews of Modern Physics*, 22:153–212, April 1950.

[10] A. A. Penzias and R. W. Wilson. A Measurement of Excess Antenna Temperature at 4080 Mc/s. *Astrophys.J.*, 142:419–421, July 1965.

[11] R. H. Dicke, P. J. E. Peebles, P. G. Roll, and D. T. Wilkinson. Cosmic Black-Body Radiation. *Astrophys.J.*, 142:414–419, July 1965.

[12] V. Mukhanov. *Physical Foundations of Cosmology.* November 2005.

[13] P.A.R. Ade et al. Planck 2013 results. I. Overview of products and scientific results. 2013.

[14] P.A.R. Ade et al. Planck 2013 results. XV. CMB power spectra and likelihood. *Astron.Astrophys.*, 571:A15, 2014.

[15] P.A.R. Ade et al. Planck 2013 results. XXII. Constraints on inflation. 2013.

[16] P.A.R. Ade et al. Planck 2013 Results. XXIV. Constraints on primordial non-Gaussianity. 2013.

[17] P.A.R. Ade et al. Planck 2015 results. XIII. Cosmological parameters. 2015.

[18] P.A.R. Ade et al. Planck 2015. XX. Constraints on inflation. 2015.

[19] P.A.R. Ade et al. Planck 2015 results. XVII. Constraints on primordial non-Gaussianity. 2015.

[20] P.A.R. Ade et al. Detection of B-Mode Polarization at Degree Angular Scales by BICEP2. *Phys.Rev.Lett.*, 112:241101, 2014.

[21] Michael J. Mortonson and Uro Seljak. A joint analysis of Planck and BICEP2 B modes including dust polarization uncertainty. 2014.

[22] Raphael Flauger, J. Colin Hill, and David N. Spergel. Toward an Understanding of Foreground Emission in the BICEP2 Region. 2014.

[23] Michael Czerny, Takeshi Kobayashi, and Fuminobu Takahashi. Running Spectral Index from Large-field Inflation with Modulations Revisited. 2014.

[24] Carlo R. Contaldi, Marco Peloso, and Lorenzo Sorbo. Suppressing the impact of a high tensor-to-scalar ratio on the temperature anisotropies. 2014.

[25] Yungui Gong and Yungui Gong. The challenge for single field inflation with BICEP2 result. *Phys.Lett.*, B734:41–43, 2014.

[26] Jing-Fei Zhang, Yun-He Li, and Xin Zhang. Sterile neutrinos help reconcile the observational results of primordial gravitational waves from Planck and BICEP2. 2014.

[27] Luis A. Anchordoqui, Haim Goldberg, Xing Huang, and Brian J. Vlcek. Reconciling BICEP2 and Planck results with right-handed Dirac neutrinos in the fundamental representation of grand unified E_6. *JCAP*, 1406:042, 2014.

[28] P. A. R. Ade, N. Aghanim, Z. Ahmed, R. W. Aikin, K. D. Alexander, M. Arnaud, J. Aumont, C. Baccigalupi, A. J. Banday, D. Barkats, and et al. Joint Analysis of BICEP 2 /K e c k A r r a y and Planck Data. *Physical Review Letters*, 114(10):101301, March 2015.

[29] Alan H. Guth. Inflationary universe: A possible solution to the horizon and flatness problems. *Phys. Rev. D*, 23:347–356, Jan 1981.

[30] A.A. Starobinsky. A new type of isotropic cosmological models without singularity. *Physics Letters B*, 91(1):99 – 102, 1980.

[31] Andreas Albrecht and Paul J. Steinhardt. Cosmology for grand unified theories with radiatively induced symmetry breaking. *Phys. Rev. Lett.*, 48:1220–1223, Apr 1982.

[32] A. D. Linde. A new inflationary universe scenario: A possible solution of the horizon, flatness, homogeneity, isotropy and primordial monopole problems. *Physics Letters B*, 108:389–393, February 1982.

[33] P.J. Steinhardt. *The Very Early Universe: Proceedings of the Nuffield Workshop, Cambridge, 21 June to 9 July, 1982*. Cambridge University Press, 1983.

[34] A. Vilenkin. Birth of inflationary universes. *Phys. Rev. D*, 27:2848–2855, June 1983.

[35] Leonard Susskind. The Anthropic landscape of string theory. 2003.

[36] Robert H. Brandenberger. Alternatives to the inflationary paradigm of structure formation. *Int.J.Mod.Phys.Conf.Ser.*, 01:67–79, 2011.

[37] Robert H. Brandenberger. The Matter Bounce Alternative to Inflationary Cosmology. 2012.

[38] Paolo Creminelli, Alberto Nicolis, and Enrico Trincherini. Galilean Genesis: An Alternative to inflation. *JCAP*, 1011:021, 2010.

[39] Ghazal Geshnizjani and Nahid Ahmadi. Can non-local or higher derivative theories provide alternatives to inflation? 2013.

[40] P.P. Avelino and R.Z. Ferreira. Bouncing Eddington-inspired Born-Infeld cosmologies: an alternative to Inflation ? *Phys.Rev.*, D86:041501, 2012.

[41] G.W. Gibbons and Neil Turok. The Measure Problem in Cosmology. *Phys.Rev.*, D77:063516, 2008.

[42] Stefan Hollands and Robert M. Wald. Comment on inflation and alternative cosmology. 2002.

[43] Lev Kofman, Andrei D. Linde, and Viatcheslav F. Mukhanov. Inflationary theory and alternative cosmology. *JHEP*, 0210:057, 2002.

[44] Stefan Hollands and Robert M. Wald. An Alternative to inflation. *Gen.Rel.Grav.*, 34:2043–2055, 2002.

[45] Eiichiro Komatsu and David N. Spergel. Acoustic signatures in the primary microwave background bispectrum. *Phys.Rev.*, D63:063002, 2001.

[46] N. Bartolo, E. Komatsu, S. Matarrese, and A. Riotto. Non-Gaussianity from inflation: theory and observations. *Phys. Rept.*, 402:103–266, November 2004.

[47] S. Weinberg. *Cosmology.* Oxford University Press, 2008.

[48] C. W. Misner, K. S. Thorne, and J. A. Wheeler. *Gravitation.* 1973.

[49] K.A. Olive et al. Review of Particle Physics. *Chin.Phys.*, C38:090001, 2014.

[50] Georges Aad et al. Observation of a new particle in the search for the Standard Model Higgs boson with the ATLAS detector at the LHC. *Phys.Lett.*, B716:1–29, 2012.

[51] Serguei Chatrchyan et al. Observation of a new boson at a mass of 125 GeV with the CMS experiment at the LHC. *Phys.Lett.*, B716:30–61, 2012.

[52] Daniel Baumann. TASI Lectures on Inflation. 2009.

[53] Masahide Yamaguchi. Supergravity based inflation models: a review. *Class.Quant.Grav.*, 28:103001, 2011.

[54] Daniel Baumann and Liam McAllister. Advances in Inflation in String Theory. *Ann.Rev.Nucl.Part.Sci.*, 59:67–94, 2009.

[55] David H. Lyth and Antonio Riotto. Particle physics models of inflation and the cosmological density perturbation. *Phys.Rept.*, 314:1–146, 1999.

[56] Andrei D. Linde. Hybrid inflation. *Phys.Rev.*, D49:748–754, 1994.

[57] Edmund J. Copeland, Andrew R. Liddle, David H. Lyth, Ewan D. Stewart, and David Wands. False vacuum inflation with Einstein gravity. *Phys.Rev.*, D49:6410–6433, 1994.

[58] Andrew R. Liddle, Anupam Mazumdar, and Franz E. Schunck. Assisted inflation. *Phys.Rev.*, D58:061301, 1998.

[59] C. Armendariz-Picon, T. Damour, and Viatcheslav F. Mukhanov. k - inflation. *Phys.Lett.*, B458:209–218, 1999.

[60] Konstantinos Tzirakis and William H. Kinney. Non-canonical generalizations of slow-roll inflation models. *JCAP*, 0901:028, 2009.

[61] Eva Silverstein and David Tong. Scalar speed limits and cosmology: Acceleration from D-cceleration. *Phys.Rev.*, D70:103505, 2004.

[62] Shamit Kachru, Renata Kallosh, Andrei D. Linde, Juan Martin Maldacena, Liam P. McAllister, et al. Towards inflation in string theory. *JCAP*, 0310:013, 2003.

[63] J.J. Blanco-Pillado, C.P. Burgess, James M. Cline, C. Escoda, M. Gomez-Reino, et al. Racetrack inflation. *JHEP*, 0411:063, 2004.

[64] David Langlois and Sebastien Renaux-Petel. Perturbations in generalized multi-field inflation. *JCAP*, 0804:017, 2008.

[65] Clifford Cheung, Paolo Creminelli, A. Liam Fitzpatrick, Jared Kaplan, and Leonardo Senatore. The Effective Field Theory of Inflation. *JHEP*, 0803:014, 2008.

[66] Steven Weinberg. Effective Field Theory for Inflation. *Phys.Rev.*, D77:123541, 2008.

[67] Leonardo Senatore and Matias Zaldarriaga. The Effective Field Theory of Multifield Inflation. *JHEP*, 1204:024, 2012.

[68] Kazuharu Bamba and Sergei D. Odintsov. Inflationary cosmology in modified gravity theories. *Symmetry*, 7(1):220–240, 2015.

[69] Richard L. Arnowitt, Stanley Deser, and Charles W. Misner. The Dynamics of general relativity. *Gen.Rel.Grav.*, 40:1997–2027, 2008.

[70] Juan Martin Maldacena. Non-Gaussian features of primordial fluctuations in single field inflationary models. *JHEP*, 0305:013, 2003.

[71] Viatcheslav F. Mukhanov. Gravitational Instability of the Universe Filled with a Scalar Field. *JETP Lett.*, 41:493–496, 1985.

[72] Misao Sasaki. Large Scale Quantum Fluctuations in the Inflationary Universe. *Prog.Theor.Phys.*, 76:1036, 1986.

[73] T.S. Bunch and P.C.W. Davies. Quantum Field Theory in de Sitter Space: Renormalization by Point Splitting. *Proc.Roy.Soc.Lond.*, A360:117–134, 1978.

[74] J. M. Bardeen, P. J. Steinhardt, and M. S. Turner. Spontaneous creation of almost scale-free density perturbations in an inflationary universe. *Phys. Rev. D*, 28:679–693, August 1983.

[75] Steven Weinberg. Adiabatic modes in cosmology. *Phys.Rev.*, D67:123504, 2003.

[76] Ewan D. Stewart and David H. Lyth. A More accurate analytic calculation of the spectrum of cosmological perturbations produced during inflation. *Phys.Lett.*, B302:171–175, 1993.

[77] D. S. Salopek and J. R. Bond. Nonlinear evolution of long-wavelength metric fluctuations in inflationary models. *Phys. Rev. D*, 42:3936–3962, Dec 1990.

[78] Andrew R. Liddle, Paul Parsons, and John D. Barrow. Formalizing the slow roll approximation in inflation. *Phys.Rev.*, D50:7222–7232, 1994.

[79] James E. Lidsey, Andrew R. Liddle, Edward W. Kolb, Edmund J. Copeland, Tiago Barreiro, et al. Reconstructing the inflation potential : An overview. *Rev.Mod.Phys.*, 69:373–410, 1997.

[80] H. V. Peiris, E. Komatsu, L. Verde, D. N. Spergel, C. L. Bennett, M. Halpern, G. Hinshaw, N. Jarosik, A. Kogut, M. Limon, S. S. Meyer, L. Page, G. S. Tucker, E. Wollack, and E. L. Wright. First-Year Wilkinson Microwave Anisotropy Probe (WMAP) Observations: Implications For Inflation. *Astrophys.J.*, 148:213–231, September 2003.

[81] D.N. Spergel et al. First year Wilkinson Microwave Anisotropy Probe (WMAP) observations: Determination of cosmological parameters. *Astrophys.J.Suppl.*, 148:175–194, 2003.

[82] G. Hinshaw et al. Three-year Wilkinson Microwave Anisotropy Probe (WMAP) observations: temperature analysis. *Astrophys.J.Suppl.*, 170:288, 2007.

[83] D.N. Spergel et al. Wilkinson Microwave Anisotropy Probe (WMAP) three year results: implications for cosmology. *Astrophys.J.Suppl.*, 170:377, 2007.

[84] E. Komatsu et al. Five-Year Wilkinson Microwave Anisotropy Probe (WMAP) Observations: Cosmological Interpretation. *Astrophys.J.Suppl.*, 180:330–376, 2009.

[85] G. Hinshaw, D. Larson, E. Komatsu, D.N. Spergel, C.L. Bennett, et al. Nine-Year Wilkinson Microwave Anisotropy Probe (WMAP) Observations: Cosmological Parameter Results. 2012.

[86] Scott Dodelson. *Modern Cosmology.* Academic Press, Elsevier Science, 2003.

[87] Uros Seljak and Matias Zaldarriaga. A Line of sight integration approach to cosmic microwave background anisotropies. *Astrophys.J.*, 469:437–444, 1996.

[88] Matias Zaldarriaga, Uros Seljak, and Edmund Bertschinger. Integral solution for the microwave background anisotropies in nonflat universes. *Astrophys.J.*, 494:491–502, 1998.

[89] Antony Lewis, Anthony Challinor, and Anthony Lasenby. Efficient computation of CMB anisotropies in closed FRW models. *Astrophys. J.*, 538:473–476, 2000.

[90] Cullan Howlett, Antony Lewis, Alex Hall, and Anthony Challinor. CMB power spectrum parameter degeneracies in the era of precision cosmology. *JCAP*, 1204:027, 2012.

[91] E. Komatsu, N. Afshordi, N. Bartolo, D. Baumann, J. R. Bond, E. I. Buchbinder, C. T. Byrnes, X. Chen, D. J. H. Chung, A. Cooray, P. Creminelli, N. Dalal, O. Dore, R. Easther, A. V. Frolov, J. Khoury, W. H. Kinney, L. Kofman, K. Koyama, L. Leblond, J.-L. Lehners, J. E. Lidsey, M. Liguori, E. A. Lim, A. Linde, D. H. Lyth, J. Maldacena, S. Matarrese, L. McAllister, P. McDonald, S. Mukohyama, B. Ovrut, H. V. Peiris, A. Riotto, Y. Rodrigues, M. Sasaki, R. Scoccimarro, D. Seery, A. Sefusatti, K. M. Smith, A. A. Starobinsky, P. J. Steinhardt, F. Takahashi, M. Tegmark, A. J. Tolley, L. Verde, B. D. Wandelt, D. Wands, S. Weinberg, M. Wyman, A. P. S. Yadav, and M. Zaldarriaga. Non-Gaussianity as a Probe of the Physics of the Primordial Universe and the Astrophysics of the Low Redshift Universe. In *astro2010: The Astronomy and Astrophysics Decadal Survey*, volume 2010 of *Astronomy*, page 158, 2009.

[92] Alejandro Gangui, Francesco Lucchin, Sabino Matarrese, and Silvia Mollerach. The Three point correlation function of the cosmic microwave background in inflationary models. *Astrophys.J.*, 430:447–457, 1994.

[93] Limin Wang and Marc Kamionkowski. Cosmic microwave background bispectrum and inflation. *Phys. Rev. D*, 61:063504, Feb 2000.

[94] Daniel Babich, Paolo Creminelli, and Matias Zaldarriaga. The Shape of non-Gaussianities. *JCAP*, 0408:009, 2004.

[95] Paolo Creminelli and Matias Zaldarriaga. Single field consistency relation for the 3-point function. *JCAP*, 0410:006, 2004.

[96] P. Creminelli, G. D'Amico, M. Musso, and J. Noreña. The (not so) squeezed limit of the primordial 3-point function. *JCAP*, 11:38, November 2011.

[97] Paolo Creminelli, Alberto Nicolis, Leonardo Senatore, Max Tegmark, and Matias Zaldarriaga. Limits on non-gaussianities from wmap data. *JCAP*, 0605:004, 2006.

[98] L. Senatore, K. M. Smith, and M. Zaldarriaga. Non-Gaussianities in single field inflation and their optimal limits from the WMAP 5-year data. *JCAP*, 1:28, January 2010.

[99] Andrei D. Linde and Viatcheslav F. Mukhanov. Nongaussian isocurvature perturbations from inflation. *Phys.Rev.*, D56:535–539, 1997.

[100] N. Bartolo, S. Matarrese, and A. Riotto. Nongaussianity from inflation. *Phys.Rev.*, D65:103505, 2002.

[101] David H. Lyth, Carlo Ungarelli, and David Wands. The Primordial density perturbation in the curvaton scenario. *Phys.Rev.*, D67:023503, 2003.

[102] Francis Bernardeau and Jean-Philippe Uzan. NonGaussianity in multifield inflation. *Phys.Rev.*, D66:103506, 2002.

[103] David Seery and James E. Lidsey. Primordial non-Gaussianities from multiple-field inflation. *JCAP*, 0509:011, 2005.

[104] Filippo Vernizzi and David Wands. Non-gaussianities in two-field inflation. *JCAP*, 0605:019, 2006.

[105] David Wands. Multiple field inflation. *Lect.Notes Phys.*, 738:275–304, 2008.

[106] C. T. Byrnes, S. Nurmi, G. Tasinato, and D. Wands. Scale dependence of local f_{NL}. *JCAP*, 2:34, February 2010.

[107] Mohsen Alishahiha, Eva Silverstein, and David Tong. DBI in the sky. *Phys.Rev.*, D70:123505, 2004.

[108] Xingang Chen, Min-xin Huang, Shamit Kachru, and Gary Shiu. Observational signatures and non-Gaussianities of general single field inflation. *JCAP*, 0701:002, 2007.

[109] Nima Arkani-Hamed, Paolo Creminelli, Shinji Mukohyama, and Matias Zaldarriaga. Ghost inflation. *JCAP*, 0404:001, 2004.

[110] N. Bartolo, M. Fasiello, S. Matarrese, and A. Riotto. Large non-Gaussianities in the effective field theory approach to single-field inflation: the bispectrum. *JCAP*, 8:8, August 2010.

[111] David Seery and James E. Lidsey. Primordial non-Gaussianities in single field inflation. *JCAP*, 0506:003, 2005.

[112] Johannes Noller and Joao Magueijo. Non-Gaussianity in single field models without slow-roll. *Phys.Rev.*, D83:103511, 2011.

[113] Steven Weinberg. Quantum contributions to cosmological correlations. *Phys.Rev.*, D72:043514, 2005.

[114] Peter Adshead, Richard Easther, and Eugene A. Lim. Cosmology With Many Light Scalar Fields: Stochastic Inflation and Loop Corrections. *Phys.Rev.*, D79:063504, 2009.

[115] Peter Adshead, Richard Easther, and Eugene A. Lim. The 'in-in' Formalism and Cosmological Perturbations. *Phys.Rev.*, D80:083521, 2009.

[116] David Seery. One-loop corrections to the curvature perturbation from inflation. *JCAP*, 0802:006, 2008.

[117] David Seery. One-loop corrections to a scalar field during inflation. *JCAP*, 0711:025, 2007.

[118] Martin S. Sloth. On the one loop corrections to inflation and the CMB anisotropies. *Nucl.Phys.*, B748:149–169, 2006.

[119] Martin S. Sloth. On the one loop corrections to inflation. II. The Consistency relation. *Nucl.Phys.*, B775:78–94, 2007.

[120] Julian Schwinger. Quantum variables and the action principle. *Proceedings of the National Academy of Sciences of the United States of America*, 47(7):pp. 1075–1083, 1961.

[121] Pradip M. Bakshi and Kalyana T. Mahanthappa. Expectation value formalism in quantum field theory. i. *Journal of Mathematical Physics*, 4(1), 1963.

[122] Pradip M. Bakshi and Kalyana T. Mahanthappa. Expectation value formalism in quantum field theory. ii. *Journal of Mathematical Physics*, 4(1), 1963.

[123] L.V. Keldysh. Diagram technique for nonequilibrium processes. *Zh.Eksp.Teor.Fiz.*, 47:1515–1527, 1964.

[124] R.D. Jordan. Effective Field Equations for Expectation Values. *Phys.Rev.*, D33:444–454, 1986.

[125] E. Calzetta and B.L. Hu. Closed Time Path Functional Formalism in Curved Space-Time: Application to Cosmological Back Reaction Problems. *Phys.Rev.*, D35:495, 1987.

[126] Ali Kaya. In-in formalism, pseudo-instantons and rethinking quantum cosmology. 2013.

[127] Xingang Chen. Primordial Non-Gaussianities from Inflation Models. *Adv.Astron.*, 2010:638979, 2010.

[128] Xingang Chen, Richard Easther, and Eugene A. Lim. Large Non-Gaussianities in Single Field Inflation. *JCAP*, 0706:023, 2007.

[129] Xingang Chen, Richard Easther, and Eugene A. Lim. Generation and Characterization of Large Non-Gaussianities in Single Field Inflation. *JCAP*, 0804:010, 2008.

[130] Dhiraj Kumar Hazra, L. Sriramkumar, and Jerome Martin. BINGO: A code for the efficient computation of the scalar bi-spectrum. 2012.

[131] Karyn M. Apfeldorf, Horacio E. Camblong, and Carlos R. Ordonez. Field redefinition invariance in quantum field theory. *Mod.Phys.Lett.*, A16:103–112, 2001.

[132] Jaume Garriga and Viatcheslav F. Mukhanov. Perturbations in k-inflation. *Phys.Lett.*, B458:219–225, 1999.

[133] Frederico Arroja and Takahiro Tanaka. A note on the role of the boundary terms for the non-Gaussianity in general k-inflation. *JCAP*, 1105:005, 2011.

[134] R. Holman and Andrew J. Tolley. Enhanced Non-Gaussianity from Excited Initial States. *JCAP*, 0805:001, 2008.

[135] William H. Press, Saul A. Teukolsky, William T. Vetterling, and Brian P. Flannery. *Numerical recipes in C (2nd ed.): the art of scientific computing.* Cambridge University Press, New York, NY, USA, 1992.

[136] J. R. Cash and Alan H. Karp. A variable order runge-kutta method for initial value problems with rapidly varying right-hand sides. *ACM Trans. Math. Softw.*, 16(3):201–222, September 1990.

[137] Jonathan S. Horner and Carlo R. Contaldi. Non-Gaussianity Unleashed. 2013.

[138] Kate Gregory and Ade Miller. *C++ AMP: Accelerated Massive Parallelism with Microsoft® Visual C++®.* OReilly Media, Inc., 2012.

[139] A.D. Linde. Chaotic inflation. *Physics Letters B*, 129(34):177 – 181, 1983.

[140] Viatcheslav F Mukhanov and GV Chibisov. Quantum fluctuations and a nonsingular universe. *JETP Letters*, 33:532–535, 1981.

[141] VF Mukhanov and GV Chibisov. Vacuum energy and large-scale structure of the universe. *Zh. Eksp. Teor. Fiz*, 83:487, 1982.

[142] Stephen W Hawking. The development of irregularities in a single bubble inflationary universe. *Physics Letters B*, 115(4):295–297, 1982.

[143] Alan H Guth and So-Young Pi. Fluctuations in the new inflationary universe. *Physical Review Letters*, 49(15):1110, 1982.

[144] A.A. Starobinsky. Dynamics of phase transition in the new inflationary universe scenario and generation of perturbations. *Physics Letters B*, 117(34):175 – 178, 1982.

[145] James M. Bardeen, Paul J. Steinhardt, and Michael S. Turner. Spontaneous creation of almost scale-free density perturbations in an inflationary universe. *Phys. Rev. D*, 28:679–693, Aug 1983.

[146] Neal Dalal, Olivier Dore, Dragan Huterer, and Alexander Shirokov. The imprints of primordial non-gaussianities on large-scale structure: scale dependent bias and abundance of virialized objects. *Phys.Rev.*, D77:123514, 2008.

[147] Tommaso Giannantonio, Cristiano Porciani, Julien Carron, Adam Amara, and Annalisa Pillepich. Constraining primordial non-Gaussianity with future galaxy surveys. *Mon.Not.Roy.Astron.Soc.*, 422:2854–2877, 2012.

[148] Hiroyuki Funakoshi and Sebastien Renaux-Petel. A Modal Approach to the Numerical Calculation of Primordial non-Gaussianities. *JCAP*, 1302:002, 2013.

[149] Peter Adshead and Richard Easther. Constraining Inflation. *JCAP*, 0810:047, 2008.

[150] William H. Kinney. A Hamilton-Jacobi approach to nonslow roll inflation. *Phys.Rev.*, D56:2002–2009, 1997.

[151] Richard Easther and William H. Kinney. Monte Carlo reconstruction of the inflationary potential. *Phys.Rev.*, D67:043511, 2003.

[152] Sirichai Chongchitnan and George Efstathiou. Dynamics of the inflationary flow equations. *Phys.Rev.*, D72:083520, 2005.

[153] Andrew R Liddle. Inflationary flow equations. *Phys.Rev.*, D68:103504, 2003.

[154] Antony Lewis and Sarah Bridle. Cosmological parameters from CMB and other data: a Monte- Carlo approach. *Phys. Rev.*, D66:103511, 2002.

[155] Carlo R. Contaldi. BICEP's acceleration. *JCAP*, 1410(10):072, 2014.

[156] Raquel H. Ribeiro. Inflationary signatures of single-field models beyond slow-roll. *JCAP*, 1205:037, 2012.

[157] Xingang Chen. Running non-Gaussianities in DBI inflation. *Phys.Rev.*, D72:123518, 2005.

[158] E. Sefusatti, M. Liguori, A. P. S. Yadav, M. G. Jackson, and E. Pajer. Constraining running non-gaussianity. *JCAP*, 12:22, December 2009.

[159] C. L. Bennett, D. Larson, J. L. Weiland, N. Jarosik, G. Hinshaw, N. Odegard, K. M. Smith, R. S. Hill, B. Gold, M. Halpern, E. Komatsu, M. R. Nolta, L. Page, D. N. Spergel, E. Wollack, J. Dunkley, A. Kogut, M. Limon, S. S. Meyer, G. S. Tucker, and E. L. Wright. Nine-year Wilkinson Microwave Anisotropy Probe (WMAP) Observations: Final Maps and Results. *Astrophys.J.Suppl.*, 208:20, October 2013.

[160] Planck Collaboration, P. A. R. Ade, N. Aghanim, C. Armitage-Caplan, M. Arnaud, M. Ashdown, F. Atrio-Barandela, J. Aumont, C. Baccigalupi, A. J. Banday, and et al. Planck 2013 results. XVI. Cosmological parameters. *Astron.Astrophys.*, 571:A16, November 2014.

[161] L. Verde. Non-Gaussianity from Large-Scale Structure Surveys. *Advances in Astronomy*, 2010:64, 2010.